

INVESTIGATIONS INTO THE DYNAMICS OF AEROSOLS IN  
ENCLOSURES AS USED FOR AIR POLLUTION STUDIES



CENTRALE LANDBOUWCATALOGUS

0000 0086 6851

Promotor: dr. E.H. Adema, hoogleraar in de leer der luchthygiëne  
en luchtverontreiniging

Co-promotor: dr. W. Stöber hoogleraar aan de Westfälische  
Wilhelms-Universität te Münster

118746-03  
U.D.C. 541.182.2/.3:614.71/.72:

JOH.F. VAN DE VATE

551.575/.576

INVESTIGATIONS INTO THE DYNAMICS OF AEROSOLS IN  
ENCLOSURES AS USED FOR AIR POLLUTION STUDIES

**Proefschrift**

ter verkrijging van de graad  
van doctor in de landbouwetenschappen,  
op gezag van de rector magnificus  
dr. H.C. van der Plas,  
hoogleraar in de organische scheikunde,  
in het openbaar te verdedigen  
op woensdag 24 september 1980  
des namiddags te vier uur in de aula  
van de Landbouwhogeschool te Wageningen

RECTOR  
MAGNIFICUS  
LANDBOUWHOGESCHOOL  
WAGENINGEN

15N - 118746 - 03

## STELLINGEN

1.

De recente resultaten van Harrison betreffende het gedrag van aerosol-deeltjes in een ruimte met houten wanden, leiden tot een verband tussen diffusie-grenslaagdikte en aerosol-diffusiecoëfficiënt dat sterk afwijkt van de theorie en van andere waarnemingen betreffende dit verband.

*A.W. Harrison, J. Coll. Interf. Sci. 69 (1979), 563.*

*Dit proefschrift: §2.2.2, in het bijzonder vergelijking (15).*

2.

Facy's schatting van het belang van thermoforese ten opzichte van diffusioforese van aerosol-deeltjes in de nabijheid van verdampende of condenserende druppels is een grootte-orde te laag.

*L. Facy, "Radioactive precipitations and fall out", in: "Nuclear Radiation in Geophysics", eds. H. Israel en A. Krebs (Springer, Heidelberg, 1962), p.226.*

3.

De waarnemingen van Van de Vate waaruit Van der Hage concludeert dat de nucleatie-snelheid van water op hydrofobe deeltjes veel groter is dan volgens de klassieke theorie berekend kan worden, zijn in dit verband multi-interpretabel.

*J.C.H. van der Hage, "Condensation of water on insoluble substrates", proefschrift Universiteit van Utrecht, 1974, p.55.*

4.

Deeltjes groter dan enkele micrometers kunnen in de buitenlucht niet verzameld worden met een van de luchtbeweging onafhankelijk rendement als een monster-aanzuigmond in rust wordt gebruikt.

5.

Bij epidemiologisch onderzoek betreffende luchtverontreinigend stof is de aerosolmonstername tot nu toe onvoldoende gezondheidsrelevant geweest.

*"Sulfur Oxides and Suspended Particulate Matter", Environmental Health Criteria 8, World Health Organization, Geneva, 1979, sections 2.2.3 and 8.3.*

6.

De grote stroom resultaten van meetnetten voor neerslag-samenstelling is voorlopig niet bruikbaar voor de doeleinden die men zich daarbij voorstelt betreffende kennis van verontreiniging van bodem, water en lucht.

De bezwaren van natuurwetenschappelijke zijde tegen sub-Avogadro verdunningen in de homeopathie ( $< 10^{-24}$ , c.q. "potenties"  $> D24$ ) moeten zich ook richten tegen de zeer lage partiële zuurstof-drukken ( $< 10^{-22}$  kPa) in de gas-vast chemie van metaaloxiden met defect-structuren.

*O. Leeser, Lehrbuch der Homöopathie (3e druk, K.F. Haug, Ulm, 1963), p. 535.*

*L.M. Atlas, G.J. Schleman, "Defect equilibria of  $PuO_{2-x}$ , 1100 to 1600 °C in: Proc. Int. Symp. "Thermodynamics", Vienna, 22-27 July, 1965 (IAEA, Vienna, 1966), vol. II, p. 407.*

*K.L. Komarek, M. Silver, "Thermodynamic properties of zirconium-oxygen, titanium-oxygen and hafnium-oxygen alloys", in: Proc. Int. Symp. "Thermodynamics of Nuclear Materials", Vienna, 21-25 May, 1962 (IAEA, Vienna, 1962), p. 749.*

## 8.

Antoni van Leeuwenhoek was de eerste belangrijke natuurwetenschappelijke onderzoeker van aerosoldeeltjes.

*"Alle de brieven" van Antoni van Leeuwenhoek (Amsterdam/Lisse: Swets & Zeitlinger, 1939-1979); bijv. kaarsrook: deel I, p.182; tabaksrook: deel I, p.220; mistdeeltjes: deel III, p.300; tin- en loodrook: deel V, p.108.*

## 9.

De onomkeerbare klimaatbeïnvloeding ten gevolge van kooldioxide-emissie door de verbranding van fossiele brandstoffen is waarschijnlijk een groter probleem dan de mogelijke effecten van radio-actief afval van nucleaire energie-opwekking

## 10.

Hoewel een belangrijk deel van de taak van de Landbouwhogeschool te Wageningen is gericht op monocultures, is het toch niet gewenst de doctoraten-oogst aan deze instelling te beperken tot die in Landbouwwetenschappen.

## 11.

Het past een christen om zorgen te hebben over het milieu maar niet om milieu-activist te zijn.

## 12.

Polemiek in de kerkelijke pers strijdt met christelijke grondregels.

*Matthéus 18: 15-17.*

## 13.

Het zou beter zijn als men zijn schoolgeld weer kan terughalen.

*A. Kuyper, "Ons program" (Höveker en Wormser, A'dam, 1880), p.223.*

Stellingen bij het proefschrift "Investigations into the dynamics of aerosols in enclosures as used for air pollution studies".

Joh. F. van de Vate  
Wageningen, 24 september 1980.

## VOORWOORD

Dit proefschrift wil op een bescheiden wijze tot uitdrukking brengen de prachtige samenhang waarin God Zijn schepping gemaakt heeft en nog steeds zo in stand houdt, waaruit Zijn almacht en trouw blijkt. Hem ben ik dank verschuldigd dat ik met dit proefschrift te midden van veel andere activiteiten een stukje van die schepping mag ontplooiën.

Mijn ouders wil ik in dit voorwoord een voorname plaats geven. Zij hebben in de financieel moeilijke jaren na de Tweede Wereldoorlog mij in de gelegenheid gesteld een universitaire studie te volgen. In het bijzonder wijlen mijn vader heeft mij opgevoed in het zien van het esthetische van de omringende werkelijkheid en in het bijzonder van de natuurwetenschappelijke verschijnselen en wetmatigheden, een instelling van veel belang voor een natuurwetenschappelijk onderzoeker.

Prof.Dr. E.H. Adema, mijn promotor, ben ik erg erkentelijk voor zijn belangrijke begeleiding bij het in definitieve vorm brengen van dit proefschrift en vooral voor zijn welwillendheid een al grotendeels gevormde dissertatie onder zijn supervisie te nemen. De kritische commentaren op concepten van deze dissertatie door twee van zijn vak-groep-medewerkers Dr.Ir. Eltjo Buringh en Ir. Peter Hofschreuder zijn belangrijk geweest voor zowel vorm als inhoud van dit proefschrift. Ik ben hen daarvoor erg dankbaar.

I feel strongly obliged to acknowledge my co-promotor Prof.Dr. W. Stöber for his various activities in relation to this thesis. His critical reading of the manuscript in its final form, advices on various aerosol subjects dealt with in this thesis, and further comments have been greatly appreciated.

Prof.Dr. F.H. Schmidt wil ik ook graag hier vermelden. Het spijt me dat U in een bepaald stadium van mijn promotie hebt moeten terug-treden. Uw commentaar op dit proefschrift heb ik echter erg gewaardeerd en is met vrucht verwerkt.

Het Energieonderzoek Centrum Nederland verdient veel waardering voor de ter beschikking stelling van verschillende technische faci-li-teiten onontbeerlijk voor het verschijnen van dit proefschrift. Vooral wil ik Prof.Dr. J.A. Goedkoop en Dr. A. Tolk noemen bij mijn dankwoord vanwege hun stimulerende belangstelling voor het aerosolonderzoek dat ik bij het ECN nu bijna 13 jaar heb mogen leiden. Bovendien heeft het

commentaar van eerstgenoemde bij het manuscript van dit proefschrift belangrijk bijgedragen aan een goede weergave van mijn ideeën hierin.

De experimentele uitvoering van het onderzoek vermeld in dit proefschrift heb ik samen met Leo Hermans en Adri Plomp mogen doen. Bij het uitwerken van de vele waarnemingen ben ik bevestigd in mijn overtuiging dat zonder hun inzet en bijzondere experimenteer-vaardigheid dit proefschrift niet de noodzakelijke basisgegevens had gekregen. Zij weten dat ik de kwaliteit van hun werk hoog schat.

Ik wil zeker ook Ir. J.R.D. Stoute noemen die mij op plezierige wijze ingewijd heeft in de aerosolmysterieën. Discussies met Dr.Ir. J.A.M. Kops, Dr. H.M. ten Brink en technische hulp van verschillende medewerkers van de ECN-groep Aerosolonderzoek hebben bijgedragen tot dit proefschrift; hen wil ik ook bijzonder bedanken.

Mevrouw Admiraal-Ypma verdient veel waardering voor de verzorging van het type-werk.

Ik ben aan mijn vrouw, Agathe, bijzondere dank verschuldigd vanwege haar opofferende, voortdurende aanmoediging bij de studie voor en het schrijven van dit proefschrift. Ze heeft zonder enig teken van ongenoegen gedragen dat mijn afwezigheid in de huiselijke kring gedurende anderhalf jaar nog groter was dan normaal. Ook waardeer ik de morele steun die mijn kinderen me gaven door zo consequent de houding van hun moeder na te volgen.

## CONTENTS

	<u>Page</u>
LIST OF SYMBOLS	10
1. INTRODUCTION	13
1.1. General	13
1.2. Atmospheric aerosols	17
1.3. Review of literature	18
1.3.1. Early period	18
1.3.2. Nuclear safety research	21
1.3.3. Smog chamber studies	24
1.3.4. Summary	25
1.4. Objectives	26
2. THEORY	27
2.1. Coagulation	27
2.2. Deposition of enclosed aerosols	28
2.2.1. General	28
2.2.2. Stirred diffusive deposition	31
2.2.3. Stirred gravitational deposition	34
2.2.4. Stirred thermophoretic deposition	35
2.2.5. Stirred diffusiophoretic deposition	42
2.2.6. Stirred photophoretic deposition	45
2.2.7. Stirred electrophoretic deposition	47
2.3. Particle shape, density and size distribution	50
2.4. Size distribution of enclosed aerosols	53
2.5. Non-stirred aerosol deposition	56
2.5.1. Non-stirred aerosol settling	56
2.5.2. Non-stirred diffusive deposition	57
2.5.3. Atmospheric stability of box atmospheres	58
2.5.4. Rotating drums	60



	<u>Page</u>
3. MATERIALS AND METHODS	62
3.1. Aerosol formation	62
3.2. Containments	63
3.3. Analytical and sampling techniques	65
3.3.1. Sampling for electron microscopy	65
3.3.2. Particle number concentration	68
3.3.3. Mass concentration	69
3.3.4. Size distribution	69
3.4. Materials	72
3.5. Experimental errors	73
4. RESULTS AND DISCUSSIONS	74
4.1. Primary particles	74
4.2. Coagulation	77
4.3. Aerosol deposition in unheated dry vessels	79
4.3.1. Quasi-monodisperse aerosols	79
4.3.2. Influence of aerosol formation parameters	82
4.3.3. Influence of vessel height	86
4.3.4. Measurement of dynamic shape factors from decay curves of mass and number concentrations	89
4.3.5. Influence of the initial mass concentration	97
4.3.6. Non-stirred conditions	100
4.3.6.1. Non-stirred settling	100
4.3.6.2. Stratification	102
4.3.7. Stirred electrophoresis	105
4.3.8. Summary	107
4.4. Aerosol decay in heated dry vessels	108
4.4.1. General observations and considerations	108
4.4.2. Effect of heating power	111
4.4.3. Effects of aerosol material, temperature and gas phase on thermophoresis	113
4.4.4. Hampered settling on heated vessel floors (low heating rates)	115
4.4.5. Summary	117

	<u>Page</u>
4.5. Aerosol decay in vessels with a heated pool of water on the floor	117
4.5.1. General observations and discussions	117
4.5.2. Theory	122
4.5.3. Experimental results and discussions	124
4.5.4. Summary	131
4.6. Photochemical reaction chambers (smog chambers)	132
4.6.1. General	132
4.6.2. Thermophoretic effects	132
4.6.3. Photophoretic effects	133
4.6.4. Diffusional and gravitational effects	134
4.6.5. Coagulation combined with deposition	135
4.6.6. Experiments and discussions	136
4.6.7. Summary	141
5. GENERAL SUMMARY	143
REFERENCES	145
TABLES	152

## LIST OF SYMBOLS

- A - proportionality constants in (19), (89) and (90)
- B - proportionality constant in (27)
- D - diffusion coefficient in (10)
- E - electric field strength in (41)  
- proportionality constant in (87) and (88)
- F(d) - slip correction factor for particle of diameter d in (8)
- G - factor in (91) and (92)
- $\Delta H_v$  - latent heat of vaporization in (34) and (88)
- I - flux, of particles in (14), of light in (37)
- K - coagulation constant in (1)
- Kn - Knudsen number ( $= \frac{\lambda}{r} = \frac{2\lambda}{d}$ )
- M - molecular mass in (62)
- N - number
- Q - heating power
- R - gas constant  
- proportionality constant in (48) and (49)
- S - surface area
- %S - percentage of supersaturation in (93)
- T - Kelvin temperature
- U - force
- X - mole fraction
- b - exponent to n in section 4.3.2
- c - concentration  
- slip coefficients in (28<sup>c</sup>)
- d - particle diameter
- f - factor of increase of  $d_a$  due to compaction in (79)
- $f_n$  - factor of increase of  $d_a$  due to n primaries in section 2.3

- g - gravitational acceleration
- h - height of aerosol chamber
- k - Boltzmann constant
- l - mean free path of molecules  
-  $\frac{2}{3}V$  in (55)
- m - mass of aerosol particle
- n - number  
- gas/particle interaction coefficient ( $n_{th}$ ) in (23)
- p - pressure
- q - electric charge
- r - radius of droplet
- r - radius of particle
- t - time
- v - velocity
- x - distance
- $\alpha$  - thermophoretic constant in (20)  
- coefficient of thermal expansion in (55)
- $\beta$  - decay constant of aerosol removal in (5)
- $\delta$  - thickness of boundary layer in (11)
- $\epsilon$  - absolute dielectric constant in (44)
- $\eta$  - gas viscosity
- $\kappa$  - dynamic shape factor in (47)
- $\lambda$  - thermal conductivity in (25)
- $\mu$  - mobility in (6)
- $\rho$  - density
- $\sigma$  - standard deviation
- $\omega$  - angular velocity of rotation

## Subscripts

- a - aerodynamic
- B - according to Brock in (28<sup>c</sup>)
- crit - in (31)
- d - diffusive in (16)  
- vapour in (61)
- diff - diffusiophoretic in (32)
- D - according to Derjaguin in (28<sup>d</sup>)
- e - mass (or volume) equivalent in (46)  
- electric in (41)
- eff - effective
- E - according to Epstein in (28<sup>b</sup>)
- f - floor in (18)
- g - gas in (22)  
- geometric in (51)
- m - mass  
- measured in (29)  
- momentum in (28<sup>c</sup>)
- max - maximum
- n - number
- p - particulate  
- photophoretic in (37)
- S - according to Stetter in (28<sup>a</sup>)
- s - sedimentation in (17)
- sp - spatial in (73)
- t - thermal in (28<sup>c</sup>)
- th - thermophoretic in (19)
- v - vapour in (88)

## 1. INTRODUCTION

### 1.1. General

Commonly "aerosol" is defined as a heterogeneous system of finely dispersed solid or liquid matter suspended in a gas. Since, in contrast to hydrosols, the aerosol system is inherently unstable, the problem of the size range of the dispersed phase reduces to the sensitivity and the quickness of the means to observe it. Usually, interest is limited to the size range of 0.01 to 100  $\mu\text{m}$ .

For a long time aerosols have been recognized as an important part of nature. In 1885 Sir Oliver Lodge [1] remarked: "If the atmosphere were purely gaseous and held no minute foreign bodies in suspensions, . . . , the sun would glare down directly with blinding intensity and objects not directly in sunlight would be in almost complete shadow". Besides, cloud formation by condensation of water vapour would be strongly hampered, leading to a different world climate. On the other hand, for modern traffic and shipping, the presence of fog causes severe problems, so that the considerable efforts to investigate the role and the behaviour of condensation nuclei and to forecast visibility are of more than academic interest.

For centuries anthropogenic aerosols have been considered as air pollution to be combatted, the main part of these aerosols originating from combustion. Recently, interest paid to pollution of the air by particulate matter has increased strongly. There were various reasons for this change in view of airborne particulate matter. One of the reasons has been the insight that the gaseous air contaminants like  $\text{SO}_2$  [2] and  $\text{NO}_x$  [3], originally considered to be main air pollutants, appeared to have enhanced toxicity in the presence of aerosols probably due to conversion at the particle's surface or due to a postulated increased inhalability (concentrating and vehicle function of the particle). This synergism of gaseous contaminants and aerosols is the proposed explanation for smog catastrophies like the one of 1952 in London [4]. Effects owing to anthropogenic aerosols other than on human health or living nature, which have placed them more and more on the environmental foreground are e.g.:

- decreased visibility (mainly related to sulphate particles),

- a possible influence on the world's climate,
- changes in the composition of precipitation (acidification),
- enhanced corrosion of materials,
- other consequences of atmospheric interactions with particles, like radical scavenging, photocatalysis, formation of photoactive compounds ( $\text{HNO}_2$ ).

Nearly every handbook on aerosols commences with a survey of the various names attributed to aerosols according to their composition, formation, appearance, etc. To avoid adding to the confusion caused by the sometimes controversial definitions, the existence of this extensive literature e.g. [5] may merely be mentioned here. In the present work, however, other terms like "nucleus" are also used. Concentrations of nuclei are measured by means of condensation nuclei counters (pg. 68); nuclei play a role in aerosol formation inside enclosures with a heated layer of liquid (section 4.5). The use of the term nucleus in aerosol science stems from meteorology where aerosols play an important role in water droplet and ice nucleation.

This study concerns the behaviour of enclosed aerosols. Originally, it was carried out with the aim to derive rules which could refine the evaluation of reactor safety with regard to severe hypothetical accidents of nuclear power reactors [6]. However, the applicability of the results is much wider, amongst others to atmospheric research (to which the present study is generally dedicated). One of the experimental problems of atmospheric research is the principal impossibility of avoiding interferences due to the surroundings. When investigating a localized air parcel *in situ* one should follow this parcel during its transport which can be done e.g. by means of balloon-borne instruments. However, interference from mixing in of air from outside the parcel will be unavoidable in this approach. The alternative of placing the parcel inside an enclosure eliminates the air mixing interference but now the walls of the enclosure will influence the properties of the air parcel. Nevertheless, the latter technique is most widely used in atmospheric research. Obviously, atmospheric research and other investigations on air-borne material require some knowledge about the influence of the dimensions and parameters of the enclosure confining the air or cloud of particles to be examined. In air pollution research

this is the case, for example if the kinetics of a slow chemical reaction involving aerosols must be investigated. For this purpose the often used (dynamic) flow reactor has limited use because the relevant trace-analytical determinations need large samples which can only be obtained at higher flow velocities limiting this type of reactors to reactions of relatively fast kinetics.

However, knowledge of the stability of aerosols in vessels may be useful for still more purposes. Either the aerosol container may be used as a supply of atmospheric nuclei with a concentration having a known time dependence, or the enclosure may be used for research on aerosols in a defined environment. Moreover, the properties of the aerosol particles can be examined by investigating the decay rate of an enclosed aerosol. Finally, using a known aerosol the enclosure can be characterized as to its properties as an aerosol enclosure.

Consequently, this study has been carried out in view of the importance of the knowledge of the processes in enclosed aerosols for:

- the use of enclosures under controlled laboratory conditions:
  - a) in atmospheric research for the study of aerosol processes in the atmosphere like coagulation, sedimentation, condensation, scavenging, nucleation and chemical reactions,
  - b) in environmental sciences for the study of the totality of aerosol processes playing a role in air pollution,
  - c) in microbiology, particularly aerobiology of airborne microbes,
  - d) as a tool for assessment of aerosol properties;
- experimental simulation of post-accident situations of nuclear reactors or other potentially hazardous industrial installations;
- the characterization of aerosols stored in a container as a supply, for calibration etc. of aerosol measuring apparatus.

From the review of available literature of research on enclosed aerosols (see next section) it may become clear that there is a considerable and widespread interest in this field, but also that results are rather incoherent. This is also one of the motivations for the present study.

The majority of the aerosols in this study used was generated by the so-called Exploding Wire technique which will be explained later on. Although the motivation for the use of aerosols from an Exploding Wire in the present research stems from nuclear safety, it must be emphasized here that these aerosols have aerodynamics similar to the so-called



condensation aerosols. These aerosols play an important role in air pollution since they are typically anthropogenic owing to their formation by wide-spread high-temperature processes such as occurring in combustion engines and iron works. In a separate study on the morphology and chemical composition of atmospheric particles, the author has shown [7] the occurrence of important concentrations of these chain-like particles near busy roads and in industrial areas. Figure 1 allows comparison between these atmospheric aerosols and the aerosols from an Exploding Wire.

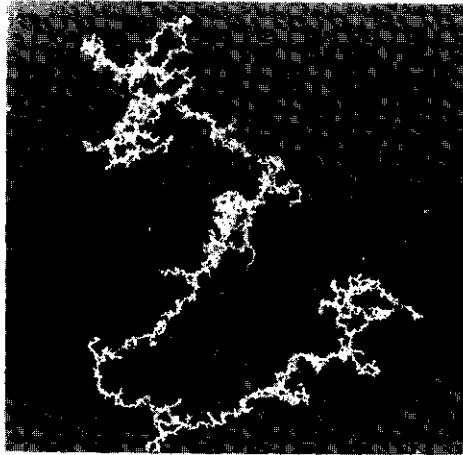


Fig. 1a. Condensation aerosol of copper oxide formed by the Exploding Wire technique. The platinum shadow illustrates the three-dimensional character of the aggregates.

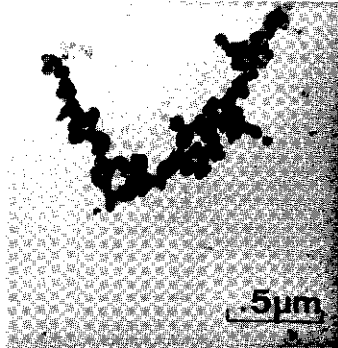
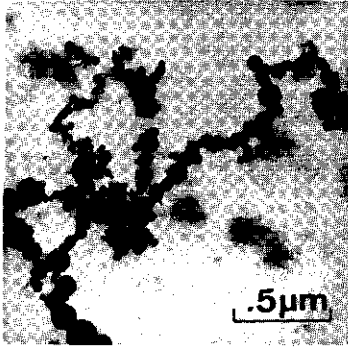


Fig. 1b. Iron oxide aerosol sampled in an industrial area with iron works.

Fig. 1c. Aerosol particle (presumably carbonaceous material) sampled near a busy road.

## 1.2. Atmospheric aerosols

Aerosols in the troposphere have various origins. Nature itself gives the largest contribution ( $\sim 4 \times 10^{15}$  g.yr<sup>-1</sup>) [8]. Anthropogenic sources, though important locally or regionally, emit globally with a much lower rate ( $\sim 3 \times 10^{14}$  g.yr<sup>-1</sup>) [8]. Meteoritic dust is insignificant ( $2 \times 10^{11}$  g.yr<sup>-1</sup> [8]). It is most functional to describe the atmospheric aerosol in terms of its size distribution. According to Whitby [9] (supported by experimental evidence, also from many other studies) the number size spectrum of the atmospheric aerosol basically consists of three modes

- a "transient nuclei" mode with a geometric median diameter of 0.017  $\mu\text{m}$  and a geometric standard deviation of 1.74,
- an "accumulation" range with a geometric median diameter of 0.34  $\mu\text{m}$  and a geometric standard deviation of 2.05,
- a "coarse particle" region with a geometric median diameter of about 8.8  $\mu\text{m}$  and a geometric standard deviation of 2.33.

Sources mainly emit into the smallest or largest mode. When aerosol formation is via the molecular stage (photochemical, combustion, etc.) transient nuclei will be produced. Coarse particles are produced by

mechanical means like grinding, by wind, etc. Due to the high rate of coagulation of nuclei these small particles are quickly transported from the transient nuclei mode to the accumulation mode. The accumulation mode is relatively stable since the combined atmospheric deposition process (diffusion removal and inertial removal) is least effective for these particles. Since most of the surface area of airborne particulates is concentrated in the accumulation mode, coagulation of transient nuclei is predominantly with this mode. Background aerosols in remote areas have mainly sizes which fall in the accumulation mode. However, when the sun is shining in these areas considerable amounts of transient nuclei can be found (Great Smoky Mountains), and when arid regions (Sahara desert) are concerned, dust storms can give a major contribution of coarse particles. Worlds largest natural aerosol source is the ocean ( $10^{15}$  g.yr<sup>-1</sup>) [8]. The marine aerosol is produced by the bursting-bubble mechanism which is a mechanical process. However, the droplets initially formed evaporate to particles which are much smaller. The marine aerosol size spectrum consists roughly of two modes: one coinciding with the coarse particle mode, the other mode extending from the accumulation mode into the transient nuclei [10].

In urban regions the various anthropogenic sources can give the whole spectrum of the three modes. These emissions are extensively studied like fly-ash, traffic aerosols, and various industrial emissions. A separate category is the secondary formed aerosol, e.g. sulphate particles from the primary SO<sub>2</sub> emission and photochemical smog from sun irradiation of complex mixtures of nitrogen oxides and unsaturated hydrocarbons (sometimes also SO<sub>2</sub> is involved in this photochemical system). Such secondary aerosols mainly appear in the accumulation mode due to either condensation on existing accumulation particles or rapid coagulation of homogeneously formed clusters or nuclei with these accumulation particles.

### 1.3. Review of literature

#### 1.3.1. Early period

Already during more than half a century aerosol behaviour in enclosures was subject of research although with widely different objectives.

Investigations on enclosed aerosol date back to at least 1916. In that

year Kennedy [11] published his study on the decay of nuclei produced by a Bunsen burner in a vessel. The aim of the study was to obtain information about the electric charges on particulate matter under circumstances simulating atmospheric conditions. Particle number concentrations were measured by means of an (Aitken) nucleus counter (pg. 68). The decay appeared to be a second order process which was attributed to the coagulation of the small particles. This was found to hold over a concentration range from  $8 \times 10^5 \text{ cm}^{-3}$  to  $7 \times 10^4 \text{ cm}^{-3}$ . For lower concentrations the rate of disappearance was faster than that due to coagulation. In 1928 W.D. Flower [12] confirmed Kennedy's conclusions on coagulation as the dominating process in high number concentration aerosols in enclosures. Flower has used particles formed by heating a platinum wire in air and has measured relative number concentrations by means of the ultra-microscope. In 1933 P.J. Nolan published his study using the same measuring technique on the influence of condensation nuclei and dust particles on atmospheric ionisation [13]. He followed the decay of an enclosed aerosol consisting of atmospheric nuclei and particles over a period of 150 hours. This decay appeared to obey an exponential law except for the first day during which the rate of decay was higher. In agreement with Kennedy, Nolan attributed the initial high decay rate to coagulation, whereas the prolonged exponential decay was said to be caused by diffusion deposition from a well-stirred atmosphere on the walls of the storage balloon that was used. In 1935 J.J. Nolan and V.H. Guerrini published their study on the parallel plate single-stage diffusion battery [14] in which study the authors investigated the concentration decay in a gasometer in order to see whether the storage of nuclei would change the size spectrum of the nuclei used. It looked as if the processes of diffusion and settling operate to remove the particles at the extremes of the size distribution. Six years later P.J. Nolan re-examined his previous results [14] together with the results of Rauscher [15] and again concluded that the exponential decay is mainly due to diffusion taking place in a boundary layer. In 1955 Pollak and O'Connor [16], assisted by Fürth [17], developed a theory for the disappearance of atmospheric nuclei assuming that the "whole column of particles diffuses radially while sedimenting bodily"; thereby Pollak disavows Nolan's stirred diffusion model. They observed

also a non-exponential part in their long-term decay curves. In the same year P.J. Nolan [18] (probably convinced by Pollak's critique) gives a new approach to the problem. His analysis based on measurements of the diffusion coefficient by means of the diffusion box [14] leads also to a non-exponential decay of enclosed aerosols. Accordingly, in 1956 Pollak et al. [19] published an extensive article on the determination of the diffusion coefficient of condensation nuclei using the two different techniques. The "static" method applies the decay inside a vessel using Pollak's theory on diffusion deposition for analysis of the decay rate data. The "dynamic" method uses the diffusion box of Nolan [14]. Their "static" method, however, they state to be valid only for narrow but tall spaces with an air-column diameter of no more than a few cm. Also a boundary of 1.5 mm had to be postulated which remains free of nuclei at the start of the experiments. In 1959, O'Connor reported experimental results with nuclei stored in a 4 m<sup>3</sup> rubber balloon gasometer and showed that the "average" size of the nuclei (measured by the "dynamic" method) increased presumably due to preferential losses of smaller particles by diffusion on the wall [20]. The results presented indicate that a constant size was approached. This size was deduced from the effective diffusion coefficient obtained with the "dynamic" method. Meanwhile Nolan and Scott [21] in 1955 added to the existing knowledge of enclosed aerosols by introducing a refined "dynamic" method taking into account the relation between the effective diffusion coefficient and the flow rate through their diffusion box. The size dispersity of enclosed nuclei appeared to decrease considerably during storage. In 1965, however, McGreevy [22] showed that the "dynamic" method should be used with great care since the diffusion box measures an effective diffusion coefficient which can be seriously misleading when the size distribution is skew. For example, the presence of a significant fraction of small nuclei can suggest diffusion coefficients which are much too large. McGreevy also stated that aerosols stored for periods up to 10 days remain polydisperse. He further concluded that after about two days the size of nuclei in a container would lie between two size limits dependent on the size of the enclosure used and on the original size distribution. McGreevy's extensive publications are of great importance because his critical comments on the "dynamic method" (diffusion box) unsettles Pollak's

model of non-stirred (spatially non-uniform) aerosol deposition in chambers as this model was largely based on "dynamic" method data. Outside the field of meteorology, Langstroth and Gillespie ([23], [24]) have studied around 1950 the effect of initial mass concentration, humidity and stirring on the decay of ammonium chloride smoke inside vessels. They reported exponential decay curves for both mass and particle number. Increased humidity and stirring led to increased wall losses. In 1962 Rosinski et al. [25] reported about their investigations with enclosed aerosols originating from an Exploding Wire (pg. 62). An influence of radioactive labelling of the aerosol on the coagulation rate was observed. They found that after correction for coagulation the "decay constant" of the aerosol decreased with time. However, closer analysis of their data given in their publication does not support such a time-dependent "decay constant".

### 1.3.2. Nuclear safety research

In the mid-sixties, nuclear reactor safety motivated the initiation of various investigations of enclosed aerosols. Up to that time, in the safety evaluation of a radioactive cloud formed e.g. by a reactor accident, a 100% release to the environment was assumed. The investigations that were initiated has as their common aim to account in the safety calculations for the instability of the enclosed radioactive cloud. Reports of an expert group and symposia [26, 27] give a good survey of the efforts of the various groups in this field. Most of these groups ultimately try to develop computer models as versatile as possible regarding the description of the mechanisms active in aerosols inside containments. Since the safety of nuclear aerosols is directly related to aerosol mass, interest of these groups is mainly in gravitational aerosol deposition, the rate of which is known to be strongly coupled with any preceding coagulation. An exact formulation of coagulation, however, is very difficult (if not impossible) at least for solid aerosols. As a result, the main effort of these groups has been in coagulation. Coagulation, however, is not our primary interest since the enclosure itself is not influencing an aerosol coagulating inside it except by preventing dispersion. Nevertheless, the extent to which this work is focussed on aerosol stability inside containments justifies treatment of this study. Though it must be kept

in mind that usually rather high aerosol mass concentrations (one or more  $\text{g.m}^{-3}$ ) are concerned and, furthermore, this safety related research aims at upper estimates of the time dependent mass concentration. The most extensive series of experiments on nuclear aerosols has been done by Greenfield et al. This investigation is probably also the oldest work in this area. Aerosols have been investigated in vessel volumes varying from  $1 \text{ m}^3$  to  $6 \text{ m}^3$  [26]. In these experiments mainly sodium smoke produced from various types of sodium fires is used but the experimental programme also included  $\text{U}_3\text{O}_8$  aerosols from arc vaporization. Aerosol mass concentration versus time and depositions on walls and floor versus time have been measured. In a number of cases cascade impactor samples have been used for the determination of the size distribution. Due to the high mass concentrations in these sodium smoke experiments ( $1 - 100 \text{ g.m}^{-3}$ ) the average aerodynamic diameters observed were quite high, viz. several  $\mu\text{m}$ . The observed decay curves were non-exponential with decay rates slowing down as time proceeds. The  $\text{U}_3\text{O}_8$  aerosols having lower initial mass concentrations showed a nearly exponential decay after an initially accelerated decay. In case of the sodium smoke experiments a considerable temperature rise inside the vessels has been observed. The high mass concentrations as well as the additional thermal effects considerably complicate the interpretation of the experimental results of Atomics International. Nevertheless, they have developed a computer programme (code HAA-3) which allows the calculation of the time-dependent aerosol concentration in a closed vessel. Coagulation, stirred gravitational settling and diffusive deposition are taken into account [28]. The computed concentrations are in reasonable agreement with the experimental values [29]. Further improvements of the HAA-3 code have been reported [30].

In the same years, R.J. Davis of Oak Ridge National Laboratory has developed a special model for the estimation of aerosol concentration in a closed vessel [31]. He assumed a power-function type particle size distribution (comparable to the Junge-distribution) to be present, after coagulation within a certain size region has ceased. Then, Davis derived a concentration-time relation which he regards to be in fair agreement with the above mentioned experimental results obtained by Atomics International. Stirred settling was the only deposition process taken into account.

More recently, one of the largest nuclear aerosol projects commenced at Oak Ridge National Laboratory (USA), the ART-project (Aerosol Release and Transport). In the first stage of the ART-project main efforts are in the area of aerosol formation rate under hypothetical accident conditions. Later on, greater attention will be given to aerosol behaviour inside containments. The first preliminary results on this are available [32]. At Brookhaven National Laboratory, Castleman Jr. et al. have also carried out aerosol research which was mainly theoretical. They have solved an equation expressing the processes in high number density aerosols subject to both Brownian motion and stirred gravitational settling in a closed system [33]. Lindauer and Castleman [33] have calculated for such large initial number concentrations that after a short time an enclosed aerosol shows a lognormal size distribution with a geometric standard deviation of 1.37 irrespective of its original properties. Calculations and their sparse experimental results compare very well [34]. Schikarski's research group (Karlsruhe,FRG) has investigated enclosed aerosols of  $UO_2$  produced by the Exploding Wire technique. The German primary effort has been in development of a versatile computer programme. The most recent version of their code PARDISEKO deals with coagulation and a number of stirred deposition mechanisms (gravitational, thermophoretic and diffusive) [35]. From a number of experiments the Germans concluded that thermophoretic deposition is a dominating removal process under sodium fire circumstances [36]. This conclusion sheds controversial light on the above mentioned fit between the HAA-3 code (without thermophoresis) and the Atomic International sodium smoke results. A problem related to PARDISEKO as well as to similar codes is the use of shape factors for non-spherical particles which factors should correct for the shape dependence of coagulation and phoretic processes. In practice, time independent and empirical factors are applied which makes the validation of the codes by fit with experiment rather unreliable. In accordance with the nature of these codes (safety application) usually the aerosol concentrations are overpredicted. At Battelle's Columbus Laboratories a versatile code (HAARM-3) has been developed which represents the most recent modification of the original HAA-3 code (see above). It provides a more physically realistic modelling of the nuclear conditions it is applicable to. Treated are various types of coagulation and stirred deposition (settling, diffusion



and thermophoresis). Reasonable fit with experimental data from elsewhere is shown [37]. No experiments on enclosed aerosols have been performed at Battelle Columbus.

At Japan Atomic Energy Research Institute, aerosol codes have been developed. Also experiments on enclosed aerosols have been performed. The code (ABC) models coagulation, settling, diffusion and thermophoresis in all cases for well-stirred aerosols [38]. Significant problems were met in fitting the ABC-code with experimental data particularly those on sodium smoke aerosols. Good fit was obtained for data from specially designed experiments where thermophoresis should be the dominating process. In France a large experimental programme has been executed using large-scale spaces (several 1000 m<sup>3</sup>) almost exclusively using sodium fire aerosols.

### 1.3.3. Smog chamber studies

In view of the very high mass concentrations generally involved in the above listed nuclear oriented investigations, this research is only of limited interest here. Much lower mass concentrations are used in so-called smog chamber studies where gaseous contaminants in filtered or unfiltered ambient air are exposed to near-UV light. Some investigators interested in aerosol production in these systems have given attention to the fate of the particles produced in smog chambers. Miller [39], in a study of sulphate particulate formation in irradiated SO<sub>2</sub>/air mixtures, recognised the importance of wall losses of these particles in his 200-liter chamber. He has shown that for unfiltered air no important wall losses occur. However, this observation applies to the dark (unirradiated) conditions only, which could be different from the irradiated conditions. Miller expects important loss rates due to diffusion for the SO<sub>2</sub>/unfiltered air system due to the small nuclei formed in that case. McMurtry in his thesis [40], which is based mainly on aerosol investigations using a 65-m<sup>3</sup> air-filled teflon bag placed on a laboratory roof, also considers the error in his smog chamber data from wall losses. He regards inertial and gravitational removal to govern loss of large particles. However, the given results from experiments using e.g. 1 µm particles (70% per hour removal) are far too high for being explainable by gravitational deposition whereas inertial deposition in the non-stirred bag seems very unlikely for 1 µm particles. Probably

effects due to electrostatic charges at the teflon walls or photophoresis or thermophoresis have played a role. Another study deals with the same problem (Zalabsky [4]) as that of Miller (see above). Zalabsky has made a special study of the decay rates of platinum hot-wire aerosol and  $H_2SO_4$  aerosol (about  $0.03 \mu m$  diameter) in his 24-liter reactor. He concludes that a limited stirring (partial homogenisation of the atmosphere) could explain the results. However, there is no need to use this explanation. The observed decay curves are exponential and it can be shown that stirred diffusion to the reactor walls with a stagnant boundary layer of  $0.5 \text{ mm}$  thickness explains the observations fairly well. Zalabsky's diffusion coefficients probably are incorrect in view of the small half-life of the aerosol (27 min) which leads to a rather large boundary layer thickness  $\delta$  compared to the  $\delta$  value which can be calculated using Eq. (15) derived later on.

In a later stage (see pg. 106) the observations made by McMurry and Zalabsky will be discussed in the framework of stirred electrophoretic deposition onto the aerosol chamber walls. A picture reasonably coherent with other observations on electrophoretic deposition can be obtained.

#### 1.3.4. Summary

In summary, literature shows two or three disciplines active in the field of enclosed aerosols. In early periods of attention to this subject, the meteorologists extensively investigated the decay of nuclei in enclosures. The initial view of "stirred deposition" has been left by Pollack who assumed "non-stirred deposition" on the basis of his diffusion box observations ("dynamic method"). The critique on Pollack's "dynamic method" did not lead to reconsidering the stirred deposition model. In the nuclear safety efforts since the mid-sixties, the importance of the stirred deposition model has been recognized again. However, the attention is focussed on high mass concentrations and related processes which are not relevant to air pollution. Furthermore, the main objective of these studies is to derive merely conservative estimates of aerosol concentrations. Only on a few occasions qualitative investigations are made of the wall effects on aerosol behaviour in smog chambers.

#### 1.4. Objectives

In view of the incoherent picture of the behaviour of aerosols inside enclosures as obtained from a literature search, it is scientifically worthwhile to improve the knowledge on enclosed aerosols. It is also desirable to have a general model for aerosol removal inside enclosures allowing a mutual comparison of the various removal mechanisms responsible for the instability of enclosed aerosols. As set forth in section 1.1. (pg. 15), this knowledge can be used either to predict the behaviour of known aerosols inside enclosures in use for various purpose or to characterize an unknown aerosol aerodynamically.

## 2. THEORY

### 2.1. Coagulation

Aerosols formed at a considerable number concentrations inevitably will show significant coagulation during an initial period. The particles subject to deposition are formed and shaped by the coagulation which constitutes in this way an important pre-stage to the final deposition period. Coagulation, being a two-particle process, will decrease relatively quickly compared to the deposition processes which have first-order kinetics.

Kennedy [11] has observed that nuclei in a closed vessel disappear according to a second order process. The relationship was found to exist over a range of concentrations from  $8 \times 10^5$  to  $7 \times 10^4 \text{ cm}^{-3}$ . For lower concentrations the decay rate appeared to be faster which was attributed to some additional deposition process being of the first order and hence showing an increasing relative importance [13].

Coagulation of particles of equal size has been treated extensively by Von Smoluchowski [42a]. The decay of the particle number concentration  $c_n$  is described by

$$\frac{dc_n}{dt} = -Kc_n^2 \quad (1)$$

where K is the coagulation constant.

This equation can be integrated

$$\frac{1}{c_n} - \frac{1}{c_n(o)} = Kt \quad \text{or:} \quad c_n(t) = \frac{c_n(o)}{Ktc_n(o) + 1} \quad (2)$$

The general expression for the coagulation of a polydisperse aerosol has been given by Müller [42b]. The solution of the general equation has been obtained by Zebel [43] and also Spiegler [44], assuming the particles to be spherical droplets. This assumption has the advantage that coagulation of two particles yields a new one having a defined diameter. This is, however, far from reality for our case of condensation aerosols of branched chain-like coagulates (fig. 1). This lack of realism has been recognized by the Atomic International Group when it observed the bad fit between their HAA-3 code and the

experimental results on condensation aerosols [30].

From experiments, however, it may be concluded that the coagulation constant of an aging aerosol can be considered to be constant and slightly larger than  $10^{-9} \text{ cm}^3 \cdot \text{s}^{-1}$ . This has been explained by the compensating effects on  $K$  of the changes of particle size and dispersity of the size distribution [45].

Some investigators state that electrical charges on the aerosol particles can affect the rate of coagulation considerably [46, 47]. However, Gillespie's results [46] apply to particles having relatively high charges and, moreover, are not convincing in view of the large scatter in the results. Rosinski [47] dealing with highly radioactive aerosols presents data which are difficult to interpret and the effects observed relate only faintly to electrical influences on coagulation rates. Zebel [45] has given a treatment of electrical effects on coagulation.

## 2.2. Deposition of enclosed aerosols

### 2.2.1. General

Temperature differences between the walls and the atmosphere of an enclosure give rise to free convection flows inside. These flows can be calculated with the aid of the Prandtl relation [48, 49] for the vertical flow which develops at a heated wall, when an effective wall is assigned to the enclosure. It has been shown by Watson, Perez and Fontana [50] that the convective flows increase with increasing tank dimensions at a given temperature difference between gas and walls. This can also be deduced from the Prandtl relation (see Eq. (55), [48]). In practice free convection is always present inside a vessel due to temperature gradients induced by the environment. Application of thorough cooling of the lower vessel part can suppress unintentional convection. It has been shown by Fuchs [49] that a temperature difference of the order of  $0.01 \text{ }^\circ\text{C}$  in an enclosure with an effective wall length of one meter is capable of keeping an aerosol consisting of particles smaller than  $10 \text{ }\mu\text{m}$  homogeneously distributed inside the enclosure. This state of homogeneous aerosol distribution which generally occurs, is usually called "stirred". In some cases intentional or unintentional local heating of the enclosure may be present. Evidently, the magnitude of the convective flow will be larger in case

the enclosure is heated from below.

As mentioned above non-stirred circumstances are abnormal. The occurrence of non-stirred deposition is dealt with in a separate section (2.5) of this chapter.

The deposition on the walls is only possible when the particles penetrate into the stagnant boundary layer ( $> 1$  mm) in contact with the walls. Since the stopping distance of aerosol particles in a system with flow velocities of about  $10 \text{ cm.s}^{-1}$  is in the range of  $10^{-5} \mu\text{m}$  to  $100 \mu\text{m}$ , the aerosol particles can reach the walls only with the aid of additional mechanisms like gravitational settling, diffusion, thermophoresis, etc. Gravitational deposition will occur through this layer near upward facing horizontal surfaces. Deposition due to Brownian diffusion is active through the boundary layer towards the whole internal surface of the enclosure. Deposition in non-isothermal cases takes place through the boundary layer near the cold walls.

The number of particles  $\Delta n$  deposited during a time period  $\Delta t$  through the stagnant layer onto area  $S$  at a deposition velocity  $v$  is related to the particle number concentration  $c_n$  by

$$\Delta n = - v S c_n \Delta t \quad (3)$$

For a containment volume  $V$ ,  $c_n = \frac{n}{V}$ ,  $n$  being the total number of aerosol particles contained in the vessel. Now, (3) may be rearranged into

$$\frac{d c_n}{dt} = - v \frac{S}{V} c_n \quad (4)$$

When  $v$  is time independent, which is the case for a monodisperse aerosol in which no coagulation takes place, (4) may be solved:

$$c_n = c_n(o) \exp(- \beta t) \quad (5)$$

This is an exponential decay with a decay constant  $\beta$  equal to  $\frac{S}{Vv}$ . In case of a monodisperse aerosol the deposition velocity is equal to the terminal velocity which each particle attains due to the force causing deposition. Hence, according to the definition of the mobility  $\mu$  of a particle the deposition velocity is related to the

deposition force  $U$  by

$$\mu = \frac{\text{terminal velocity of particle}}{\text{force causing translation}} = \frac{v}{U} \quad (6)$$

The mobility  $\mu$  of an aerosol particle is dependent on particle size and shape, and on the viscosity of the gaseous medium in which it is suspended. The equation for spherical particles due to Knudsen and Weber [51] and Millikan [52] is generally accepted:

$$\mu = \frac{F(d)}{3 \pi \eta d} \quad (7)$$

$d$  = particle diameter,

$\eta$  = viscosity of the medium in which the particle moves

( $\eta$  of air of STP =  $1.83 \times 10^{-4}$  poise),

and

$$F(d) = 1 + \frac{1.66 \times 10^{-5}}{d} + \frac{5.3 \times 10^{-6}}{d} \exp(-8.33 \times 10^4 d) \quad (8)$$

with  $d$  expressed in cm.

The empirical factor  $F(d)$  (see e.g. [53]) is called slip factor. It is near unity for particles larger than a few  $\mu\text{m}$  diameter but increases strongly with decreasing particle size. For particle diameters smaller than the mean free path of the molecules,  $F(d)$  is inversely proportional to  $d$ ,  $F(d) \times d$  amounting to about 0.23 ( $d$  in  $\mu\text{m}$ ).

The mobility is a basic property of a particle since it describes its behaviour due to an external force, as a rule irrespective of the nature of the force (gravity, electrical force, thermal force, etc.). In case of nonspherical particles, however, the mobility depends on the orientation and on the nature of the force. When a nonspherical particle carrying a dipole is subjected to an electrical force, its mobility depends also on the orientation of the dipole. The same is true for inertial forces where the dynamic shape factor  $\kappa$  is orientation dependent.

Substitution of (7) into (6) yields, for spherical particles,

$$v = \mu \times U = \frac{F(d)U}{3 \pi \eta d} \quad (9)$$

In the following sections various deposition processes of stirred aerosols are dealt with.

### 2.2.2. Stirred diffusive deposition

Deposition by Brownian motion of an aerosol homogeneously distributed inside a container takes place through a boundary layer at the walls. The driving force for this transport is the concentration gradient across this boundary layer. At the walls the particle number concentration is taken zero since all particles reaching the wall are assumed to stick to it and not to be resuspended. At the inner side of the boundary layer the concentration equals the concentration of the homogeneously filled containment. Fick's law describes the diffusion of particles due to a concentration gradient  $\frac{dc_n}{dx}$

$$- \frac{dn}{dt} = DS \frac{dc_n}{dx} \quad (10)$$

where  $D$  = the diffusion coefficient of the particles in the gaseous medium. Eq. (10) may be rewritten as

$$- \frac{dc_n}{dt} = \frac{D S}{\delta V} c_n \quad (11)$$

for an aerosol in an enclosure of volume  $V$ , total surface area  $S$  and with a thickness  $\delta$  of the concentration boundary layer. The introduction of  $\delta$  as an effective boundary layer thickness is a necessary simplification which implies a linear concentration gradient near the walls. The coefficient of diffusion  $D$  of a particle is related to the mobility  $\mu$  of the particle as follows (Einstein [54])

$$\mu = \frac{D}{kT} \quad (12)$$

where:

$k$  = Boltzmann constant

$T$  = Kelvin temperature.

Substitution of equation (7) into (12) yields the size dependence of the diffusion coefficient:



$$D = \frac{kT}{3\pi\eta d} F(d) \quad (13)$$

For coarse particles ( $> 1 \mu\text{m}$ )  $D$  is inversely proportional to particle diameter ( $F(d) \approx 1$ ); nuclei ( $< 0,05 \mu\text{m}$ ) have  $D$ -values inversely proportional to  $d^2$ .

$\delta$  has been defined by Fuchs [55] as the distance from the wall at which the coefficients of molecular and convective diffusion are equal.

At the edge of the boundary layer the particle flux  $I$  due to convection equals the rate of deposition:

$$I = \frac{Dc}{\delta} n \quad (14)$$

According to Fuchs [55],  $\delta$  depends not only on the intensity of convection but also on  $D$ . Since  $D$  is size dependent, it follows that  $\delta$  will be a function of particle size too. This cannot be treated exactly, but some indications on the relation between  $D$  and  $\delta$  can be obtained from the discussions of Fuchs on this subject [55]. Fuchs explains that when  $D$  decreases, turbulent fluctuations carry the particles closer to the wall and in so doing partly compensate for the small value of  $D$ . He obtains a  $D^{\frac{1}{2}}$  dependence of  $\delta$ , where the exponent may be even smaller in reality.

In conclusion,  $\delta$  will be largely independent of the particle size of the enclosed aerosol. This is in agreement with the general approach of various authors. Fuchs [55] calculated  $\delta$ -values of  $5 \times 10^{-4}$  mm and 0.02 mm, from experiments by Shifrin [56] and Gillespie [57], respectively. Castleman [34] referring to Fuchs, assumed the thickness  $\delta$  to be 0.02 mm. Greenfield [29] obtained  $\delta = 10^{-3}$  mm from his experimental data. These  $\delta$ -values, however, are all very small (though obtained for comparable aerosols) compared to the values found by Nolan [58] and the author [59], viz.  $\delta$ -values of the order of 1 mm. Very likely, the small  $\delta$ -values are due to erroneous interpretation of measurement data. Often, incorrectly, deposition due to thermophoresis or by electrophoresis has been attributed to diffusion deposition.

Since gas molecules can classically be treated as particles, the applicability of Fuchs'  $\delta$ -model can be tested for the extremes of the range of  $10^{-4}$   $\mu\text{m}$  (molecules) to 0.1  $\mu\text{m}$  (aerosol particles). Eq. (13)

relates the diffusion coefficient  $D$  to particle diameter  $d$ . From experimental data by Cox et al. [60] on the decay of concentrations of  $SO_2$  in a vessel, one may deduce a  $\delta$  value of 2.5 cm. In addition, for water vapour diffusing from a pool into an air-filled vessel a  $\delta$  value of 3.5 cm has been found [61]. Nolan [58] using "atmospheric or room air" in a 330 litres vessel obtained a  $\delta$ -value of 0.23 cm and simultaneously estimated the average diffusion coefficient to be  $1.2 \times 10^{-5} \text{ cm}^2 \cdot \text{s}^{-1}$ . Mercer and Tillery [62] using "room air" containing particles of  $D \approx 1.3 \times 10^{-4} \text{ cm}^2 \cdot \text{s}^{-1}$  ( $d = 0.02 \mu\text{m}$ ) give experimental data on wall losses from which a  $\delta$  value of 0.6 cm can be deduced. Rooker and Davies [63] calculated  $\delta$  equal to 0.4 cm for  $\text{CaCO}_3$  nuclei of  $D = 2.2 \times 10^{-6} \text{ cm}^2 \cdot \text{s}^{-1}$ . Finally, in section 4.6.4 of this study the diffusion deposition of  $0.06 \mu\text{m}$  NaCl particles is found to take place across a boundary layer of  $\delta = 0.26$  cm. Table I\* lists the  $\delta$ -values together with the corresponding diameters  $d$  and the diffusion coefficients  $D$  of the "particles" (gas molecules are also treated as particles). Power curve fitting of these data yields

$$\delta = 4.6 D^{0.265} \quad (15)$$

with a coefficient of correlation  $r$  of 0.98 ( $n=6$ ). One can conclude that Fuchs' model (predicting the exponent of  $D$  equal to 0.25), is not far from correct. For vessels of volume  $V$  and internal wall surface area  $S$  the half-life  $t_{\frac{1}{2}}$  of aerosols disappearing by diffusion losses can be calculated, using Eqs. (15) and (16), from  $t_{\frac{1}{2}} = 0.693 \frac{\delta V}{D S} = 53 D^{-0.735}$  for a  $1 \text{ m}^3$  square box. The half-lives for particles of  $0.01 \mu\text{m}$  and  $0.1 \mu\text{m}$  are about 4 and 90 hours, respectively. These half-lives are relatively large compared to those pertaining to other processes in smog chambers where the photochemically produced nuclei "disappear" by coagulation rather quickly (1 hour half-life for  $c_n \approx 10^5 \text{ cm}^{-3}$ ). Only for low mass production rates and when sufficient aging has taken place (resulting in small particle sizes and concentrations) one may expect removal due to diffusive deposition which then can be significant prior to important particle growth due to coagulation.

The value of  $\delta$  will not be very different for various tanks since the unintentional temperature gradients will not deviate much from case to case. Furthermore the Prandtl relation shows that the free convection

\* Tables can be found on page 152 and following.

flow is only proportional to the square root of the product of the temperature difference and the total wall length (Eq. (55), [48]). When the disappearance of a monodisperse aerosol is governed by stirred diffusive deposition an exponential decay will be observed. The deposition velocity  $v_d$  equals the ratio of  $D$  to  $\delta$ , which remains unchanged during the aerosol life. Hence, by integration of (10) the general equation (5) may be obtained with a decay constant

$$\beta_d = \frac{D}{\delta} \times \frac{S}{V} \quad (16)$$

When a polydisperse aerosol decays due to stirred diffusion the coarse particles will be deposited more slowly than the fine particles since  $D$  is smaller for larger particle sizes. The decay curve of such an aerosol will show a decreasing "decay constant". The same phenomenon will be shown by a coagulating aerosol, however.

### 2.2.3. Stirred gravitational deposition

In case of stirred gravitational deposition the force  $U$  causing the deposition of the aerosol is the weight of the aerosol particles. Substitution of  $U = \frac{1}{6} \pi \rho d^3 g$  ( $\rho$  = particle density;  $g$  = gravitational acceleration) in (9) yields the Stokes settling velocity for spherical particles

$$v_s = \frac{\rho g}{18 \eta} d^2 F(d) \quad (17)$$

The use of  $\rho$  instead of the difference between the densities of particle and gas implies negligible buoyancy. According to equation (5) a monodisperse aerosol will decay exponentially with a decay constant.

$$\beta_s = v_s \frac{S_f}{V} \quad (18)$$

with  $S_f$  being the projected area of the containment floor. For simple vertical vessels  $\frac{V}{S_f}$  can be replaced by the height of the vessel.

When a polydisperse aerosol decays due to stirred gravitational deposition its size distribution will change since the coarser particles will settle preferentially leading to a decreasing average diameter. When deposition is only due to settling the average deposition velocity

decreases and consequently the aerosol stability increases. Conditions of non-stirred settling are discussed in section 2.5.

#### 2.2.4. Stirred thermophoretic deposition

In a temperature gradient a particle is subjected to a force which is called the thermophoretic force. This force,  $U_{th}$ , is proportional to the temperature gradient  $\frac{dT}{dx}$  according to Einstein [64] and Epstein [65]

$$U_{th} = A_{th} \times \frac{dT}{dx} \quad (19)$$

Using relation (6) between force  $U_{th}$ , velocity  $v_{th}$  and mobility  $\mu$ , one obtains after substitution of (7) that the thermophoretic velocity  $v_{th}$  is also proportional to the temperature gradient

$$v_{th} = \alpha \times \frac{dT}{dx} \quad (20)$$

$\alpha$  is a particle-size dependent proportionality constant which will be discussed later on. Measurements [66, 67, 68] of the thermophoretic velocity as a function of the temperature gradient have shown the correctness of (20), the value of  $\alpha$  being of almost identical magnitude regardless of particle material, e.g. its thermal conductivity.

There are various distinct theoretical treatments of the thermophoretic effect. The major part of the theories is based on the short treatment by Einstein [64]. The thermal force is considered to be the net result of the impulses in the direction of the temperature gradient imparted to the particle by impinging gas molecules.

When the particle is small compared to the mean free path ( $l$ ) of the gas molecules the problem is essentially that of thermal diffusion of a two-component gaseous system where one component has a negligible size. In case of small Knudsen numbers (particle radius  $r$  larger than the mean free path  $l$ ,  $Kn = \frac{l}{r}$ ) the temperature distribution inside the particle and the various effects of the particle on the surrounding gas have to be taken into account as was done e.g. by Epstein [65].

Then the thermophoretic force originates from "thermal creep" of gas molecules along the unevenly heated particle surface. In that case the thermophoretic force mainly arises from that part of the particle

surface where the thermal gradient along the surface is largest, viz. the "sides" of the moving particle. Clearly, in this model the heat transfer through the particle itself will play an important role in the thermophoresis of larger particles.

After Epstein's treatment the complexity of the derived relations further increased since observations have shown that any influence of thermal conductivity of the aerosol particles is absent [66, 69]. Several constants associated with the temperature jump and the thermal slip at the particle surface had to be postulated in order to fit theory and experiment [67, 69, 70].

On the other side Stetter argues that these theoretical treatments are incorrect because they are based on speculative concepts concerning thermal creep, pressure unbalance and on the unknown physical properties of colloidal matter [71]. Stetter explains [72] that thermophoresis is not caused directly by the temperature gradients themselves but via the concentration gradients in the gas due to the temperature gradients. The concentration gradients give rise to self-diffusion of the gas molecules which in a closed space must be compensated by a hydrodynamic Stefan back flow ("Rückstrom") in order to preserve pressure equilibrium. This is further illustrated by figures 2 and 3.

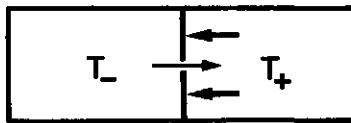


Fig. 2. Thermophoresis in a closed space with movable wall and hole simulating an aerosol particle.  $T_-$  and  $T_+$  are cold and warm parts. Due to the temperature dependent molecular concentration and velocity a diffusion flow arises through the hole from the cold to the warm part. The resulting pressure difference causes a translation of the wall to the left, being thermophoresis. The driving force is only due to pressure: diffusing molecules exert no force on the wall (Stetter [50]).

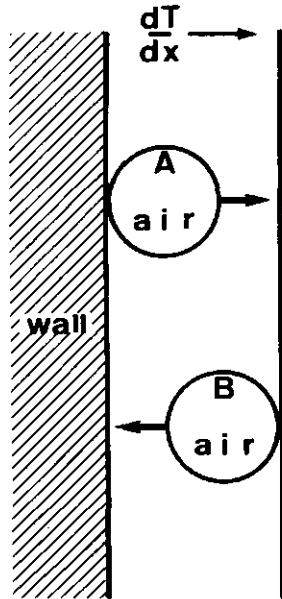


Fig. 3. Mass flows related to thermophoresis in a boundary layer at a cold wall. The temperature gradient  $\frac{dT}{dx}$  causes a diffusion air flow A to the warm gas atmosphere. Due to the induced pressure difference an air flow B results which pushes aerosol particles forward to the cold wall.

This backflow from hot to cold drags the aerosol particles with a velocity [72]

$$v_{th} = \frac{D_g}{c_g} \times \frac{dc_g}{dx} \quad (21)$$

where  $D_g$  is the diffusion coefficient of the gas molecules,  $c_g$  the number concentration of gas molecules, and  $\frac{dc_g}{dx}$  the gradient of this concentration due to the temperature field. Since  $c_g$  is inversely proportional to temperature T equation (21) can be rewritten

$$v_{th} = \frac{D}{T} \frac{g}{dx} \frac{dT}{dx} \quad (22)$$

According to Stetter [72] a factor  $\frac{1}{n_{th}}$  must be introduced in (22) for the different interactions (expressed by  $n_{th}$ ) of various gas molecules with the particle surface. This leads to

$$v_{th} = \frac{D}{n_{th} T} \times \frac{dT}{dx} \quad (23)$$

which in combination with (20) leads to  $\alpha = \frac{D}{n_{th} T}$ .

In fact the proportionality constant  $A_{th}$  (in Eq. (19)) between the thermophoretic force  $U_{th}$  on a particle and the temperature gradient  $\frac{dT}{dx}$ , can be expressed now as

$$A_{th} = \frac{k}{n_{th}} \frac{D}{D} \frac{g}{D} \quad (19a)$$

which summarises the relation between thermophoresis and the properties of the particle and of the gas.

Small particles ( $r < \lambda$ ) have  $n_{th} = 2$  if the gas molecules can be treated as rigid spheres. In the case of air, however,  $n_{th} \approx 3$  [72]. For  $r > \lambda$ ,  $v_{th}$  decreases to  $\frac{2}{5}$  of the small particle value and hence for air  $n_{th} \approx 8$ . Large particles have a relatively small effective size since the force from the back flow is limited to a boundary region of the particle surface with a thickness of the order of the mean free path in the gas phase. The remaining part of the particle surface plays no role in thermophoresis since there is no corresponding back flow in this region.

Comparing the two theories on thermophoresis in the light of the experimental results, it can be established that in the small particle region ( $Kn > 1$ ) there is good agreement between experiment and the theories of e.g. Brock [69], Waldmann [70] and Stetter [71]. The experimentally found reduced thermophoretic velocity of large particles ( $Kn < 1$ ) is quantitatively explained by Stetter [71], though Stetter uses  $n_{th}$ -values which are empirical. All theories based on Einstein's approach [64, 65, 66, 69, 70] lead to relations which either are in disagreement with observations or include accommodation constants for the particular gas-surface system which are obtained from fitting theory

and experiment for high thermal conductivity aerosols [71]. To complicate the problem, it must be remarked that Bokanov and Derjaguin [73] have shown that the thermal slip is much smaller than assumed by e.g. Brock [69]. This is also shown for diffusion slip by Whitmore [74]. To date no satisfactory theory exists that deals with the thermophoretic force in the intermediate size range  $r \approx l$ . Rotation of the particles is an aspect which has not been taken into account in either of the theories. A much smaller thermophoresis may result from the theories based on thermal slip when the Brownian rotation lowers the temperature gradient in the particle due to insufficient thermal coupling between the rotating particle and the surrounding gaseous medium.

When an enclosed aerosol is subjected to thermophoretic deposition the corresponding decay constant  $\beta_{th}$  is given by

$$\beta_{th} = \alpha \times \frac{dT}{dx} \times \frac{S_{th}}{V} \quad (24)$$

which is the combination of the Eqs. (4) and (20), and where  $S_{th}$  equals the surface area of the "cold" walls (the heat sink) and  $\alpha = \frac{D_g}{n_{th}T}$  as in (23).

The heat transfer can be related to aerosol mass transport by substitution of Newton's law of cooling

$$\frac{dT}{dx} = \frac{Q}{\lambda_g S_{th}} \quad (25)$$

which leads to

$$\beta_{th} = \frac{\alpha}{\lambda_g} \frac{Q}{V} \quad (26)$$

( $\lambda_g$  = thermal conductivity of the gas phase and  $Q$  = thermal power transferred by the enclosed gas).

According to Stetter (apart from  $n_{th}$ ) the factor  $\alpha$  is a parameter of the gas only ( $\alpha = \frac{D_g}{n_{th}T}$ , see Eq. (23)). Therefore, this must apply to  $\frac{\alpha}{\lambda_g}$  too. It can also be shown that  $\frac{\alpha}{\lambda_g}$  is independent of temperature. Gas kinetics theory [75] gives a proportionality between  $D_g$  and  $l\bar{v}_g$  and also a proportionality between  $\lambda_g$  and  $\rho_g \bar{v}_g l c_v$  where  $\bar{v}_g$  is the



average velocity of the gas molecules and  $c_v$  is the specific heat capacity (heat capacity per unit mass). Consequently,  $\frac{\alpha}{\lambda_g}$  ( $= \frac{D_g}{n_{th} \lambda_g T}$ ) is proportional to  $(n_{th} \rho_g c_v T)^{-1}$  in which  $n$ ,  $c_v$  and  $\rho T$  are all temperature-independent parameters. Taking  $n_{th} = 8$  for large particles in air,  $\frac{\alpha}{\lambda_g}$  amounts to  $0.3 \text{ cm}^3 \cdot \text{J}^{-1}$ .

In order to allow comparison between our experimental results and the values which can be derived from various theories on thermophoresis, the observed decay constants  $\beta$  are transformed to dimensionless constant  $B$  defined by Eq. (24) and

$$v_{th} = B \frac{\eta}{\rho_g T} \frac{dT}{dx} \quad (27)$$

The proportionality factor  $B \frac{\eta}{\rho_g T D_g}$  has been denoted  $\alpha$  in Eq. (20) which according to Stetter equals  $\frac{D_g}{n_{th} T}$  (Eq. (23)). Since the Schmidt number ( $\equiv \frac{\eta}{D_g \rho_g}$ ) is near unity for gases [55] (theoretically 0.83 for gas molecules of rigid spheres [75]), then  $D_g = \frac{\eta}{\rho_g}$ . Therefore, we can define a constant  $B_S$  (in 27) for Stetter's model by

$$B_S = \frac{1}{n_{th}} \quad (28a)$$

The following B-values apply to the relations derived by Epstein, Brock and Derjaguin:

$$B_E = \frac{3}{2} \frac{\lambda_g}{2\lambda_g + \lambda_p} \quad (28b)$$

$$B_B = \frac{3}{2} \frac{\lambda_g + c_t \lambda_p \text{Kn}}{2\lambda_g + \lambda_p + 2c_t \lambda_p \text{Kn}} \times \frac{1}{1 + 2c_m \text{Kn}} \quad (28c)$$

$$B_D = 2 B_B \quad (28d)$$

with:  $\text{Kn} = \text{Knudsen number} = \frac{2Z}{d}$

$c_t$  and  $c_m$  the thermal jump and isothermal slip coefficients  
2.16 and 1.23, resp. ([69]),

$\lambda_g$  and  $\lambda_p$  the thermal conductivities of carrier gas and particle,  
respectively.

The formulae of Brock and Derjaguin differ by a factor of two.

Epstein's relation has a strong dependence on  $\lambda_p$  for large  $\lambda_p$ -values in contrast to  $B_B$  and  $B_D$ , which are almost independent of  $\lambda_p$ . The experimental value  $B_m$ , which is to be compared with these theoretical values, may be obtained from the measured decay constant  $\beta_{th}$  of an aerosol in a heated aerosol vessel (Eq. (26)) by

$$B_m = \frac{V}{Q} \times \frac{\lambda_g T}{D_g} \times \beta_{th} \quad (29)$$

$\frac{\lambda_g T}{D_g}$  is a constant depending on the properties of the gas; for helium and nitrogen its values are 0.37 and 0.50 J.cm<sup>-3</sup>, respectively.

An important effect arises due to thermophoresis in an aerosol vessel with a heated floor. Particles which settle through the stagnant boundary layer at the floor experience a counter force due to the temperature gradient there. The critical diameter ( $d_{crit}$ ) of a particle that will float in this thermal boundary layer near the floor can be calculated as follows.

According to Newton's law of cooling the temperature gradient  $\frac{dT}{dx}$  which arises in the boundary layer of thermal conductivity  $\lambda_g$ , and the heat  $Q$  causing the T-gradient through a surface area  $S_f$  are related by equation (25):

$$Q = \lambda_g S_f \frac{dT}{dx}$$

A vertical temperature gradient  $\frac{dT}{dx}$  hampers settling of a particle due to a thermophoretic force (see Eqs. (6), (7), (20)).

$$U_{th} = \frac{v_{th}}{\mu} = \frac{3\pi\eta ad}{F(d)} \frac{dT}{dx} \quad (30)$$

In case of equilibrium between the gravitational and thermophoretic forces, with the particle suspended in the boundary layer,

$$d_{crit} = \left( \frac{18\eta a}{\rho_p \lambda_g F(d)} \times \frac{Q}{S_f} \right)^{\frac{1}{2}} = 10^{-3} \left( \frac{Q}{S_f \times F(d)} \right) \quad (31)$$

For  $\rho_p$  = particle density, here assumed to be 1 g.cm<sup>-3</sup>  
 $\eta$  = 10<sup>3</sup> cm.sec<sup>-2</sup>  
 $\frac{a}{\lambda_g}$  = 0.3 cm<sup>3</sup>.J<sup>-1</sup> (in case of air)  
 $\eta$  = 1.8 x 10<sup>-4</sup> poise (air)

One obtains  $d_{crit}$  in  $\mu m$  when  $\frac{Q}{S_f}$  is expressed in  $W.cm^{-2}$ .  
Fig. 4 gives  $d_{crit}$  as a function of the heat flux  $\frac{Q}{S_f}$  for the  $d_{crit}$  range of  $0.1 - 10 \mu m$ . A warm floor with a temperature of  $10 K$  higher than the aerosol above it dissipates roughly  $6 \times 10^{-3} W.cm^{-2}$ . The corresponding value of  $d_{crit}$  is about  $0.8 \mu m$ .

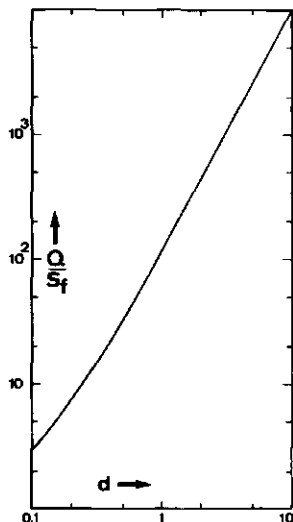


Fig. 4. Critical diameter  $d$  (in  $\mu m$ ) of a particle having unit density that will float in the boundary layer above a heated plate in air. Plate heat flux  $Q/S_f$  in  $W.m^{-2}$ .

#### 2.2.5. Stirred diffusiophoretic deposition

Diffusiophoresis is defined as the transport of aerosol particles due to the presence of a concentration gradient in the gas phase. This requires the gas to consist of two or more components. Waldmann [70] has treated the general case of a particle in a binary gas mixture of which the two components are counterdiffusing. Diffusiophoresis arises in a system with a component which evaporates and condenses this component diffuses through another, "stationary" non-condensing component. Goldsmith and May [76] have considered this case of an aerosol in condensing vapour as a superposition of the Stefan flow on the diffusion flows of the two components. According to Stetter [72], diffusing molecules exert no force on aerosol particles since at the moment of the collision the molecules are no longer diffusing (fig. 2). Hence, the

aerosol particles will obtain a velocity in the direction of the diffusing species merely due to and equal to the Stefan backflow (fig. 5) which is governed by (see also Eq. (21))

$$v_{\text{diff}} = - \frac{D_2}{c_1} \frac{dc_1}{dx} \quad (32)$$

where  $D_2$  is the diffusion coefficient of the diffusing component and  $c_1$  is the gas concentration. According to the predictions of Stetter [72] for the analogous case of thermophoresis,  $v_{\text{diff}}$  decreases with increasing particle size in the range  $\frac{r}{\lambda} \approx 1$  ( $Kn \approx 1$ ).

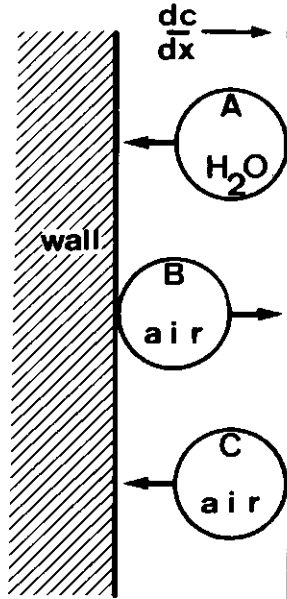


Fig. 5. Mass flows related to diffusiophoresis in a boundary layer at a cold wall on which water condenses. The concentration gradients of water vapour and air cause mass diffusion flows A and B, resp. The pressure difference due to flow B gives rise to an air counter flow C which drags aerosol particles to the blurring wall.

The size dependence in this range found experimentally by Schmitt [68] and Derjaguin [77] is in qualitative agreement with this.

In (32)  $c_1$  may be replaced by the gas pressure  $p_1$ . Since also  $\frac{dp_2}{dx} = -\frac{dp_1}{dx}$  we may write

$$v_{\text{diff}} = \frac{D_2}{p_1} \frac{dp_2}{dx} \quad (33)$$

where:  $p_2$  = particle pressure of the second diffusing vapour component.

For not too large partial pressures of the vapour component (which as a rule is the case at temperatures below the boiling point of the vapour component)  $p_1$  equals total pressure = 100 kPa.

For the water vapour-air system at s.t.p. studied by Goldsmith and May [76] equation (33) fits their results fairly well. Therefore, the conclusion of these investigators that they found excellent agreement with their modified Waldmann theory is no proof of the correctness of this theory, since Stefan flow dominated in their system.

The same applies to the experimental studies of Schmitt [68] and Derjaguin [77] since they also carried out their experiments at relatively small partial vapour pressures ( $p_1 \approx 100$  kPa).

In addition to this, experimental evidence is obtained by Whitmore and Meisen [74] that counter diffusion must not be taken into account. Hence, the above given argument of Stetter concerning the absence of a force on particles due to diffusing molecules is supported indirectly (see also fig. 2).

In the case of a partial pressure gradient of saturated vapour which is caused merely by heat flow with a corresponding temperature gradient  $\frac{dT}{dx}$ , equation (33) may be modified by means of the p-T relation of Clausius-Clapeyron

$$v_{\text{diff}} = \frac{p_2 D_2}{T^2} \times \frac{\Delta H_v}{R p_1} \times \frac{dT}{dx} \quad (34)$$

with  $\Delta H_v$  = latent heat of vaporisation of the second component.

As for stirred thermophoretic deposition - see Eqs. (24) through (26) - a decay constant  $\beta_{\text{diff}}$  may then be derived

$$\beta_{\text{diff}} = \frac{p_2 D_2}{\lambda_g T^2} \times \frac{\Delta H_v}{R p_1} \times \frac{Q}{V} \quad (35)$$

Here, implicitly, it is assumed that heat transfer is convective in the main vessel atmosphere but diffusive in the boundary layer at the walls. For the usual case of a heat flow conditioned vapour pressure gradient, thermophoresis and diffusiophoresis will occur simultaneously. Hence, a total aerosol decay will result with a decay constant

$$\begin{aligned} \beta_{\text{d+t}} = \beta_{\text{diff}} + \beta_{\text{th}} &= \left( \frac{p_2 D_2}{T^2} \times \frac{\Delta H_v}{R p_1} + \alpha \right) \frac{Q}{\lambda_g V} \\ &= \left( \frac{p_2 \Delta H_v}{RT p_1} + 1 \right) \frac{\alpha}{\lambda_g} \frac{Q}{V} \end{aligned} \quad (36)$$

When the temperature gradient  $\frac{\Delta T}{\Delta x}$  is increased (and consequently  $Q$  too)  $v_{\text{diff}}$  increases more than  $v_{\text{th}}$  due to the exponential temperature dependence of  $p_2$ . Above a certain value of  $\frac{\Delta T}{\Delta x}$  the deposition will be entirely due to diffusiophoresis. For a dynamic system this has been shown by Goldsmith and May [76]. In case of an aerosol tank with a water layer on the floor already at room temperature the two terms are nearly equal for aerosol particles larger than several tenths of a micron.

#### 2.2.6. Stirred photophoretic deposition

Photophoresis is defined as the transport of a particle due to light illumination of one side of the particle. Simplified one may regard photophoresis as a secondary effect which arises due to the heating of one side of the particle, inducing thermophoresis. Photophoresis can be negative or positive depending on the absorptive properties of the particle material. When the particle is partially transparent heating can be on the rear side of the particle resulting in a translation to the light source opposite to when the particle is strongly absorbent. Particles of reflecting materials do not show photophoresis. Tong [78] has made an extensive study of the materials dependence of photophoresis and he has measured also the effect using very large (1 to 10 mm) particles. Tong also has developed a theory on photophoresis starting from the older theories on thermophoresis like

Epstein's [65]. Unfortunately, Tong's derivation is not available. However, Tong's publication [78] gives a relation for the photophoretic force  $U_p$  of absorbing particles:

$$U_p = \frac{\pi n d}{5p} \frac{I \lambda_g}{2\lambda_g + \lambda_p} \quad (37)$$

where  $p$  = gas pressure and  $I$  = light flux. Using Eqs. (6) and (7), substitution in (37) gives for the photophoretic velocity  $v_p$

$$v_p = \frac{I}{15p} \frac{\lambda_g}{2\lambda_g + \lambda_p} F(d) \quad (38)$$

The factor  $\frac{\lambda_g}{2\lambda_g + \lambda_p}$  is typical for Epstein's model (see Eq. (28b)) which is generally considered to be incorrect. Also our findings contradict Epstein's theory and favour e.g. Stetter's model (pg. 113). Therefore we replace  $\frac{\lambda_g}{2\lambda_g + \lambda_p}$  (which is Epstein's constant  $B_E$  in Eq. (28b)) by  $\frac{1}{n_{th}}$  (which is Stetter's constant  $B_S$  in Eq. (28a)), yielding

$$v_p = \frac{2I}{45pn_{th}} F(d) \quad (39)$$

Now the decay of aerosol in a vessel due to illumination can be described by a decay constant

$$\beta_p = v_p \frac{S_p}{V} = \frac{2I}{45p n_{th}} \frac{S_p}{V} F(d) \quad (40)$$

$S_p$  is the surface area of the illuminated wall region.  $n_{th}$  usually amounts to 5 for particles of  $Kn < 1$  and is a measure of the interaction between the gas molecules surrounding the particle and the particle surface (pg. 38).

Photophoresis in the sunlit troposphere is due to a light flux of about  $0.1 \text{ W cm}^{-2}$  ( $\approx 10^2 \text{ cm.kPa.s}^{-1}$ ). Consequently, according to Eq. (39) the photophoretic velocity of aerosol in the troposphere is about  $0.01 \text{ cm. s}^{-1}$ . This is of the same order of magnitude as the (dry) deposition velocity on the soil of aerosol particles in the size range of  $0.1 - 1 \mu\text{m}$ . This means that e.g. the ubiquitous sulphate particles in the troposphere (which, when dry, are in this size range) may be deposited by photophoresis to a significant extent; 100% absorption by

sulphate particles is assumed which probably is not correct.

### 2.2.7. Stirred electrophoretic deposition

Aerosol particles carrying an electric charge are transported in an electric field. The resulting velocity  $v_e$  of electrophoretic movement is related to the strength  $E$  of the electric field and the electric particle mobility  $\mu_e$  by

$$v_e = \mu_e E \quad (41)$$

Since  $\mu = \frac{v}{U}$ , Eq. (6), and the force  $U_e$  exerted by the electric field on a particle with a charge  $q_p$  is given by

$$U_e = q_p E \quad (42)$$

it follows that

$$\mu_e = q_p \mu = q_p \frac{D}{kT} = q_p \frac{F(d)}{3\pi\eta d} \quad (43)$$

For particles of 0.03  $\mu\text{m}$  to 0.1  $\mu\text{m}$  diameter charged in Whitby's diffusion charger [79] the electrical mobility is in the range of  $10^{-3}$  to  $10^{-4} \text{ cm}^2 \cdot \text{V}^{-1} \cdot \text{s}^{-1}$ . Atmospheric particles and nuclei produced by combustion have average  $\mu_e$ -values up to  $3 \times 10^{-4} \text{ cm}^2 \cdot \text{V}^{-1} \cdot \text{s}^{-1}$  (e.g. [80] and [81]). When droplets of an aqueous solution or suspension are produced by nebulizing (pg. 63) these droplets carry charges. The particles resulting after evaporation will have 10 - 100 charges (predominantly positive). After neutralization (e.g. by exposure to <sup>85</sup>Kr radiation) the particles attain Boltzmann bipolar charge distribution (about 1 charge unit per particle of 0.4  $\mu\text{m}$ ). Then the  $\mu_e$ -value amounts to several  $10^{-4} \text{ cm}^2 \cdot \text{V}^{-1} \cdot \text{s}^{-1}$  [82].

Electrophoretic removal can be important in enclosures if the walls are electrically charged, i.e. the walls are made of high-resistivity material like plastic, or when the particles carry a large number of charges. In the past some attention has been given to electrophoretic wall deposition mainly in view of the undesirable aerosol instability in plastic aerosol chambers [80, 83, 84, 85]. Lieberman and Rosinski [83] considered the loss rate in a plastic chamber to be almost exclusively



due to stirred electrophoresis. The observed decay constants (about  $10^{-3} \text{ s}^{-1}$  in a 320-liters Lucite sphere), however, were not analyzed further. Stein et al. [80, 84, 85] in three publications in 1972 on the deposition of aerosols on charged polystyrene surfaces reports loss rates of 80% in a 20-minute period [84], the rates decreasing with increasing humidity [80]. It has also been shown that treatment of the enclosure walls with various antistatic agents can lead to almost complete elimination of electrophoretic deposition (less than a few % loss rate within 20 minutes). A model for stirred electrophoretic deposition, however, is not given. More recently, Yu [86] gave a comprehensive treatment of removal of unipolarly charged particles in vessels. Unfortunately, Yu assumed deposition from a stagnant atmosphere which is not realistic since (see below) electrophoretic deposition velocities are usually smaller than the convection velocities ( $> \text{several cm.s}^{-1}$ ) in enclosures.

Stirred electrophoretic aerosol deposition should be considered a process which (like other stirred deposition processes) is rate-limited in the stagnant boundary layer at the enclosure walls. This electrophoretic velocity in the boundary layer near the charge islands on the walls is proportional to the local electric field strength  $E$ , which is given by

$$E = \frac{q_e}{2\epsilon_o \epsilon_g S_e} = \frac{q_e}{2\epsilon S_e} \quad (44)$$

where:  $q_e$  = charge on the walls  
 $S_e$  = surface area charged  
 $\epsilon = \epsilon_o \epsilon_g$  = absolute dielectric constant of air  
 $(8.85 \times 10^{-16} \text{ C}^2 \cdot \text{cm}^{-2} \cdot \text{N}^{-1})$   
 $\epsilon_o$  = absolute dielectric constant of vacuum  
 $\epsilon_g$  = (relative) dielectric constant of air ( $\approx 1$ ).

Consequently, using Eqs. (4), (5), (41) and (44), an aerosol in an enclosure will decay due to electrophoresis with a decay constant  $\beta_e$  given by

$$\beta_e = v_e \frac{S_e}{V} = \mu_e \frac{S_e}{E \cdot V} = \frac{\mu_e q_e}{2\epsilon V} \quad (45)$$

Provided  $\mu_e$  and  $q_e$  remain constant, the electrophoretic decay will be exponential.

Usually, aerosol particles are bipolarly charged, the same being valid for the charge islands on the walls. Consequently, the deposition of particles of a certain polarity will take place only on those areas which have an opposite charge. Quantitative treatment of this different behaviour of particles of different polarities is difficult and requires exact knowledge of the aerosol charge distribution and the charging of the walls. The latter, however, at best is known only roughly as a rule; the walls have charge islands of the various polarities and of various sizes [80]. Therefore, we use a simplified quantitative approach defining an effective wall charge  $q_e$  which can be obtained by measuring the aerosol decay constant  $\beta_e$  and assuming a certain electrical mobility  $\mu_e$  of the aerosol. Electrophoretic decay can be non-exponential especially if the product  $\mu_e q_e$  has significantly different values for the polarities of the aerosol.

In general, electrophoretic deposition is undesirable. When aerosol chambers are used with walls of non-conductive materials like plastics and glass, proper actions should be taken to avoid electrophoretic removal to become important. To the author's experience treatment of the walls with a solution of any common laboratory detergent will effectively eliminate static surface charge under wet as well as dry conditions. As an indication of the care required it should be mentioned merely that simply rubbing the outside of a 20-liters perspex box containing a dense iron oxide fume resulted in clean-up of the box contents within a few seconds. This is quite reasonable in view of the possibility of charging plastic surfaces up to  $10^{-9} \text{ C.cm}^{-2}$  [87] which for an aerosol of  $\mu_e = 10^{-4} \text{ cm}^2 \cdot \text{V}^{-1} \cdot \text{s}^{-1}$  leads to half-lives of the order of 0.1 seconds in a vessel of this size.

Another type of electrophoretic deposition can prevail when the charged aerosol is enclosed in a vessel having conducting walls. Then, image charges are formed at the vessel walls which lead to Coulomb attraction of the aerosol particles too. This can be treated roughly as follows. We assume the same image charge  $q_p$  to be formed at the vessel wall by a particle carrying a charge  $q_p$  at a (small) distance of half the thickness  $\delta$  ( $\approx 1 \text{ mm}$  for  $0.1 \text{ }\mu\text{m}$  particles) of the boundary

layer at the wall. The Coulomb force  $U_e$  acting on the particle is then given by

$$U_e = \frac{q_p^2}{4\pi\epsilon(\frac{1}{2}\delta)^2} = \frac{q_p^2}{\pi\epsilon\delta^2} \quad (42')$$

The resulting average particle velocity  $v_e$  due to this image charge electrophoresis amounts to

$$v_e = \mu U_e = \frac{\mu q_p^2}{\pi\epsilon\delta^2} \quad (41')$$

and the related decay constant  $\beta_e$  is given by

$$\beta_e = v_e \frac{S}{eV} = \frac{\mu q_p^2}{\pi\epsilon\delta^2} \frac{S}{V} \quad (45')$$

Non-neutralized particles ( $q_p \approx 30$  electric charges) of about  $0.1 \mu\text{m}$  diameter ( $\mu = 1.7 \times 10^{11} \text{ m}^2 \cdot \text{s}^{-1} \cdot \text{J}^{-1}$ ) in the s.s.-walled 200-vessel (section 3.2) are subject to image charge electrophoretic deposition with a decay constant of the order of  $10^{-6} \text{ s}^{-1}$ . This is of similar magnitude as of other deposition processes. The induced charge will be smaller when the walls consist of a non-conducting material, dependent on the dielectric constant of the wall material.

### 2.3. Particle shape, density and size distribution

Conveniently, a non-spherical aerosol particle is aerodynamically characterized by two parameters, viz. the aerodynamic diameter and the dynamic shape factor [88]. The aerodynamic diameter ( $d_a$ ) of the particle is defined as the diameter of a hypothetical sphere of unit density having the same Stokes' settling velocity  $v_s$  as the particle possesses. The dynamic shape factor  $\kappa$  of the particle is the ratio of the particle's drag to the drag of a sphere with the same mass. Hence, writing  $d_e$  for the diameter of that sphere,

$$\kappa = \frac{U F(d_e)}{3\pi \eta d_e v} \quad (46)$$

This can be transformed to a relation between  $\kappa$ ,  $\rho$ ,  $d_e$  and  $d_a$  [88]

$$\kappa = \frac{\rho}{\rho_0} \frac{d_e^2}{d_a^2} \frac{F(d_e)}{F(d_a)} \quad (47)$$

where  $\rho_0$  is unit density.

Dynamic shape factors of non-spherical particles of simple shapes (e.g. cubes, cylinders and prolate ellipsoids) can be calculated approximately (Kops, [89]) and these theoretical results are well confirmed by experiment.

Aggregates of solid primaries have been studied experimentally by Stöber [90], Kops [89] and recently by Allen [91] yielding  $\kappa$  values which are related to aggregate microstructure (primaries size distribution and number  $n$  of primaries per aggregate). Stöber's investigations were focussed on aggregates of limited numbers (up to about 20) of monodisperse polystyrene spheres. Kops has studied aggregates of relatively large numbers  $n$  ( $10^2$ - $10^4$ ) of polydisperse primaries of metal, metal oxide or organic dye. Allen's group has been working on  $U(Pu)O_2$  aerosols and his results show the dynamic shape factor decreasing with increasing  $n$  which is contrary to the findings of Kops and Stöber. The latter two find a relation between  $\kappa$  and the microstructure dependent on the arrangement of the primaries in the aggregate. From Kops's work one may deduce that for aggregates of lognormally distributed primaries  $\kappa$  can be related to  $n$  by

$$\kappa = \frac{F(d_e)}{R_1 F_1(Kn)} n^{1/3} \quad (48)$$

where  $R_1 F_1(Kn)$  is a factor primarily related to the size of the primary particles [89].  $R_1$  is proportional to  $\exp(\ln^2 \sigma_g)$  while  $F_1(Kn)$  is related to the slip factor for primary particles with Knudsen number  $Kn$ .

Eq. (48) is valid for linear chains only and Kops has found also that for his aerosols this means a validity range of  $n \leq 5 \times 10^3$ . A different relation applies to larger aggregates ( $n \geq 5 \times 10^3$ ) which are composed of branched threedimensional networks

$$\kappa = \frac{F(d_e)}{R_2} \quad (49)$$

where  $R_2$  is a measure of the packing density of the aggregate.

Consequently, with increasing aggregate size (or n) initially  $\frac{k}{F(d_e)}$  showed increase in proportion to the cube root of n. Around  $n = 5 \times 10^3$  it should reach the maximum value as given by (49), according to the observations by Kops [89].

For spherical particles of known diameter d, only density  $\rho$  needs to be corrected for in order to calculate the aerodynamic diameter:

$$d_a = d \left( \frac{\rho F(d)}{\rho_o F(d_a)} \right)^{\frac{1}{2}} \quad (50)$$

In table II,  $d_a$  is given as a function of d for various values of  $\rho$ . Other diameter definitions used in this publication are:

- Stokes diameter, defined as the diameter according to the Stokes relation;
- mass equivalent diameter,  $d_e$ , defined as the diameter of a sphere with a mass equal to the particle's mass.

Dynamic shape factors have been derived and determined only for particles of simple shapes [92]. Particles consisting of more than one sphere of the same size have known shape factors [93]. Usually for such clusters a size factor  $f_n$  is used which is defined as the ratio of the aerodynamic diameter of the cluster of n spheres to the aerodynamic diameter of the individual spheres.  $f_n$ -values of compact clusters and straight chains of spheres have been determined with the aid of the spiral aerosol centrifuge [94].

Aerodynamic characterisation of branched chainlike aggregates of polydisperse primary particles was with limited success up to now. Using their electrical mobility analyzer, Vomela and Whitby [95] have obtained results which indicate that in the size range of 0.1  $\mu\text{m}$  the Stokes diameter of solid condensation aerosols is nearly equal to the equivalent mass diameter. However, the use of this analyzer for aerodynamic characterisation of aggregates is dubious due to the unknown charging properties of aggregates (which properties should be known for the analysis). Also, there may be changes in shape and orientation of the aggregates when charged and exposed to the electric field of the analyzer [96]. Moreover, a Stokes diameter cannot be converted into an aerodynamic diameter without correction (as in

Eq. (50)) for the density of fluffy aggregates, which is an undefined property in this case.

Usually, an observed size distribution, e.g. a number frequency distribution  $f_n(r)$  is fitted to a log-normal distribution:

$$f_n(r) = \frac{1}{(\ln \sigma_g) \sqrt{2\pi}} \exp \left\{ - \frac{(\ln r - \ln r_g)^2}{2 \ln^2 \sigma_g} \right\} \quad (51)$$

with the characteristic parameters:  $r_g$  = geometric mean and  $\sigma_g$  = geometric standard deviation of the particle radii distribution.

The fitting to a log-normal distribution is particularly useful when various distributions of the sample have to be converted such as the distributions of surface area, volume and mass. However, in using such conversions, particular attention must be given to the fit between data and the log-normal distribution since serious errors may arise in the new distributions due to relatively small deviations from a log-normal distribution. The relations are conveniently summarized in [97]. For example the mean particle mass  $\bar{m}$  is obtained by

$$\bar{m} = \frac{1}{6} \pi \rho (d_g)^3 \exp (4.5 \ln^2 \sigma_g) \quad (52)$$

provided  $\rho$  is size independent and the distribution is log-normal.

#### 2.4. Size distribution of enclosed aerosols

The size distribution of an aerosol aging in an enclosure will be correlated with the initial size distribution at the moment of the formation and it will show the influences of the various forces on the particulate cloud later on. In case of condensation aerosols the generally large particle concentration gives rise to a high rate of coagulation during the initial period (c.f. Eq. (1)). For a concentration of  $c_n = 10^9 \text{ cm}^{-3}$  the concentration is halved in about 1 sec. Since this "half-life" is inversely proportional to  $c_n$ , after a few minutes the concentration is practically independent of the initial (large) concentration (pg. 77). Consequently, this initial period of pure, rapid coagulation can be considered as a part of the aerosol formation, which does not help us too much in case of solid

condensation aerosols since we still remain confronted with the approximate equations for coagulation of these aerosols (pg. 27).

After the initial coagulation period the deposition processes will dominate more and more owing to their first order nature. Accordingly, the deposition processes will shape the size distribution of the enclosed aerosol in the long run. With respect to the long term size distribution it is worthwhile to consider the commonly observed exponential decay curve of unheated enclosed aerosols (pg. 19).

As observed by the author (fig. 18), also the decay of enclosed monodisperse aerosols is governed by the exponential relation (5).

Hence, we may conclude that the aerosol behaves as if it were aerodynamically monodisperse. Such a behaviour may be correlated with two principally different size distributions: either the size distribution has such a small standard deviation that it can be regarded as monodisperse, or the size distribution remains constant although strongly polydisperse. The later situation arises when the deposition forces are size independent or when they combine to give a self-preserving size distribution.

Thermophoresis and diffusiophoresis have a slight size dependence for particles larger than a few tenths of a  $\mu\text{m}$ . In those cases an exponential decay may be attributed to an uninfluenced polydisperse size distribution. Diffusion, however, is size dependent and settling even more. Consequently, the commonly observed exponential decay curves can only be explained by constant size distributions which look monodisperse or which are really monodisperse due to the generation.

In order to have a self-preserving size distribution of an enclosed aerosol formed by an instantaneous source two mechanisms are required. These must act in such a manner that the population in every size interval decays exponentially with the same half-life. The mechanisms involved must have opposite size dependences, viz. the fine and coarse particle regions must be influenced preferentially. This counterbalancing must lead to an equilibrium size distribution and hence the two influences must be of the same kinetic order. Various investigators claim that the combined action of coagulation and stirred settling results in a self-preserving size distribution [31, 33, 98].

It may be clear that the combination of coagulation and gravitational deposition alone cannot result in a constant size spectrum of an aging enclosed aerosol. With time passing, the dominance of settling of the formed large particles will increase over particle growth by coagulation due to the different kinetic orders of the regarded mechanisms: coagulation is of second order kinetics and deposition of first order.

Another combination of two processes which could lead to a self-preserving size distribution is stirred diffusive and gravitational deposition. This has been proposed originally by the author [6]. However, it can be shown that this pair of mechanisms cannot explain the exponential decay either. If the size distribution would be in such dynamic equilibrium, the normalized number of particles with size  $d$  must be independent of time  $t$ , or

$$\frac{\delta}{\delta t} \left\{ \frac{n(d,t)}{N(t)} \right\} = 0 \quad (53)$$

The left-hand side of (53) can be transformed:

$$\frac{\delta}{\delta t} \left\{ \frac{n(d,t)}{N(t)} \right\} = \{\beta(d) - \beta\} \frac{n(d,t)}{N(t)} \quad (54)$$

where  $\beta(d)$  and  $\beta$  are the total decay constants (diffusion and settling) of the number of particles with size  $d$  and of the total number of all particles, respectively.  $n(d,t)$  is the decaying number of particles with size  $d$  and  $N(t)$  the total number of all particles.

From (54) and condition (53) it follows that either  $\beta(d)$  equals  $\beta$ , or the relative number of particles of any size  $d$  is zero. The first case is impossible in case of a polydisperse aerosol since  $\beta(d)$  is a function of  $d$  for combined diffusive and gravitational deposition and consequently cannot be equal to the constant  $\beta$ . The second case is a trivial solution. In conclusion, the combination of stirred diffusion and settling cannot lead to an exponentially decaying polydisperse aerosol which has yielded  $\beta(d) = \beta$ . Hence, the deposition processes are size independent or the aerosol is practically monodisperse. The latter must be the case for unheated aerosols. The monodisperse character of an enclosed aerosol may arise from the initial period dominated by coagulation which removes preferentially



and very fast all small particles. Although only valid for a droplet aerosol, it has been shown by Castleman [99] that in the coagulation period an initially log-normal aerosol preserves its log-normal size distribution but the standard deviation  $\sigma_g$  changes rapidly to a value of about 1.4 irrespective of the initial  $\sigma_g$ . Qualitatively, an analogous treatment of the coagulation of an aerosol consisting of solid particles will yield the same result except that a smaller  $\sigma_g$  results. This is due to the fact that coagulation of  $n$  droplets leads to a droplet which has a larger aerodynamic size than an aggregate of  $n$  solid particles.

All deposition processes combined will show a minimum of deposition rate somewhere below  $1 \mu\text{m}$  and above  $0.1 \mu\text{m}$ . Thus the modal peak of an aged aerosol must be somewhere in this region with a decreasing  $\sigma_g$ . In summary, a condensation aerosol formed in an enclosure will deposit exponentially after the coagulation period since the aerosol is practically monodisperse. Which deposition process will dominate after this period depends on the aerodynamic diameter of the resulting aerosol. The deposition will further decrease the dispersity. The stronger the size dependence of the deposition rate the more rapidly will the standard deviation decrease. The influence will decrease in the sequence: sedimentation, diffusion, thermo- and diffusio-phoresis.

## 2.5. Non-stirred aerosol deposition

Non-stirred aerosol deposition can occur under various conditions and for various aerosols. The deposition velocity can be larger than the usual convective flow velocities in enclosures. In some cases, however, the flow velocities are relatively small compared to the deposition velocities resulting in non-stirred deposition. In the following sections the occurrence of non-stirred conditions will be treated for a number of cases. Additionally, attention will be given to the so-called rotating drums [100], systems for which a postulate on non-stirred conditions underlies the increased aerosol stability.

### 2.5.1. Non-stirred aerosol settling

When the particle size is so large that  $v_s$  approaches the velocity of the free convection normally keeping the aerosol stirred, there will

arise an inhomogeneous aerosol distribution. The particle diameter  $d_{\max}$  at which this occurs, can be obtained by taking the Stokes' settling velocity (17) equal to the velocity of the free convection given by the Prandtl relation [48]

$$\frac{\rho g}{18 \eta} d_{\max}^2 F(d_{\max}) = 0,5 \sqrt{g \alpha \Delta T} \bar{l} \quad (55)$$

where  $\alpha$  is the coefficient of thermal expansion of the gas ( $\frac{1}{T}$ ),  $\Delta T$  is the average temperature difference causing the convection and  $\bar{l}$  is the wall length which may be taken approximately equal to the cube root of the tank volume. For this rough calculation  $F(d_{\max})$  may be taken unity ( $d_{\max} > 1 \mu\text{m}$ ). Then the following relation holds:

$$d_{\max} = 3 \left(\frac{\eta}{\rho}\right)^{\frac{1}{2}} \left(\frac{\alpha \Delta T \bar{l}}{g}\right)^{\frac{1}{4}} \quad (56)$$

Obviously,  $d_{\max}$  is little dependent on  $\Delta T$  and  $\bar{l}$ . When we use aerodynamic diameters (pg. 50)  $\rho$  is unity.  $\Delta T$  is about  $0.01^\circ\text{C}$  for vessels in the laboratory according to the authors' experience. Hence, for the usual range of tank volumes (50 liters to  $5 \text{ m}^3$ )  $d_{\max}$  ranges from  $13 \mu\text{m}$  to  $20 \mu\text{m}$ , so that indeed only a slight dependence on the enclosure volume exists. In order to reduce  $d_{\max}$  by a factor of two,  $\Delta T$  must be smaller by more than one order of magnitude.

Clearly, aerosol research, which as a rule is limited to particle diameters of a few  $\mu\text{m}$  or less, concerns "stirred" aerosols.

### 2.5.2. Non-stirred diffusive deposition

Treatment of aerosol diffusive deposition like that of gravitational settling in the previous section 2.5.1. (with instead of  $v_s$  the convection velocity  $v_d = \frac{D}{\delta}$ ) leads to the maximum diffusion coefficient  $D_{\max}$  for which the stirred model still holds

$$D_{\max} = 0.5 \delta \sqrt{g \alpha \Delta T} \bar{l} \quad (57)$$

in which  $\delta = 4.6 D^{0.265}$  (Eq. (15)) according to our model (pg. 33). For an extreme case of  $\Delta T = 10^{-4} \text{ K}$  and for characteristic vessel dimensions of  $1 \text{ m}$ ,  $D_{\max}$  amounts to  $0.3 \text{ cm}^2 \cdot \text{s}^{-1}$ . This means that

usually a homogeneous spatial distribution exists even for low-molecular gases having diffusion coefficients of the order of  $0.1 \text{ cm}^2 \cdot \text{s}^{-1}$ . This conclusion is contrary to the prevailing opinion that diffusive deposition takes place from a stagnant atmosphere (see e.g. Goldberg et al. [101] and Pich [20, 103]). They stated that their models for non-stirred diffusive aerosol behaviour are realistic. However, the above given evidence shows that in reality usually diffusive deposition is of the stirred type.

### 2.5.3. Atmospheric stability of box atmospheres

When the gas phase consists of two components of different molecular weights, the atmospheric conditions in the aerosol box may be non-uniform. From a heated layer of liquid on the floor molecules diffuse upwards against gravity. When these vapour molecules are much heavier than those of the gas in the box a situation may arise where a major part of the atmosphere in the box is stagnant. Then aerosol deposition cannot be considered stirred deposition any longer and the rules derived hitherto cannot be applied. This situation has not been considered in literature. In this case the density  $\rho$  of the atmosphere decreases with increasing height  $h$

$$\frac{d\rho}{dh} < 0 \quad (58)$$

Apart from the boundary layers near the walls the temperature  $T$  decreases also with increasing height  $h$ . Hence,

$$\frac{dT}{dh} < 0 \quad (59)$$

The boundary condition for the stable case is now given by combination of (58) and (59)

$$\frac{d\rho}{dT} > 0 \quad (60)$$

When  $\frac{d\rho}{dT}$  has a negative value, the driving-force of natural convection is larger than the buoyancy force and consequently the atmosphere will become stirred.

(60) can be transformed by substitution of

$$\rho = \rho_d X_d + \rho_g X_g \quad (61)$$

with X the molefraction and the subscripts d and g referring to the vapour and gas components. The density of an ideal gas at atmospheric pressure is related to the temperature T and its molecular mass M by

$$\rho = \frac{273}{22.4 \times 10^3} \frac{M}{T} = 0.012 \frac{M}{T} \quad (62)$$

since 1 mole of gas (M grams) has a volume of  $22.4 \times 10^3 \text{ cm}^3$  STP.

Now (60) becomes

$$\frac{d\rho}{dT} = 0.012 \left\{ (M_d - M_g) \times \frac{d}{dT} \left( \frac{X_d}{T} \right) - \frac{M_g}{T^2} \right\} > 0 \quad (63)$$

It is difficult to calculate  $X_d$  since the mole fraction of vapour in the box as a function of height and temperature will depend on the degree of mixing of upwards diffusing vapour and gas and the slow vapour deficient stream downwards from the cold vertical walls. However, an upper limit to  $X_d$  can be taken when aerosol particles which act as condensation nuclei are present in the box. This means that it may be assumed that at every point inside the box the vapour is only slightly supersaturated at the local temperature. The atmosphere may be supersaturated if aerosol is absent or if the aerosol particles are smaller than the critical size required for condensation nuclei. For a saturated vapour the relation of Clausius-Clapeyron in its mole analogy is valid

$$\frac{d}{dT} (X_d) = \frac{X_d \times \Delta H_v}{RT^2} \quad (64)$$

Substitution of (63) and further differentiation of (64) yields

$$\frac{d\rho}{dT} = \frac{0.012}{T^2} \left\{ (M_d - M_g) \frac{X_d}{RT} (\Delta H_v - RT) - M_g \right\} \quad (65)$$

Since R equals 8.31 J/mole.K and  $\Delta H_v$  usually is larger than 10 kJ/mole,  $\Delta H_v - RT$  is large and positive for  $T \leq 1200$  K.

Three cases may be distinguished:

1.  $M_d < M_g$

This means that  $\left\{ (M_d - M_g) \frac{X_d}{RT} (\Delta H_v - RT) - M_g \right\}$  is negative and consequently  $\frac{d\rho}{dT} < 0$ , which indicates a stirred atmosphere.

2.  $M_d > M_g$ , but

$$\frac{X_d}{RT} (\Delta H_v - RT) < \frac{M_g}{M_d - M_g}$$

yields  $\frac{d\rho}{dT} < 0$ : the atmosphere is stirred.

Although the vapour molecules are heavier than the gas molecules, yet the natural convection will mix the atmosphere because either the molecular mass difference  $M_d - M_g$  or the vapour content of the atmosphere  $X_d$  is too small. The last case corresponds with a system of vapour at a temperature far below the boiling point of the liquid.

3.  $M_d > M_g$  and

$$\frac{X_d}{RT} (\Delta H_v - RT) > \frac{M_g}{M_d - M_g}$$

gives a stable atmosphere:  $(M_d - M_g)X_d$  is large enough. This usually will be the case at temperatures near the boiling point of a liquid having a large molecular mass  $M_d$ . In all other cases atmospheres will be convectively stirred and the air-borne particles will deposit according to stirred deposition rules.

#### 2.4.5. Rotating drums

In 1958 Goldberg [100] proposed the use of a cylindrical chamber rotating around its horizontal axis. Such rotating vessels should allow aerosols contained in them to remain air-borne during much longer periods than in stationary vessels. As shown by Fuchs [104] important conditions for proper functioning of a rotating drum are

- the atmosphere filling the drum should rotate bodily
- there should be no significant convection.

According to Fuchs the aerosol concentration decreases exponentially under these conditions with a decay constant equal to  $\frac{2 \omega^2 v_s}{g}$  ( $\omega =$

angular velocity of drum rotation,  $v_s$  = Stokes' settling velocity,  $g$  = gravitational acceleration). Frostling [105] gives some experimental results concerning the aerosol stability in a rotating drum.

Frostling's data shows that the aerosol stability is hardly improved compared to the theoretical improvement by several orders of magnitude which would follow from the relation derived by Fuchs. Obviously, the afore mentioned conditions are not fulfilled in Frostling's experiments. Very probably, the absence of free convection is a condition which cannot be met. In the previous sections it has been made plausible that already minute heat flows lead to well-stirred atmospheres thereby violating the secondly mentioned condition. Additionally, a rotating drum is a very unattractive aerosol chamber from the view point of the experimentalist. Such drums have very limited sampling possibilities, viz. only at the axis.

### 3. MATERIALS AND METHODS

#### 3.1. Aerosol formation

The major part of this research concerns condensation aerosols generated by means of the Exploding Wire technique; by this technique the energy stored in a battery of low-inductance capacitors is dissipated in a wire of the materials to be dispersed. The wire evaporates explosively, followed by condensation to particles. There were various arguments issuing from the original aim of this study (nuclear reactor safety) which were in favour of the use of this formation method. Besides, a few general aspects of this technique plead for a more wide-spread use of it. Firstly, as a discontinuous source its generation usually takes place within a millisecond and consequently, the moment of birth of the aerosol is accurately known. Secondly, the formation can be repeated with an excellent reproducibility provided care is taken to have a constant electrical circuit. Thirdly, many formation parameters can be varied easily. Finally, the technique itself has no special side effects such as continuous overpressure in the aerosol tank; the amounts of heat and electrical charge involved are of no consequence to the aerosol system created.

A drawback of the Exploding Wire technique is the limited amount of stored energy on the capacitor bank which means that only limited amounts of material can be dispersed. Furthermore, only electrically conductive materials are explodable; trials to disperse isolating materials on a metal support were unsuccessful.

The Exploding Wire equipment consists of 4 parallel capacitors with a total capacity of 30.8  $\mu\text{F}$  which can be loaded up to 18 kV. The circuit is fired with a triggered air gap switch. The circuit including the coaxial cable to the Exploding Wire - mounted inside an aerosol tank - has a resonance period of 28  $\mu\text{sec}$ , an inductance of 650 nH and a resistance of 22 m $\Omega$ . The Exploding Wire rig, called SPARK, is a mobile unit, so that it can be connected to various aerosol tanks. Depending on the wire resistance the stored energy is dissipated in the wire with efficiencies of 50 to 100 %. Application of a shunt parallel to the Exploding Wire allows casually required low efficiencies.

The energy dissipated in an Exploding Wire was measured with the aid of an identical wire in a bomb calorimeter. Initially the wires were mounted by clamping with screws but it appeared that this resulted in unreliable energy dissipations in cases wires were shunted. Later on those wires were connected by soldering and in this way reproducible energy dissipations were observed.

In some cases aerosols were produced by spraying a solution or suspension and drying the droplets to solid particles. The atomizers applied were: a Collison atomizer (Aerosol Products (Colchester) Ltd., London) and a Wiesbadener Doppelinhalator (Wiesbadener Inhalatoren-Vertrieb, Karl Blümel, Wiesbaden).

### 3.2. Containments

During the course of the aerosol research various aerosol containments were used at ECN. Table III gives a survey of them.

The aerosol tank "100" is a vertical cylindrical oil storage tank made of steel. The tank was mainly used for study of the effect of temperature gradients. The sampling ports are 15, 85 and 155 cm above its bottom. The "200" tank is a  $1 \text{ m}^3$  steel containment. Due to the dimensions ( $2 \times 1 \times 0.5 \text{ m}^3$ ) this tank may be placed in positions so that different vessel heights may be used and yet the same total internal wall surface area is maintained. Fig. 6 shows the positions of the sampling ports and further details of the tanks "100" and "200".

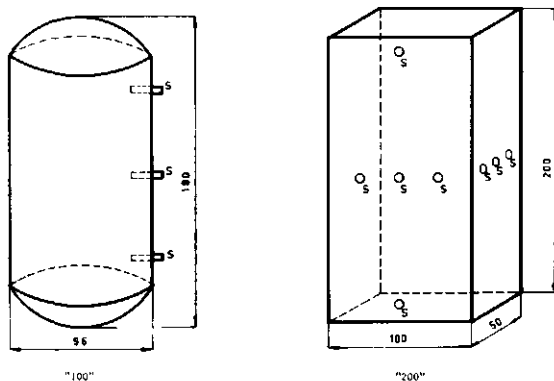


Fig. 6. The aerosoltanks "100" and "200". S are sampling ports.  
Dimensions in cm.



The "300" tank is a 75-liters stainless steel tank. This tank has been designed in order to study the aerosol behaviour at temperatures up to 200 °C. For that purpose "300" was placed inside an industrial furnace provided with an internal forced circulation of heated air. Provisions were made to enable

- conditioning and analysis of the tank atmosphere;
- explosion of wires with the aid of the SPARK rig.

Lucite tanks of 150 liters capacity (PERVEX) were especially designed for study of the effect of temperature gradients. A brass floor enabled homogeneous floor heating whereas by means of a quartz heating dish an inhomogeneously heated floor can be created. The temperature field and air velocity have been measured by means of thermocouples and a hot-wire anemometer.

The largest aerosol tank used is the 20 m<sup>3</sup> ENAK vessel. This is a disused reactor vessel placed upside down on a steel bottom plate. In order to carry out safe experiments with radioactive aerosol it was necessary to guarantee a negative pressure inside ENAK. Fig. 7 gives a sketch of the tank with its auxiliary equipment for sampling and pressure control.

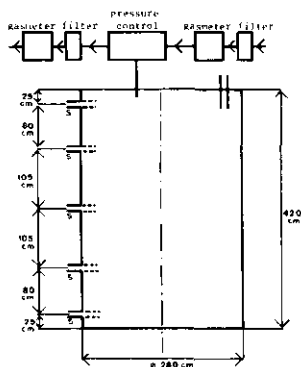


Fig. 7. The ENAK vessel. S are sampling ports.

Although in some cases the vessels contained filtered air prior to the experiments, as a rule the experiments were performed with unfiltered laboratory air. As a result of the air-conditioning this air was of sufficient quality ( $c_n \leq 10^3 \text{ cm}^{-3}$ ,  $c_m < 1 \text{ } \mu\text{g}\cdot\text{m}^{-3}$ ) in particular for the Exploding Wire experiments which were performed with concentrations far in excess to  $10^3 \text{ cm}^{-3}$  and  $1 \text{ } \mu\text{g}\cdot\text{m}^{-3}$ .

### 3.3. Analytical and sampling techniques

#### 3.3.1. Sampling for electron microscopy

Direct sampling on an electron microscope grid was achieved by electrostatic precipitation. The point-to-plane modification of the electrostatic precipitator (ESP) developed by Morrow and Mercer [106] was used and also further tested. The grids were covered with a  $200 \text{ \AA}$  carbon film. The electron microscope used has been a Philips EM 200. In principle electrostatic precipitation of aerosols works as follows. An aerosol particle entering a stable high-voltage corona discharge in air is charged by collision with ions of the negative charge cloud. The charged particle moves in the electrical field towards the positive electrode where it is deposited. The strong turbulence in the precipitation space (due to the so-called ionic wind) causes a homogeneous filling of the space. Due to this the grid shows also homogeneous covering by the aerosol particles. The precipitation process does not influence the aerosol sample provided that the precipitation target becomes not too crowded. Fig. 8 shows one of the ESP's used. Using a NaCl aerosol and two identical ESP's in series, the efficiency of the ESP as a function of particle size has been determined according to

$$\eta(d) = 1 - \frac{N_2(d)}{N_1(d)} \quad (66)$$

were  $N_1(d)$  and  $N_2(d)$  are the numbers of particles with size  $d$  precipitated in the first ESP and the second ESP, respectively. Fig. 9 shows the relation between the sampling efficiency and the particle size.  $\eta(d)$  values for  $d > 0.3 \text{ } \mu\text{m}$  have been measured with the aid of monodisperse aerosols of polystyrene spheres.

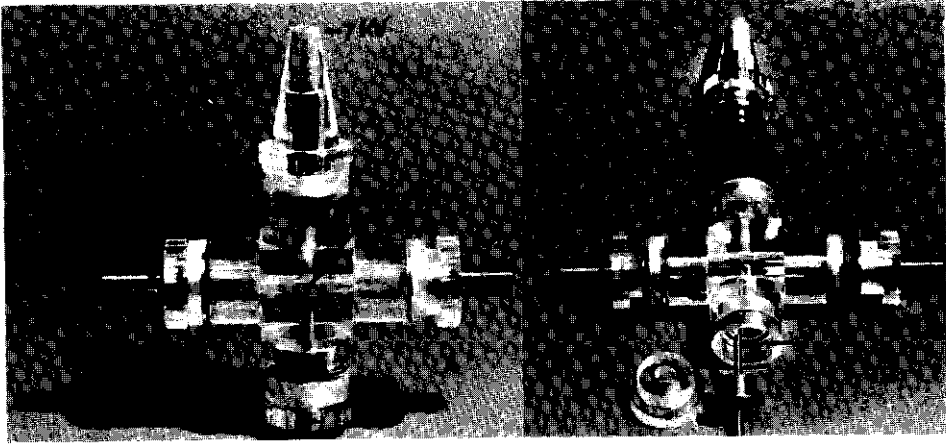


Fig. 8. ECN point-to-plane electrostatic precipitator, assembled (A) and disassembled (B). Aerosol flow and HV as indicated. Particles entering the corona discharge become all negatively charged and consequently are deposited on a carbon foil covered electron microscope grid which is placed on top of the grounded electrode (a).

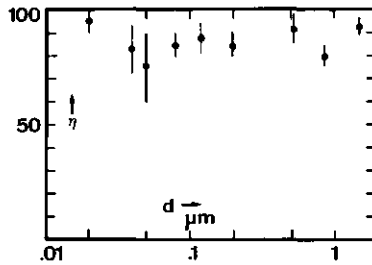


Fig. 9. Sampling efficiency ( $\eta$ ) of electrostatic precipitator as a function of particle size  $d$  (in  $\mu\text{m}$ ). Below  $0.3 \mu\text{m}$  crystalline NaCl particles were used, beyond  $0.3 \mu\text{m}$  polystyrene spheres.

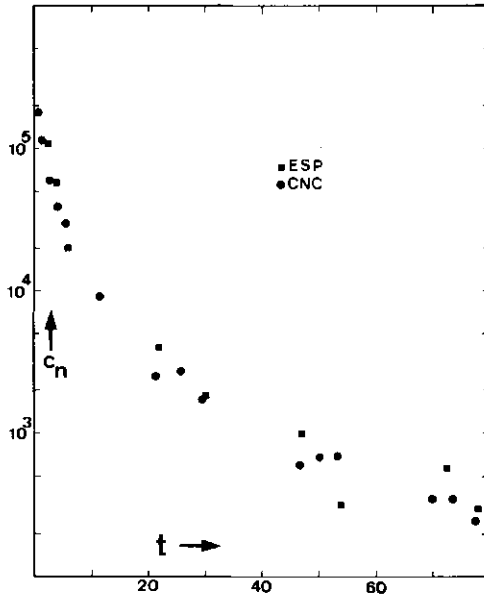


Fig. 10. Comparison of measuring data of an aging aerosol obtained by means of a Gardner condensation nucleus counter and by counting of particles on an electron micrograph taken from a grid loaded with aerosol sampled with the ESP. Number concentrations  $c_n$  (in  $\text{cm}^{-3}$ ) as a function of time  $t$  (in hours).

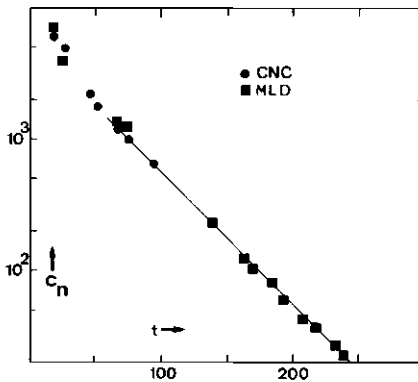


Fig. 11. Comparison of measurements with commercial (Gardner) condensation nuclei counter (CNC) and high sensitivity counter (MLD). Au-aerosol in  $1 \text{ m}^3$  ("200") tank in 2 meters height position.  $c_n$  in  $\text{cm}^{-3}$  and time  $t$  in hours.

Obviously the precipitation efficiency is not very dependent on the particle size of the sampled aerosol if the size range is mainly below 1  $\mu\text{m}$ . Thus the particle size distribution of a sampled aerosol is hardly influenced. An average sampling efficiency of 85 % has been used for estimating the particle number concentration. The ESP shows identical properties in air and other gases such as pure nitrogen or helium.

### 3.3.2. Particle number concentration

Two methods have been applied for the determination of the number of aerosol particles in containments.

Since the overall efficiency of the ESP has been estimated to be about 85 %, it is possible to calculate the particles number concentration from the number of particles on electron micrographs of known areas of the grid and from the sample volume.

The second method applied for measurement of the particle number concentration is that of the condensation nuclei counter. In principle this instrument detects all nuclei above about 0.01  $\mu\text{m}$  by condensing water on them in an expansion chamber. The concentration is measured by comparing the initial intensity of a light beam with the intensity after passage through the chamber. The condensation nuclei counters used (Small Particle Detector, Gardner Ass., Inc.) have a measuring range of  $2 \times 10^2$  to  $10^6 \text{ cm}^{-3}$ . The condensation nuclei counter has been compared with the ESP-counting method by measuring the decay of an enclosed aerosol. Fig. 10 shows that there is a reasonable agreement between the results of both techniques. This is in accordance with separate findings to which the author contributed [107].

An improved version of the condensation nuclei counter has been built by the author. Instead of using the extinction of the cloud, the scattered light intensity is measured. In this way the detection limit for aerosol particles could be lowered more than an order of magnitude. The apparatus (MLD) has been calibrated by means of a divider of a similar type as originally used for the Pollak counters [108]. One absolute concentration value has been obtained with the aid of the ESP-electron microscope technique described above. Fig. 11 shows the good agreement between the measuring data obtained with the Gardner counter (CNC) and MLD.

### 3.3.3. Mass concentration

The aerosol is sampled by loading cellulose nitrate membrane filters (Sartorius, Göttingen) of the type MF 100. The efficiency of these filters is virtually 100 % [109]. For suction a syringe is used with a flow rate of about  $200 \text{ cm}^3 \cdot \text{min}^{-1}$ . The volume of the syringe is either  $100 \text{ cm}^3$  or  $1000 \text{ cm}^3$ . Initially, mass concentrations have been measured by weighing the filter loads. The detection limit (some  $10 \text{ } \mu\text{g}/\text{m}^3$ ) was too high for our purposes. Better, mass concentration data have been obtained by preirradiating the wire material and counting the activity of the filter load. The count rate has been converted into mass with the aid of a filter loaded with a known amount of material of the same specific activity.

### 3.3.4. Size distribution

As shown in 3.3.1, a representative sample of aerosol particles can be obtained by means of the point-to-plane precipitator. Electron micrographs of the sampled particulate matter have been analysed using the semiautomatic size analyser TGZ-3 (Zeiss). During the last part of this study a spiral centrifuge according to Stöber [110] became available. The Stöber centrifuge facilitates separation and classification of aerosol particles according to their aerodynamic diameters in the size range between  $1.5 \text{ } \mu\text{m}$  and about  $0.1 \text{ } \mu\text{m}$ . The device consists essentially of a rotor with a vertical axis. As the aerosol flows outwards through a spiral duct in the rotor, the aerosol particles are deposited along a thin strip on the outer wall of the duct. The deposition place of an aerosol particle can be converted into an aerodynamic diameter by means of a calibration curve which is obtained with the aid of monodisperse polystyrene aerosols. The deposition pattern for an aerosol consisting of singlets and clusters of polystyrene spheres is shown in fig. 12. Calibration data have been obtained using polydisperse polystyrene aerosol which compare nicely with the data from the deposit location of the monodisperse polystyrene aerosol (fig. 13). Since the range of commercially available sizes of monodisperse polystyrene latices does not extend below  $0.1 \text{ } \mu\text{m}$  diameter, these polydisperse aerosols are an important tool for calibration of the centrifuge. With the aid of this calibration curve an aerodynamic

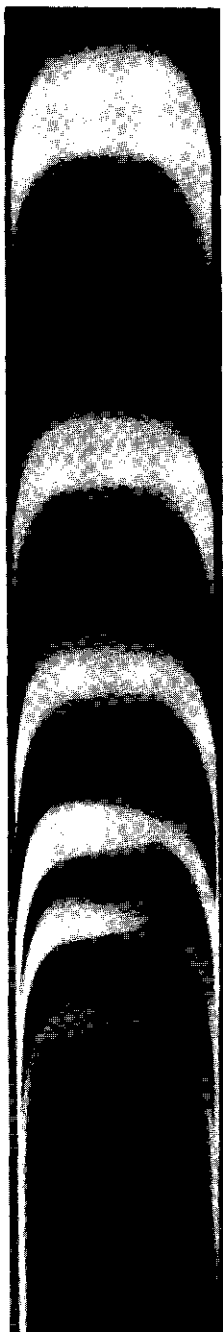


Fig. 12. Deposition pattern of polystyrene aerosol (consisting of single spheres and multipliers) along a sampling foil from the Stöber centrifuge. From l to r: single spheres, doublers, triplets, etc.

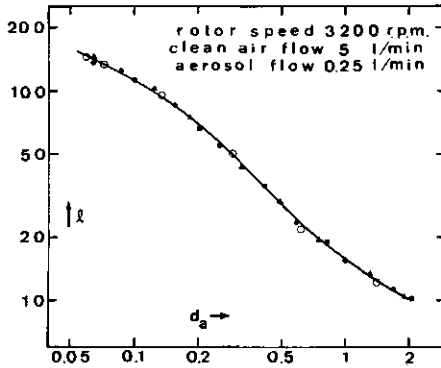


Fig. 13. Calibration curve (deposition place  $l$  in cm as a function of  $d_a$  in  $\mu\text{m}$ ) of the Stöber centrifuge obtained with monodisperse (o) as well as with polydisperse (■●▲) polystyrene aerosols

diameter can be attributed to an arbitrary particle according to its deposition place in the centrifuge.

In order to obtain the aerodynamic diameter distribution of an aerosol the particle density as a function of deposition place must be measured by counting of particles on an electron micrograph of a certain area. However, there are various size dependent effects disturbing the direct relation between particle deposit density and the original abundance in the aerosol. In the coarse region ( $> 0.8 \mu\text{m}$  dia) there is a size dependent loss at the centrifuge entrance. Furthermore, the double vortex in the channel (due to Coriolis forces) contributes to a locally non-uniform deposit of the aerosol.

Using the polydisperse polystyrene aerosol the location dependent (and consequently size dependent) correction factors have been determined and are shown in fig. 14.



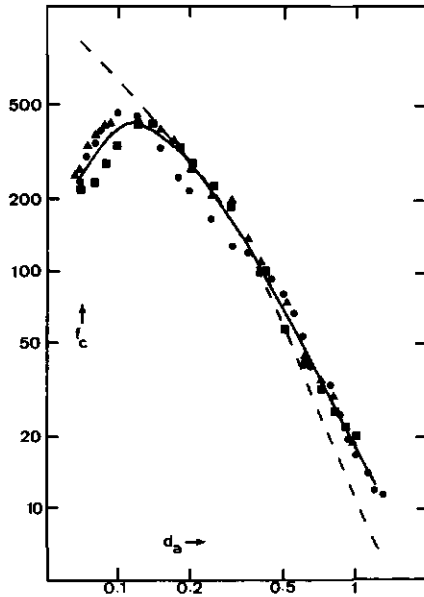


Fig. 14. Experimentally determined correction factors  $f_c$  for the Stöber centrifuge as compared to the (dashed) curve  $\frac{\delta}{\delta d_a} \{Z(d_a)\}$  obtained from fig. 13;  $d_a$  in  $\mu\text{m}$ .

### 3.4. Materials

Gold wires used had a 99.9 wt.% purity. Other materials exploded (Cu, U, etc.) were of technical quality.

Sodium chloride aerosols have been obtained by spraying aqueous solutions of NaCl p.a. Polydisperse polystyrene aerosols have been produced in the same way using solutions of polystyrene (Dow Chem.) in xylene p.a. In the latter case obviously the all-glass Wiesbadener Doppelinhalator has been used in view of the plastic components of the Collision atomizer.

Monodisperse polystyrene latices of Dow Chem. and Pechiney-Saint Gobain have been used. Since the sizes quoted by the manufacturers are unreliable according to literature [111], all sizes were electron microscopically redetermined. Table IV represents the results and allows comparison with data from literature and from manufacturers.

The carrier gas of the aerosol was mostly air but in some cases nitrogen or helium with impurity levels below 10 ppm was used.

### 3.5. Experimental errors

The basic measuring data comprises those concerning number concentration ( $c_n$ ), mass concentration ( $c_m$ ) and various particle sizes. Inaccuracy in time data is negligible compared to other uncertainties. Mass concentration measurements have an accuracy which depends mainly on the volume measurement in the range of higher  $c_m$ -values ( $\approx \pm 10\%$ ) but near the lowest limit of mass detection, the accuracy of  $c_m$  is worse ( $\leq \pm 25\%$ ). Particle number concentration data as obtained with the Gardner condensation nuclei counter is accurate within  $\pm 20\%$  generally  $|107|$ ; however, in the low  $c_n$  range ( $< 10^3 \text{ cm}^{-3}$ ) accuracy is about  $\pm 30\%$ .  $c_n$ -values as obtained from counting particles on electron micrographs of samples taken by means of ESP have an accuracy slightly less than those from the CNC (see e.g. fig. 10). As a result, average particle mass, calculated as the ratio of  $c_m$  to  $c_n$ , is obtained with  $\pm 30\%$ . Most of the calculations involve half-lives ( $t_{\frac{1}{2}}$ ) or decay constants ( $\beta$ ) which originate from decay data on aerosol concentration.  $\beta$  or  $t_{\frac{1}{2}}$  were obtained graphically with an accuracy better than  $10\%$ ; however, sometimes accuracy was worse.

Aerodynamic diameters as determined by means of the Stöber centrifuge are known better than  $\pm 1\%$  in the size range larger than  $0.1 \mu\text{m}$ . Spatial dimensions of particles as measured from electron micrographs are usually accurate within  $\pm 10\%$ . In the size range  $0.005 - 0.05 \mu\text{m}$  (primary particles) considerable uncertainty exists in size data amounting to about  $\pm 25\%$ .

Systematic errors in the experimental observation could have resulted from sampling artefacts. Sampling was done with linear velocities of a few  $\text{cm}\cdot\text{s}^{-1}$  or more. Under these conditions no artefacts due to non-isokinetics or non-axiality can have taken place for particles in our aerodynamic diameter range of  $0.1 - 1 \mu\text{m}$ . Also losses of such particles in the sampling lines used ( $\leq 20 \text{ cm}$  length and I.D.  $\geq 5 \text{ mm}$ ) are negligible.

#### 4. RESULTS AND DISCUSSIONS

##### 4.1. Primary particles

Size and shape of the primary particles formed immediately after the explosion of an Exploding Wire depend on various parameters. In case of gold the particles are spherical with formation of crystalline faces in a few cases. However, particles of metal oxide like MgO or  $\text{Fe}_2\text{O}_3$ , clearly show crystalline properties (figs. 15 and 1b resp.). Obviously, high-melting materials such as these metal oxides ( $\text{U}_3\text{O}_8$  is another example) easier form monocrystalline particles after their formation in the molecular form than lower-melting metals like gold.

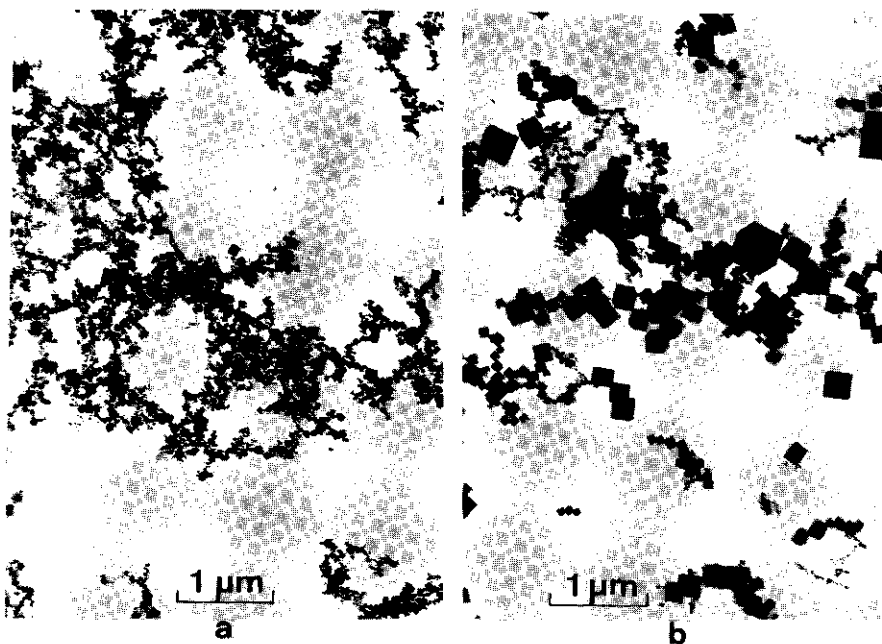


Fig. 15. MgO aerosol; a) from electrical explosion of Mg ribbon in air, b) formed by burning a Mg ribbon in air.

As may be expected the size of the primary particles formed immediately after the explosion is found to be dependent on the specific explosion energy (Espec) (see fig. 15a and 15b). Since the size of the primary particles forms a record of the way of aerosol formation, this important aspect of the aerosol formation was studied in more detail. Espec was measured with the bomb calorimeter (pg. 62). The primary particle size was measured by means of the TGZ-3 (pg. 69) after taking an electron micrograph of a sample obtained with the ESP (pg. 65). Although the sample consisted of coagulated primary particles, the good resolution of the electron microscope allows the measurement of the diameter distribution (diameters of the order of  $0.01 \mu\text{m}$ ) of the primary particles. Table V summarizes the data about the relation between the geometric median diameter ( $d_{1g}$ ), the geometric standard deviation ( $\sigma_{1g}$ ) and Espec for gold aerosols. The diameter distribution is nicely log-normal and  $d_{1g}$  decreases with increasing Espec, whereas  $\sigma_{1g}$  is  $1.5 \pm 0.1$  irrespective of Espec. Both effects have been observed by others, e.g. Phalen [112]. Our results of  $d_{1g}$  compare very well with those of Tomaides [113] and Barkow [114] presumably because their specific explosion energy data are measured values or because the energy losses in the electrical circuit were negligible. Results of other investigators (see ref. [112]) have systematically larger Espec values, presumably, due to the assumption of complete energy dissipation in the EW. Fig. 16 shows the dependence of  $d_{1g}$  on Espec. A reasonable qualitative explanation for the observed dependence of  $d_{1g}$  on Espec may be the following one.

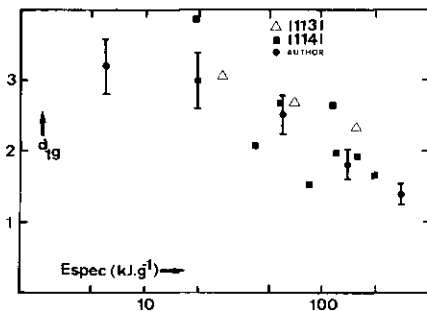


Fig. 16. Geometric median diameter ( $10^{-4} \mu\text{m}$ ) of primary particles of gold aerosols as a function of specific explosion energy (Espec).

At a certain moment after the explosion an expanding sphere of vaporized material is present, the radius of the vapour sphere at the moment of condensation being larger for larger *Espec*. So at this moment the vapour concentration is lower, leading to smaller particles assuming homogeneous condensation and a nuclei concentration independent of *Espec*.

The surface energy stored in the dispersity of the aerosol can be taken as the energy used for aerosol formation from the wire material. The specific surface energy can be calculated according to Ulich and Jost [115]. The ratio of this specific surface energy to the specific formation energy (*Espec*) measured by means of the bomb calorimeter is given in table V. This ratio decreases with increasing *Espec*, as more energy is wasted by heat dissipation. The interaction between the electric discharge and the wire, obviously is stronger in case of smaller *Espec*, probably due to less radial expansion of the discharge.

Using Eq. (52) the mean mass  $\bar{m}_1$  of the primary particles has been calculated and given in Table V. Taking into account an initial mass concentration  $c_m(o)$  of about  $10 \text{ mg.m}^{-3}$  one calculates an initial number concentration  $c_n(o)$  of about  $10^7 \text{ cm}^{-3}$  assuming instantaneous distribution in the space. In this way, however, an upper limit of  $c_n(o)$  is used. To the author's experience the homogeneous space distribution is reached only after about 15 minutes in case of a  $1 \text{ m}^3$  vessel, thereby enhancing coagulation in the early period of the aerosol life.

Closer examination of the relation between  $\bar{m}_1$  and *Espec* (Table V) leads to the conclusion that for higher specific formation energies (*Espec*  $\geq 20 \text{ kJ.g}^{-1}$ ) these two properties are almost inversely proportional, the product (*Espec*). $\bar{m}_1$  being  $(1.7 \pm 0.6) \times 10^{-14} \text{ kJ}$ . This indicates that the explosive particle formation is a three-dimensional process of evaporation and condensation as indicated above. Further discussion of the Exploding-Wire formation mechanism is regarded to be beyond the scope of this thesis.

#### 4.2. Coagulation

Coagulation is an inherent property of aerosols. Whether coagulation of an aerosol in a chamber is an important process depends on the number concentration as well as on the containment size and shape, the former being the most important parameter. In case of instantaneous aerosol formation such as by Exploding Wires, coagulation is dominant during an initial period. Enhanced coagulation takes place when the aerosol cloud is expanding in the aerosol vessel immediately after the local explosion (during about 15 minutes in a  $1 \text{ m}^3$  vessel). Therefore, the measured or extrapolated initial particle number concentration will always be smaller than calculated from exploded mass, chamber volume and primary particle size. Fig. 17 show the coincidence of number concentration data during the period (about 5 hours) dominated by coagulation, as observed in various chambers.

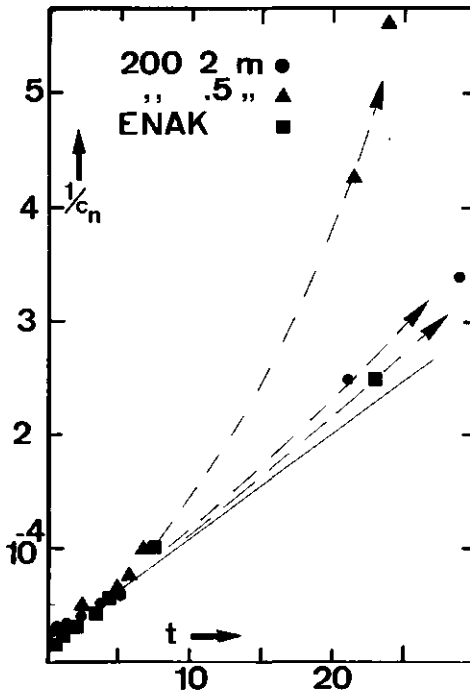


Fig. 17. Reciprocal value of the particle concentration  $1/c_n$  ( $\text{cm}^3$ ) as a function of time  $t$  (in hours) in various tanks.

After this period the decay curves diverge for different vessels. The decay due to coagulation can be described by Eqs. (1) and (2) within the measuring uncertainty. The coagulation constant calculated from a great number of experiments with Exploding Wire aerosols in containments of wide variety ranges from  $1.2 \times 10^{-9}$  to  $2.5 \times 10^{-9} \text{ cm}^3 \text{ sec}^{-1}$  which is a reasonable value for particles in the size range of 0.02 to 0.07  $\mu\text{m}$  [116].

In the initial period of pure (second order) coagulation the average mass  $\bar{m}$  per particle changes relatively fast compared to the later periods in which the (first order) deposition processes dominate. The rate of change of  $\bar{m}$  can be related to the coagulation constant K

$$\frac{d\bar{m}}{dt} = \frac{d}{dt} \left( \frac{c_m}{c_n} \right) = \frac{1}{c_n} \left( c_n \frac{dc_m}{dt} - c_m \frac{dc_n}{dt} \right) \quad (67)$$

In the absence of deposition  $\frac{dc_m}{dt} = 0$  and  $-\frac{dc_n}{dt} = Kc_n^2$ . If we assume the initial mass concentration equal to  $c_m(0)$ , then

$$\frac{d\bar{m}}{dt} = Kc_m(0) \quad (68)$$

Starting with an instantaneous aerosol concentration  $c_m(0) \approx 1 \text{ mg.m}^{-3}$  and taking  $K = 2 \times 10^{-9} \text{ cm}^3 \cdot \text{s}^{-1}$ , one arrives at  $\frac{d\bar{m}}{dt} \approx 10^{-14} \text{ g.h}^{-1}$ . This means that primary particles smaller than 0.1  $\mu\text{m}$  coagulate to particles of  $10^{-14} \text{ g}$  average mass in a time period of about one hour. Such particles have mass equivalent diameters ( $\rho = 1 \text{ g.cm}^{-3}$ ) of 0.3  $\mu\text{m}$ . Moreover, due to the second order kinetics of the coagulation process the rate of coagulation is so strongly dependent on initial number concentration  $c_n(0)$  that a period  $t(10\%)$  can be defined after which the number concentration is independent of  $c_n(0)$  within 10%. In Eq. (2) (section 2.1)  $\frac{1}{c_n(0)}$  should equal  $0.1 K t(10\%)$  under these conditions. Consequently, taking  $c_n(0) = 10^7 \text{ cm}^{-3}$  and  $K = 2 \times 10^{-9} \text{ cm}^3 \cdot \text{s}^{-1}$ ,  $t(10\%)$  amounts to 500 seconds or about 10 minutes. As a result, all aerosols of initial number concentrations larger than  $10^7 \text{ cm}^{-3}$  will have number concentrations equal to about  $10^6 \text{ cm}^{-3}$  within 10% of that value 10 minutes after their formation.

### 4.3. Aerosol deposition in unheated dry vessels

In this section experimental results will be discussed on the deposition of aerosols in unheated dry vessels. The theoretical background has been given in the sections 2.2.1 through 2.2.3 and 2.2.5 as far as stirred systems are concerned. In section 4.3.6 the occurrence of non-stirred deposition is discussed in view of some limited experimental data with reference to the theoretical section 2.5 on this subject.

#### 4.3.1. Quasi-monodisperse aerosols

In order to evaluate the relative importance of the various deposition processes responsible for aerosol decay in unheated containments, the decay of monodisperse polystyrene aerosols was studied in the 200 vessel (fig. 6) in its 2 m height position. The aerosols were produced directly in the vessel by spraying an aqueous suspension of polystyrene spheres (section 3.1) and subsequent drying in the vessel atmosphere. Electric discharging by means of a so-called neutralizer was considered unnecessary because of the electrically conductive metal vessel walls. The initial number concentration was kept sufficiently low ( $< 10^3 \text{ cm}^{-3}$ ) to have a negligible influence of coagulation on the number concentration decay even in the case of the lowest deposition rate. The number concentration was measured by taking electrostatically precipitated samples of known volume (section 3.3.2). This technique allows simultaneous measurement of the concentrations of multiplets by counting the singlets, doublets etc. individually.

Apart from an initial short period of filling of the vessel space and build up of multiplet particles the number concentration decays exponentially. Fig. 18 shows this for a few runs. The decay constants  $\beta$  obtained from such plots are given in Table IV. Particles with sizes larger than about  $0.5 \mu\text{m}$  dia have a deposition velocity equal to the Stokes settling velocity given by (17). In this range the measured decay constants equal  $\beta_s$  (as calculated from (17) and (18)) using  $\rho = 1.06 \text{ g.cm}^{-3}$ . This is shown in fig. 19, in which the fit between the measuring data beyond  $0.5 \mu\text{m}$  and equation (18) is evident. The deposition velocities of the multiplets and their related decay constants  $\beta_s$  have been calculated using the size factors  $f_n$  as reported by Stöber [94] and given in table IV.



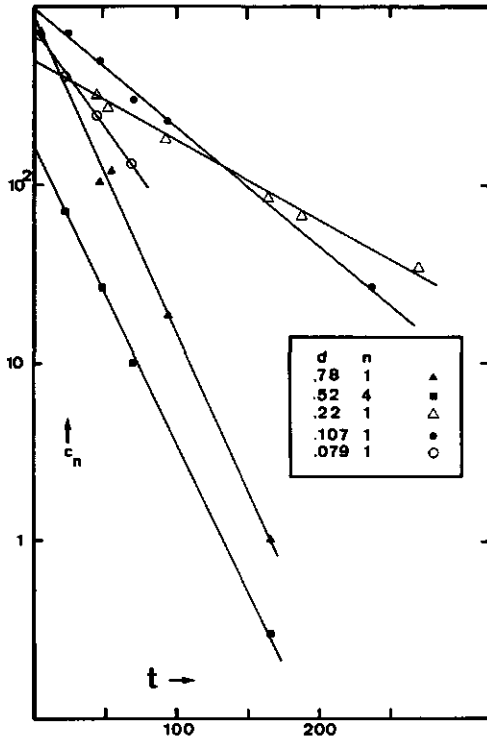


Fig. 18. Decay curves of some monodisperse aerosols in 200-vessel (2 m height).  $c_n$  in  $\text{cm}^{-3}$ ,  $t$  in hours,  $d$  in  $\mu\text{m}$ ;  $n$  = number of spheres per particle.

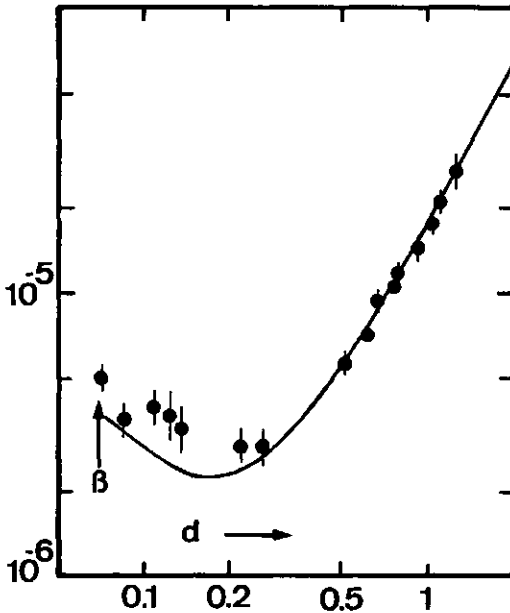


Fig. 19. Measured (solid dots) and calculated (line) decay constants  $\beta$  (in  $\text{s}^{-1}$ ) of quasi-monodisperse polystyrene aerosols in 200-vessel (2 m height) as a function of the diameter of the particles ( $d$  in  $\mu\text{m}$ ). See also Table IV.

The agreement between measured and calculated decay constants in the range of  $d > 0.5 \mu\text{m}$  supports the correctness of the stirred-settling model and, additionally, justifies Stöbers  $f_n$ -values and the underlying model of the aerodynamics of multiplet clusters [94].

In the small particle region an increase of the measured  $\beta$ -values, due to diffusional deposition, is to be expected. This is observed below  $0.2 \mu\text{m}$  dia (fig. 19). In this size region the wall loss of the aerosol will be governed by diffusion, and to some extent also by settling. A total decay constant  $\beta$  has been calculated for this combined diffusion and settling. The resulting  $\beta$ -values are listed in the last column of Table IV. The equations (15), (16), (17) and (18) have been used. The measured and calculated  $\beta$ -values agree only to a certain degree. The observed decay constants are roughly 30 % too high. This

could be due to an additional deposition mechanism. Probably, the electric charges on the particles (from their formation by spraying, which charges were not removed by a neutralizer) could have caused electrophoretic deposition. However, since the vessel walls consisted of steel, which is electrically conducting, this electrophoresis should have been due to image charges on the walls. A brief calculation using Eq. (45') shows the correct order of magnitude of this electric effect, namely about  $10^{-6} \text{ s}^{-1}$  (see pg. 50).

#### 4.3.2. Influence of aerosol formation parameters

The stability of an aerosol enclosed in a containment is directly related to the aerodynamic properties of the aerosol particles which in turn bear a relation to the way of formation of the particles. The Exploding Wire technique is particularly useful for the study of the effect of aerosol formation because the specific formation energy (Espec) of the aerosol generation can be easily measured and can be varied within reasonable limits. Fig. 20 shows the decay curves of gold aerosols formed with different Espec and with almost identical initial mass concentration  $c_m(o) = 5 \text{ mg m}^{-3}$  in the unheated 200-vessel. Obviously, aerosol stability increases with increasing specific formation energy. This can be understood because specific formation energy affects directly particle size (section 4.1). The fact that curves A ( $270 \text{ kJ.g}^{-1}$ ) and B ( $130 \text{ kJ.g}^{-1}$ ) coincide, puts in doubt on the correctness in this experiment of the value of  $270 \text{ kJ.g}^{-1}$ . Likely, incorrect mounting of the wire has occurred, leading to a lower Espec not much different from  $130 \text{ kJ.g}^{-1}$  in case A.

Increasing Espec the geometric median diameter  $d_{1g}$  decreases, the standard deviation remaining unchanged. According to Kops [89] (2.3) the aerodynamic diameter of a coagulate is proportional to the diameter of the constituting primary particles. However, the relation between aerodynamic diameter  $d_a$  of an aggregate and the number of primary particles  $n$  per aggregate is also of importance. Obviously, when  $d_a$  is proportional to  $n^{1/b} \times d_{1g}$ , there will be no influence of Espec on aerosol stability (still assuming  $c_m(o)$  constant) for  $b = 3$ . The value of  $b$  has been found to depend on  $n$ , viz.  $b = 3$  for  $n \geq 10^4$  and  $b = 6$  for  $n \leq 10^4$  [89]. After about 10 hours  $c_n \approx 10^4 \text{ cm}^{-3}$ ,  $c_m \approx 4 \text{ mg m}^{-3}$ . Since the primary particle diameter is of the order of  $0.02 \text{ }\mu\text{m}$ , it may be calculated that  $n \approx 10^3$  which in view of Kops' findings means  $b = 6$ .

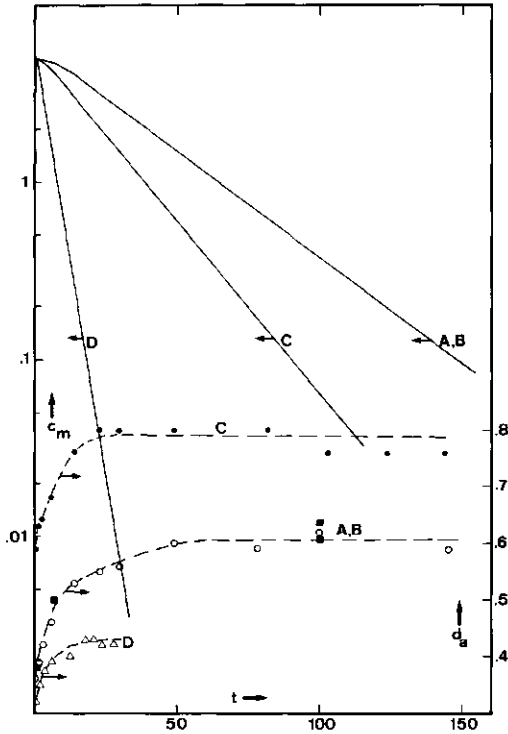


Fig. 20. Mass concentration ( $c_m$ , in  $\text{mg}/\text{m}^3$ ) and aerodynamic diameter ( $d_a$ , in  $\mu\text{m}$ ) of gold aerosol as a function of time ( $t$ , in hours) after explosive formation in 200 vessel (height = 2 m). A and B:  $\text{Espec} = 270$  and  $130$  kJ/g resp., no heating; C:  $\text{Espec} = 20$  kJ/g, no heating; D:  $\text{Espec} = 270$  kJ/g, heating power level = 200 W (see section 4.4.1.).

Consequently, for higher  $\text{Espec}$  smaller aerodynamic diameters ( $d_a \propto n^{1/6} d_{1g}$ ) are produced which in turn yields more stable aerosols in accordance with the observations (fig. 20). The  $b = 6$  region for  $n \leq 10^4$  is typical for finely dispersed coagulates of solid primary particles.

Any aerosol of liquid matter may form new spherical droplets upon coagulation and, consequently, the value of  $b$  will amount to 3 then. This means that a liquid aerosol (droplets in air, like mist, fog or

smog) after a certain period of coagulation aging will have an aerodynamic diameter irrespective of its original dispersion (usually related to the number of nuclei present at the moment of aerosol formation by condensation). Only the amount of condensable vapour (being the product of the rates of production or evaporation and time) determines the aerodynamic properties after this coagulation period. More insight has been obtained by measuring the aerodynamic diameter distribution of the aerosol during its decay in the vessel. The Stöber spiral centrifuge was used for this purpose. Mass aerodynamic size distributions were obtained with this apparatus by radioactive labelling of the gold aerosol by means of irradiation with neutrons of the gold wire prior to their explosive conversion into aerosol. Fig. 21 shows the logarithmic normal character of the aerodynamic size distribution found in this way.

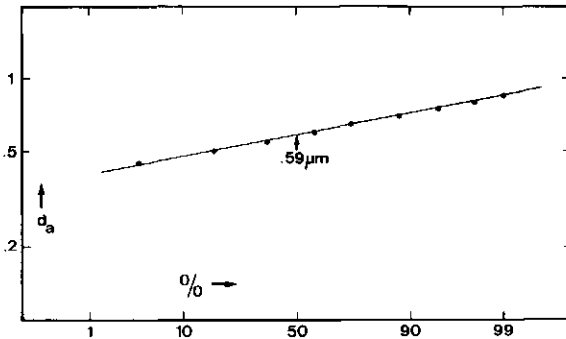


Fig. 21. Log-probability plot showing the log-normal character of the aerodynamic diameter ( $d_a$ , in  $\mu\text{m}$ ) distribution of a gold aerosol ( $c_m(o) = 5 \text{ mg/m}^3$ ,  $\text{Espec} = 130 \text{ kJ/g}$ ) after 100 hours aging in 200 vessel.

With a few exceptions (probably due to instrumental malfunctions) always log-normal distributions were obtained. The geometric median aerodynamic diameters increase initially (fig. 20). After about 20 hours the aerodynamic diameter  $d_a$  levels off and reaches an almost stationary value. During the initial period of 20 hours coagulation

governs the size distribution. Within a very short period ( $\leq 1$  hour) the geometric median  $d_a$  has reached a value of  $0.3 - 0.4 \mu\text{m}$ . Therefore, losses by diffusion to the walls will have been very small, which is also illustrated by the relatively small decrease of the mass concentration in this period and by the subsequent exponential decay of the aerosol mass concentration (fig. 20). When an additional and different deposition process would have been active in this initial stage, a change in the decay constants should have been observed during the course of the experiments.

The nearly constant aerodynamic size of the aerosol after about 20 hours is in agreement with the exponential aerosol decay. As concluded from the experiments with monodisperse particles (pg. 81), particles having aerodynamic diameters of  $0.5 \mu\text{m}$  and larger are removed predominantly by gravitational settling. Hence, the observed decay constant equals  $\beta_g$ . Using Eqs. (17) and (18) the "effective" aerodynamic diameter of the aerosol can be calculated. The results are represented in Table VI which table allows also comparison with the directly measured diameter.

There is a reasonable agreement (within 5%) between the aerodynamic diameters obtained by different methods. This supports the idea that stirred gravitational settling is the dominant deposition mechanism. However, for some unexplainable reason there is a small but systematic difference, viz. the "effective" aerodynamic diameter is systematically higher than the calculated one. This could be due to a small error in the calibration of the centrifuge used.

As explained in section 2.4 the exponential decay is an interesting phenomenon. When stirred gravitational settling is the only deposition process (as proved above) such a strongly size dependent process should influence the size distribution of the depositing aerosol considerably by removing the heaviest particles preferentially, which in turn would lead to a continuously changing decay constant. This conflicts with the findings. The explanation is found in the observed small geometric standard deviations  $(\sigma_a)_g$ . Table VI shows  $(\sigma_a)_g$  values of  $1.18 - 1.22$  which means that the aerosol is almost monodisperse! This proves that the observed decay curves are exponential due to the fact that the aerosol particles have an aerodynamic size distribution which remains almost unchanged during further deposition because the size distribution

is so narrow ( $\sigma_g \approx 1.2$ ) and not because of a self-preserving size distribution process, which could be an alternative explanation (pg. 54). Preferentially, coagulation is between particles of different size ( $K$  increases with increasing size dispersity  $|43|$ ) thereby removing the smallest particles and adding only slightly to the size of the coarse ones. Moreover, the  $n^{1/6}$  dependence of  $d_a$  of solid aggregates could be part of the explanation of this narrow  $d_a$ -distribution. As a result, any additional particle attached to a coarse one produces only a small increase of the aerodynamic diameter of the coagulate.

#### 4.3.3. Influence of vessel height

The vertical dimensions of an aerosol enclosure are of importance for stirred gravitational settling of the particles onto the vessel floor (section 2.2.3). Generally, the effective vessel height  $h$  (defined as the ratio of the vessel volume to the surface area of the horizontal projection of the upward facing vessel walls) is the relevant parameter in the aerosol decay constant. However, the (well-defined) height of a vessel may be used in case of vessels of simple shapes.

The aerosol will coagulate rapidly when it is formed instantaneously (e.g. by "explosive" generation). Coagulation will continue to govern the number concentration (meanwhile coarsening the particle size distribution) until the coagulation rate  $(\frac{dc_n}{dt})_{coag}$  is negligible (say 10%) compared to the rate of stirred gravitational deposition  $(\frac{dc_n}{dt})_s$ . This transition is defined by a point of time  $t_t$  given by

$$\left(\frac{dc_n}{dt}\right)_{coag} = 0.1 \left(\frac{dc_n}{dt}\right)_s \quad (69)$$

which by using equations (1) and (4), can be transformed into

$$Kc_n(t_t) = 0.1 \beta_s = 0.1 \frac{v}{h} \quad (70)$$

For vessels with a large height, this leads to a relatively small  $c_n(t_t)$  value. Consequently, in tall vessels coagulation can proceed relatively long and as a result particles grow to larger sizes. As an example, for an aerosol of  $0.5 \mu m$  aerodynamic diameter in a vessel of  $h = 1 m$  the concentration  $c_n(t_t)$  below which coagulation has almost

ceased is  $10^3 \text{ cm}^{-3}$ .

Some experiments were performed in the matchbox-like 200-vessel (see Table III) which vessel has been designed in view of having the possibility of variation of vessel height by means of merely changing vessel orientation. This is an attractive approach because it involves the variation of only one vessel parameter (viz. height) keeping other parameters (e.g. wall surface area) unchanged. The experimental results for gold aerosols of  $5 \text{ mg.m}^{-3}$  initial mass concentration are summarized in Table VII. Clearly, lowering the vessel height  $h$  from 2 m to 0.5 m decreases the ultimate ( $t \rightarrow \infty$ ) aerodynamic diameter of the aerosol from  $1.0 \mu\text{m}$  to  $0.72 \mu\text{m}$  in accordance with the considerations given above. Fig. 22 further elucidates this, in particular in terms of  $\bar{m}$ , the average mass per particle. All these curves show the same typical course, viz. a fast initial increase of  $\bar{m}$  followed by a maximum and a long-lasting decrease which likely approaches a final  $\bar{m}$  value. The fast initial increase of the average mass  $\bar{m}$  per particle, obviously, is due to coagulation since it is mainly the result of the fast decrease of the number concentration  $c_n$ . The long-term decrease of the average mass  $\bar{m}$  per particle must be the result of the selective removal of the coarse particles due to gravitational settling because the effect shown is clearly height related. The maximum shifts to later points of time and reaches higher values for larger vessel heights. This behaviour can be understood from equations (69) and (70). The decrease of  $c_n(t_t)$  for taller vessels implies that  $\bar{m}$  reaches a higher value at a later point of time. Or, in other words, the stirred gravitational deposition removes particles with a higher rate for decreasing heights, thereby shortening the period of "pure" coagulation and giving rise to a lower maximum value of  $\bar{m}$ .



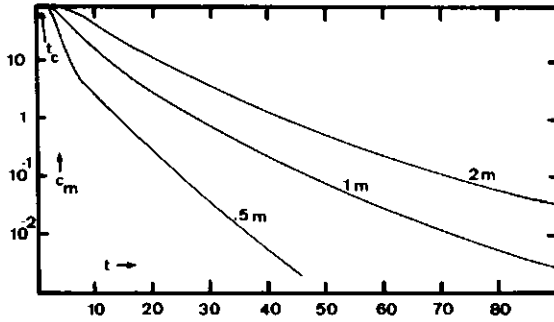


Fig. 22a. Decay of the mass concentration of gold aerosol in "200"-tank. The height of the tank is varied by turning the tank at time  $t_c$ .  $E_{spec} = 20 \text{ kJ/g} \cdot c_m$  in  $\text{mg} \cdot \text{m}^{-3}$  and  $t$  in hours.

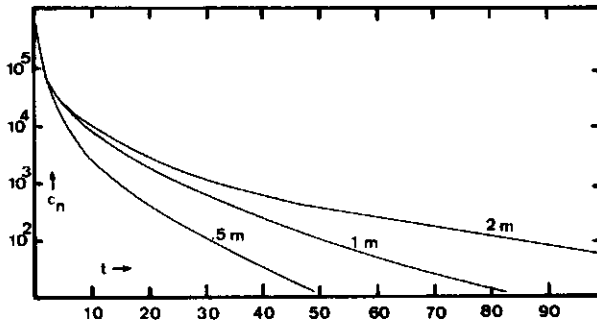


Fig. 22b. Decay of the particle number concentration of gold aerosol in "200"-tank. The height of the tank is varied.  $E_{spec} = 20 \text{ kJ/g}$ ;  $c_m(o) = 100 \text{ mg/m}^3$ .  $c_n$  in  $\text{cm}^{-3}$  and  $t$  in hours.

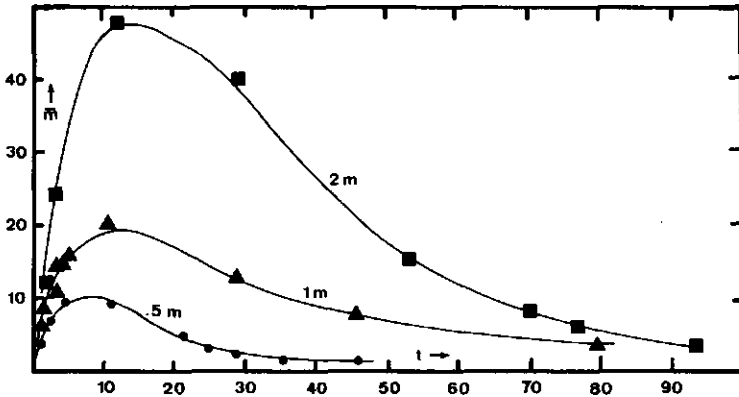


Fig. 22c. Course of the mean particle mass of gold aerosol in "200"-tank. The influence of height variation is shown.  $E_{spec} = 20 \text{ kJ/g}$ ;  $c_m(o) = 100 \text{ mg/m}^3$ .  $\bar{m}$  in 0.1 pg and  $t$  in hours.

#### 4.3.4. Measurement of dynamic shape factors from decay curves of mass and number concentration

From the above given results (sections 4.3.1 and 4.3.2) it became clear that aerosol decay constants can be used for calculation of aerodynamic properties of aerosols, the aerodynamic diameter  $d_a$  and the dynamic shape factor  $\kappa$  (Eq. (47)).

This decay curve method will be applied in this section to a large number of experimental data which are available on aerosol decay in various vessels. Also experiments have been performed specially focussed on comparing the decay curve method with alternatives for measurement of aerodynamic aerosol properties, like the spiral centrifuge. A survey of these possibilities for assessment of aerodynamic properties is given.

Three different experimental approaches are possible.

- A) Firstly, one may use a  $d_a$ -classifying aerosol sampling device like the Stöber centrifuge. This is the technique originally applied at ECN by Kops [89]. Mass and number of aerosol particles in  $d_a$ -fractionated

samples give the average mass  $\bar{m}$  per aggregate of known  $d_a$ . In combination with (47)  $\kappa$  can now be calculated as a function of  $d_a$ , these measurements making use of

$$d_e = \sqrt[3]{\frac{6\bar{m}}{\pi\rho}} \quad (71)$$

$d_e$  calculated in this way is not the real average mass equivalent diameter, but due to lack of information on the mass spectrum of the aerosol particles probably a slightly different  $d_e$  value should be used actually, the difference being related to the standard deviation of the mass distribution.

- B) The second approach utilizes aerosol behaviour inside aerosol chambers. Decay curves of mass ( $c_m$ ) and number ( $c_n$ ) concentrations are the basic experimental data. These decay curves are exponential after an initial (coagulation) period. Usually, the dispersity of the aerodynamic diameter distribution is small ( $\sigma_g \approx 1.2$ ) after this coagulation period (pg. 85). For particles larger than  $0.5 \mu\text{m}$  the decay constant  $\beta_s$  is related to  $d_a$  (pg. 81). Using Eqs. (17) and (18)  $d_a$  can be calculated now from  $\beta_s$  and  $h$

$$\beta_s = v_s \frac{S_f}{V} = \frac{v_s}{h} = \frac{\rho_o g}{18 \eta} d_a^2 F(d_a) \frac{1}{h} \quad (72)$$

where  $v_s$  is the Stokes settling velocity. The inverse chamber height  $\frac{1}{h}$  equals the ratio of floor surface area  $S_f$  to chamber volume  $V$  for chambers of undefined height.  $\beta_s$  values were obtained from  $c_m$  decay curves. It has been shown that  $d_a$  values calculated from these decay curves by means of (72) correspond very well to those from  $d_a$  distributions measured with the aid of a spiral centrifuge (section 3.3.4). Similarly, the behaviour of monodisperse aerosols in a  $1 \text{ m}^3$  chamber supports this also (pg. 81). The average mass  $m$  of a particle (necessary for calculation of  $d_e$ ) is found by dividing the values of  $c_m$  and  $c_n$  obtained for the same period  $\beta_s$  is pertaining to. Mass concentration decay curves should be used to obtain  $\beta_s$  for two reasons. Firstly, mass concentration is not affected by coagulation. No other deposition processes than stirred settling being active, these measuring data are the most relevant for calculations using (72).

Secondly, the number concentration data are far less accurate. This is true in particular in the lower concentration range which must be used in order to avoid influence of coagulation on the decay rate.

C) A third approach should be mentioned here, although it is limited to cluster-type aggregates only. This method is based on Kops's investigations into the aerodynamics of aggregates [89] and an additional analysis of his results by Walkenhorst [117]. The cluster-type aggregates generally have spherical appearance in spite of their marked fluffiness. This spherical appearance fits the independence of  $\kappa$  on  $n$ , provided these (larger) aggregates also have a nearly constant packing density  $\rho_{sp}$ . The clusters have a spatial diameter  $d_{sp}$  when observed by low resolution techniques. They can be described by the following relations:

- the equality of the mass of the cluster-type aggregate and its mass equivalent particle, leading to

$$\rho_{sp} d_{sp}^3 = \rho_e d_e^3 \quad (73)$$

- the equality of the settling velocities of these aggregates and their aerodynamic equivalent, yielding

$$\rho_{sp} d_{sp}^2 F(d_{sp}) = \rho_o d_a^2 F(d_a) \quad (74)$$

Substitution of (73) and (74) into (47) yields

$$\kappa = \frac{d_{sp}}{d_e} \frac{F(d_e) \cdot F(d_a)}{F^2(d_{sp})} \approx \frac{d_{sp}}{d_e} F(d_e) \cdot F(d_a) \quad (75)$$

$F^2(d_{sp}) \approx 1$  for the large cluster-type particles. Table VIII shows that the experimental data from Kops [89] lead to  $\kappa$  values which are nearly independent of the aggregate size. The dynamic shape factor equals  $15.5 \pm 1.5$ .

In case of these aerosols also microstructure data (geometric median diameter  $d_{lg}$  and geometric standard deviation  $\sigma_{lg}$ ) were available, enabling simultaneous calculation of the average number  $\bar{n}$  of primary

particles per coagulate from  $\bar{n}$ ,  $\rho$ ,  $d_{lg}$  and  $\sigma_{lg}$

$$\bar{n} = \frac{6\bar{m}}{\pi\rho d_{lg}^3 \exp(4.5 \ln^2 \sigma_{lg})} \quad (76)$$

Fig. 23 represents the results of  $\kappa$  measurements as a function of the number  $n$  of primaries per aggregate from centrifuge analysis of four runs with  $U_3O_8$  aerosols and one run with Cu oxide aerosol in the 100-vessel. Table IX gives additional information. Closer examination of these data has revealed  $\frac{\kappa}{F(d_e)}$  to obey Eq. (48) very well in case of  $U_3O_8$ .  $R_1 F_1(Kn)$  equals 3.1 in the range of  $n$  up to  $8.1 \times 10^3$ . This fits fairly Kops observations on four different materials [89] from which a value of 2.9 for  $R_1 F_1(Kn)$  can be derived for our primary particle size ( $0.026 \mu m$ ). The copper oxide run shows a similar relation though with a worse fit to Eq. (48) (see fig. 23).

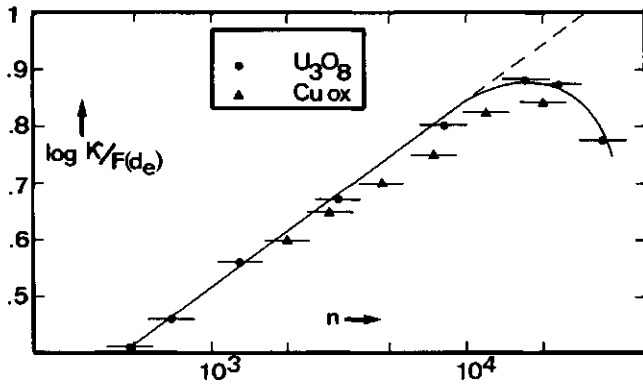


Fig. 23. Ratio of dynamic shape factor  $\kappa$  to the slip correction factor  $F(d_e)$  of aggregates of  $U_3O_8$  and copper oxide as a function of the number  $n$  of primary particles per aggregate. Results from centrifuge analysis (method A).

Larger aggregates with  $n > 10^4$  deviate from Eq. (48) and its underlying theory on chain-like aggregates. However,  $\frac{\kappa}{F(d_e)}$  does not approach a constant value, which implies a constant packing density as found by Kops [89] and reflected by Eq. (49). Instead  $\frac{\kappa}{F(d_e)}$  and  $\kappa$  go through

a maximum and decrease for  $n > 2 \times 10^4$ . This decrease was also observed by Allen [91] in the measuring range of  $5 \times 10^2 < n < 10^4$ , though at much lower  $\kappa$  values. The implications of this phenomenon will be dealt with later on.

The decay curves gave  $d_a$  values (Eq. (72)) which are in good agreement with the centrifuge measurements (Cu oxide: 0.45  $\mu\text{m}$  and 0.41  $\mu\text{m}$ , resp., and  $\text{U}_3\text{O}_8$ : identical, viz. 0.78  $\mu\text{m}$ ). Again small standard deviations (1.26 and 1.22) have been obtained which once again explain the observed exponential decay of the aerosols. This agreement, together with the above given evidence, gives additional confidence to measuring method B. The results on  $\log \frac{\kappa}{F(d_e)}$  obtained with this technique (7.0 and 8.0 for  $\text{U}_3\text{O}_8$  and Cu oxide, resp.) have been plotted in fig. 24.

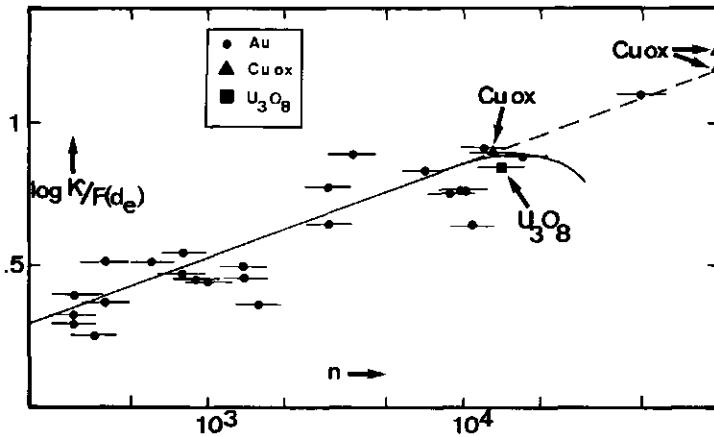


Fig. 24.  $\frac{\kappa}{F(d_e)}$  as a function of the number  $n$  of primary particles per aggregate of various materials (mainly Au(●) but also  $\text{U}_3\text{O}_8$ (■) and Cu oxide(▲) as obtained from analysis of decay curves (method B). The solid line represents the results produced by the spiral centrifuge (method A). The dashed line gives the extension for  $n > 10^4$  (method B).

Obviously, the centrifuge results (method A) and the decay curve results (method B) compare very well. About thirty sets of experimental data ( $c_m$ ,  $c_n$ , microstructure) on aerosol behaviour inside various chambers

(from 75 liters to 20 m<sup>3</sup>) have been available for analysis according to method B. These sets comprise experiments with gold and copper oxide aerosols, both generated by means of the Exploding Wire technique. The  $c_m$ ,  $c_n$  and microstructure data have been treated in a way similar to the U<sub>3</sub>O<sub>8</sub> and Cu oxide experimental data above. Fig. 24 represents these additional data together with the relation  $\frac{\kappa}{F(d_e)} = 0.33 n^{1/3}$  obtained for the U<sub>3</sub>O<sub>8</sub> aerosols. Although with considerable scatter, all the measuring points are grouped around this line; statistical analysis gave (with a coefficient of correlation  $r = 0.94$ ) a best fit to  $\frac{\kappa}{F(d_e)} = 0.28 n^{0.348}$ . The scatter around the best-fitting curve is due to the uncertainty in the available information on the primary particles sizes  $d_{lg}$ . From equation (76) it is obvious that  $n$  is very sensitive to changes in  $d_{lg}$  due to its proportionality to  $d_{lg}^{-3}$ . Consequently, also these measurements support the validity of Eq. (48) over a large range of  $n$  values and in turn indicate that these aerosols behave as "chainlike" aggregates.

The phenomenon of decreasing or constant  $\kappa$  with increasing  $n$  requires further discussion. In summary, Allen [91] found  $\kappa$  decreasing even at small  $\kappa$  values in the range  $5 \times 10^2 < n < 10^4$ . In contrast to this, Kops [89] and the author (both using the centrifuge) found the deviation from Eq. (48) to occur for  $n > 5 \times 10^3$ . With method B, however, no indication is found of this deviation from Eq. (48) up to  $n = 10^5$  (fig. 24). An explanation for these discrepancies could be the following. Close examination of electron micrographs has shown that larger aggregates consist of typical ringshaped elements of a certain ring size. This gives the impression that during coagulation the chains can grow to critical sizes before there is a significant chance to have the chain touching the body of the aggregate. That the chains are not rigidly fixed to the body of the aggregate has been observed by Whytlaw-Gray [118] by means of his ultra microscope: "The chains or strings seem flexible, and twist and whirl about in a striking way". This critical size of the chains before closing to rings will be influenced by external forces like those in turbulences. Obviously, the same is valid to the aggregate's packing density. This could be an explanation for the different findings between method A (centrifuge) and method B (decay curves). During the transport of the aggregates to the centrifuge they could have been compacted in this way whereas in the chamber atmospheres there are not such forces. An additional process may be

responsible for the greatly differing results of Allen et al. [91]. These investigators have used a continuous aerosol source, producing primary particles which are brought into an aging chamber of 25 liter from which the centrifuge samples were taken. This should lead to considerable coagulation of primaries with larger aggregates which results in higher packing densities than when coagulation takes place between chain-like structures. Due to this coagulation in their aging chamber between primaries and already formed aggregates one may expect an increasing packing density for larger aggregates in agreement with Allen's observations. However, also external forces e.g. from turbulences could have influenced the shape of their aggregates giving rise to the low  $\kappa$  values.

To our experience usually solid aggregates have aerodynamic diameters in the range of 0.1  $\mu\text{m}$  up to about 2  $\mu\text{m}$ . When exposed to atmospheres of high relative humidity (> 95%) sorption of water vapour into the regions of contact between the primaries will occur because of the negative curvature of these regions. This condensed water exerts internal forces on the aggregate due to its surface tension. According to experience of the author this will cause compaction of the aggregate to a dense close-packed cluster. Such a change of shape should affect the aggregate's aerodynamic behaviour. This could be of importance for aerosol behaviour in the human respiratory tract. Assuming the Lung Model of the Task Group on Lung Dynamics of the International Commission on Radiological Protection to be roughly correct, the aggregates should be able to penetrate into the pulmonary region where they are deposited with an efficiency of about 30%. It is well-known that the human respiratory system has a relative humidity of about 99%. Any shape change due to condensation of water on inhaled aggregates, resulting in an increased aerodynamic diameter, should influence the deposition efficiency in the pulmonary region.

The shape change ultimately leads to a nearly spherical particle which in fact is the mass equivalent of the aggregate, with a diameter  $d_e$  and density  $\rho$  (we assume the amount of condensed water to be negligible). The aerodynamic diameter  $d'_a$  of the new particle is given by the equality between the Stokes settling velocities of the mass equivalent of the aggregate and the aerodynamic equivalent



$$\frac{\rho_e g d_e^2 F(d_e)}{18 \eta} = \frac{\rho_o g (d'_a)^2 F(d'_a)}{18 \eta} \quad (77)$$

Combination of (77) with the relation Eq. (47) for the dynamic shape factor  $\kappa$  of the aggregate leads to

$$d'_a = d_a \sqrt{\kappa \frac{F(d_a)}{F(d'_a)}} \quad (78)$$

Table X gives the factor  $f$  by which the aerodynamic diameter of an aggregate is increased due to the compaction

$$f = \frac{d'_a}{d_a} = \sqrt{\kappa \frac{F(d_a)}{F(d'_a)}} \quad (79)$$

using the centrifuge measurements on copper oxide and  $U_3O_8$  aerosols from Table IX. In the region of  $n < 10^4$  (low  $d_a$  values) where there is no important discrepancy between the findings by Kops and by the author,  $f$  increases with increasing  $n$ . The foregoing analysis of the causes of the discrepancy for the region  $n > 10^4$  suggests that  $\frac{\kappa}{F(d_e)} = 0.33 n^{1/3}$  should be valid. Since in this range all slip factors tend to become unity,  $f$  should follow

$$f = \sqrt{\kappa} = \sqrt{0.33 n^{1/3}} \quad (80)$$

which means that  $f$  should begin to increase in absence of slip. The value of  $f$  will be about 4 at  $d_a \approx 1 \mu m$ . If it is true that  $\kappa$  has a maximum value (as Kops [89] observed) amounting to about 15 (Table VIII)  $f$  should level off to around 4.

In summary, as a rule the shape change of a solid aggregate in a humid atmosphere results in a significant increase of the aerodynamic diameter. The aggregates possessing submicron aerodynamic diameters are transformed into spherical particles with an aerodynamic diameter of  $1 \mu m$  to  $3 \mu m$ . Consequently, the deposition of aggregates in the pulmonary region will be enhanced.

#### 4.3.5. Influence of the initial aerosol concentration

The initial mass concentration  $c_m(o)$  of an aerosol formed in a vessel influences its behaviour. It is possible to identify the differences in aerosol behaviour due to  $c_m(o)$  variation by keeping other parameters constant. Qualitatively, the most remarkable feature is the large and direct influence of  $c_m(o)$  variation on the coagulation process. This is due to the second order kinetics of the coagulation process, its initial rate being proportional to  $c_n^2(o)$ , which in turn is proportional to  $c_m^2(o)$ . Dependent on the decay constant  $\beta$  of the aerosol removal process (which is stirred gravitational settling in case of not too low  $c_m(o)$ ), considerable aerosol mass removal rates will result (pg. 86). Higher  $c_m(o)$  values lead to higher  $d_a$  values of the aerosol via the coagulation, which means an increased decay constant  $\beta_s$  for stirred settling.

This is actually what is observed and is illustrated in fig. 25.

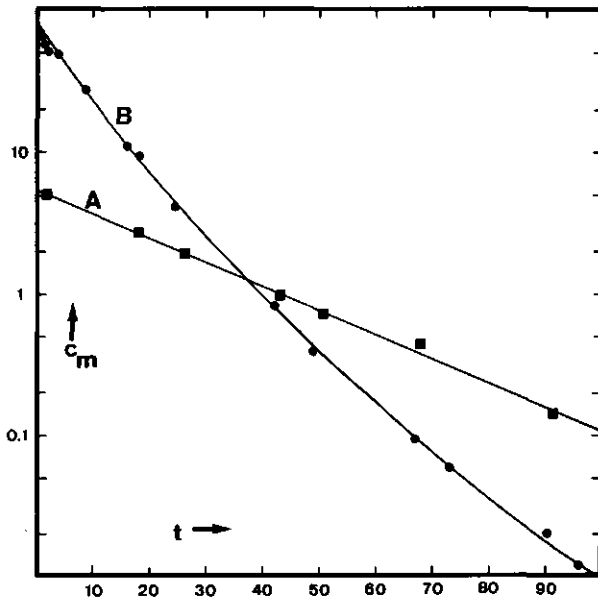


Fig. 25. Mass concentration  $c_m$  (in  $\text{mg.m}^{-3}$ ) of gold aerosol only differing in initial mass concentration as a function of time  $t$  (in hours).  $E_{\text{spec}} = 20 \text{ kJ.g}^{-1}$ . 200-vessel in 2 m-height position.

The results displayed concern two gold aerosols decaying in the 200-vessel in its 2m upright position. Though the values of  $c_m(o)$  differ considerably (80 and 5  $\text{mg}\cdot\text{m}^{-3}$ ), the aerosol formation has been kept carefully identical (20 kJ/g resulting in primary particles of  $d_{1g} = 0.030 \mu\text{m}$  and  $\sigma_{1g} = 1.5$ ).

A more quantitative description of the aerosol stability can be given by comparing the calculated and observed decay constants. The approach of the previous section can be used for the analysis of the aerosol processes. Moreover, an important simplification can be achieved by taking into account that after a certain period the number concentration is almost independent of  $c_n(o)$  (pg. 78). Using the average mass  $\bar{m}(o)$  at  $t = o$  (which according to Table V is about  $6 \times 10^{-16} \text{g}$ ) the initial number concentrations of  $1.4 \times 10^8 \text{ cm}^{-3}$  and  $8.9 \times 10^6 \text{ cm}^{-3}$  are obtained for  $c_m(o) = 80 \text{ mg}\cdot\text{m}^{-3}$  case B and  $5 \text{ mg}\cdot\text{m}^{-3}$  case A resp. By combination of Eqs. (47) and (72) one obtains a relation between the decay constant  $\beta_s$ , the dynamic shape factor  $\kappa$  and the mass equivalent diameter  $d_e$  of the aerosol

$$\beta_s = \frac{g\rho d_e^2 F(d_e)}{18 \eta \kappa} \frac{1}{h} \quad (81)$$

Substitution of Eq. (71) into (81) and using  $\frac{\kappa}{F(d_e)} = \frac{\bar{n}^{1/3}}{3}$  (4.3.4) as well as  $\bar{n} \approx \frac{\bar{m}}{\bar{m}(o)}$ , yields

$$\beta_s = \frac{g}{\eta} \frac{1}{h} \left\{ \frac{6\rho}{\pi} \bar{m}(o) \bar{m} \right\}^{1/3} F^2(d_e) \quad (82)$$

This can be reduced to

$$\beta_s = 0.16 \bar{m}^{-1/3} F^2(d_e) \quad (83)$$

for our case of the two gold aerosols ( $\rho = 19 \text{ g}\cdot\text{cm}^{-3}$ ,  $h = 200 \text{ cm}$  and  $\bar{m}(o) \approx 6 \times 10^{-16} \text{ g}$  (Tabel V)) in the 200-vessel.  $F(d_e)$ , the slip correction factor for a particle  $d_e$ , can be obtained from  $\bar{m}$  using Eqs. (8) and (71).  $F(d_e)$  amounts to about 1.5.

Since  $\bar{m} = \frac{c_m}{c_n}$ , and also  $c_n = \frac{1}{Kt}$  (for  $t > 10$  minutes, see pg. 78) (83) can be further transformed into

$$\beta_s = 0.16 K^{1/3} (c_m t)^{1/3} F^2(d_e) \quad (84)$$

This relation describes the aerosol deposition rate as a function of mass concentration and time, assuming coagulation to be the dominant process shaping the size distribution.

Three different points of time after aerosol formation have been arbitrarily chosen for evaluation of equation (84), viz. 0.25; 2.5 and 5 hours. Table XI allows comparison between the calculated and measured (from fig. 24) half-lives ( $K = 1.5 \times 10^{-9} \text{ cm}^3 \cdot \text{s}^{-1}$ ; see pg.78). The agreement between calculation and measurement is generally good. Particularly, the matching is very good in case B, the high mass concentration aerosol. This is surprising in view of the uncertainty involved in the measured half-life of case B as may be obvious from fig. 25. Less satisfactory is the trend in the calculated half-lives, especially in case A. This trend is not borne out by the fact that the decay is observed to be nicely exponential. An explanation may be found in the  $c_n$ -value ( $= \frac{1}{Kt}$ ) substituted in Eq. (83), leading to a cube root in relation to  $\beta_s$  in Eq. (84). The  $c_n$ -value calculated in this manner could have been too high due to the neglect of enhanced coagulation during the expansion of the aerosol cloud after its formation (see pg. 76). This can be translated as a  $c_n$ -value too large or a  $t$ -value too small. Consequently,  $\beta_s$  has been calculated too small ( $t_{\frac{1}{2}}$  too high) and this error is larger the shorter the time period after aerosol production (smaller  $t$ -values). Obviously, this applies also to case B though to a less extent. Removal of the trend in  $t_{\frac{1}{2}}$  requires a correction of  $-0.25\text{h}$  at  $t=0.25\text{h}$  which is the cloud expansion time (pg.76).

One feature of the decay curves of fig. 25 has not yet been dealt with, viz. the increasing half-life of the aerosol B as time proceeds. To our opinion this is a typical feature of higher  $c_m(o)$  aerosols. The following explanation could be valid. Coagulation initially increases  $\bar{m}$  and  $d_a$ , leading to relatively large values of  $\bar{m}$  and  $d_a$ . Soon after or during this period stirred settling starts removing the larger particles at a high rate from the atmosphere. Consequently,  $\bar{m}$  and  $d_a$  will begin to decrease and this leads to an increasing aerosol stability and increased half-life. It is impossible to make a quantitative model for the behaviour of such aerosols of high initial mass concentrations without using complicated analysis of the time dependent aerosol size distribution.

Increase of the initial mass concentration to high levels, should give rise to inhomogeneous filling of the vessel since the large particles which are formed either directly or by coagulation, will have large settling velocities compared to the convective flows in the vessel. Eq. (56) allows calculation of the maximum particle size which can remain well-stirred in a vessel. No special experiments have been performed in order to investigate this effect. A few observations on this subject will be made in the next section.

#### 4.3.6. Non-stirred conditions

As treated in section 2.5 and mentioned in the previous section, particles can be too large to keep them well-stirred. The other extreme case could be that particles are so small that their diffusive deposition velocity is comparable to the atmospheric flow velocities. Decreased atmosphere flow velocities may be caused by certain thermodynamic conditions existent in the vessel atmosphere (pg. 58). Experimental results for such cases, however, with the exception of diffusion, are dealt with in the following sections.

##### 4.3.6.1. Non-stirred settling

In a number of cases aerosols of larger initial aerosol mass concentrations ( $> 100 \text{ mg.m}^{-3}$ ) have been investigated but only in our smallest vessel ("300", see Tabel III). This leads to spatial inhomogeneity. Fig. 26 shows two experiments with  $c_m(o) \approx 100 \text{ mg.m}^{-3}$  where aerosol mass concentrations have been measured at two heights (10 cm and 40 cm). There is an initial period of non-stirred settling with higher concentrations in the lower part of the 300-vessel. After this exceptional period, aerosol deposition is again of the stirred type. Then the aerosols disappear with half-lives of about 4 hours which means that the aerosol has an effective aerodynamic diameter of about  $0.8 \mu\text{m}$ . Eq. (56) tells us that an effective temperature difference  $\Delta T$  of  $10^{-7} \text{ K}$  between walls and vessel atmosphere is large enough to keep the deposition of such aerosols well stirred. Only special measures (the upper part of the vessel warmer than the lower part) can prevent the aerosol from being well-stirred.

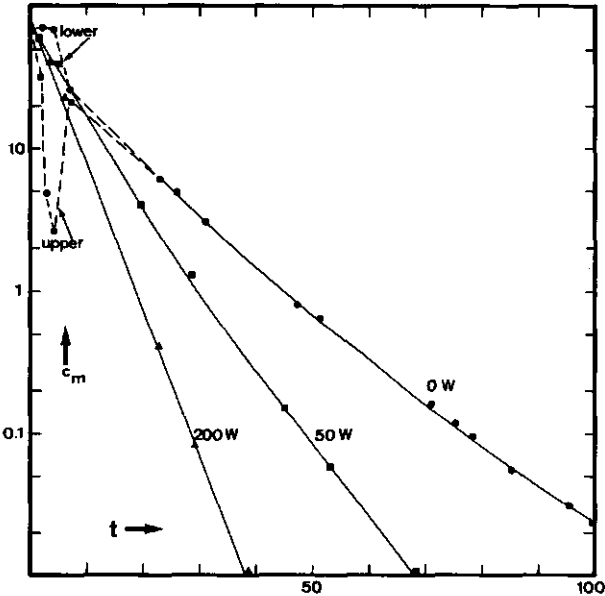


Fig. 26. Mass concentration  $c_m$  (in  $\text{mg}\cdot\text{m}^{-3}$ ) as a function of time  $t$  (hours) of gold aerosol in 100-vessel (90% thermal insulation of the walls). Heater on floor center: 0 W, 50 W and 200 W. Local inhomogeneities are visible up till 7 hours at "lower" and "upper" sampling ports in absence of heating.

Another extreme case investigated has been a gold aerosol of  $c_m(o) = 500 \text{ mg}\cdot\text{m}^{-3}$  in the 100-vessel (Table III). Although a half-life as small as 3 hours has been observed (consequently  $d_a \approx 1.8 \mu\text{m}$ ) the aerosol was removed by stirred deposition, as could be established from the equality of samples taken at different heights. From Eq. (56) it follows that  $\Delta T$  must have been larger than  $10^{-6}$  K.

The convective flows inside aerosol vessels arise from heat transfer between the laboratory atmosphere and the vessel. The response of the vessel walls as a transfer medium for heat is of importance for the coupling between the two media. For the smaller 300-vessel (75 liters) with relatively thick walls, obviously, a smaller effective  $\Delta T$  exists between gas and wall compared to the larger 100-vessel ( $1.2 \text{ m}^3$ ).

From Eq. (25) one obtains lowest estimates of related heating powers of the order of  $\mu\text{W}$  in the vessels. The power densities in the surrounding atmosphere will be roughly of the order of  $1 \text{ W.m}^{-3}$ . This means that considerable "damping" by the walls of the heat flows must occur before the critical  $\mu\text{W}$  levels inside the vessels are achieved.

#### 4.3.6.2. Stratification

In section 2.5 a boundary condition has been derived for the occurrence of atmospheric stability in a containment with a heated pool of liquid on the floor. Experiments have been conducted in order to validate this boundary condition. Twelve different vapour/gas systems were studied in PERVEX, the rectangular 150 liter plexiglass box with a brass floor. The floor and a pool of liquid above it were heated homogeneously, as a rule with a power level of 60W. The box pressure was atmospheric. The vertical temperature profile was measured by means of a movable thermocouple. This vertical temperature scanning in the box has revealed that two significantly different profiles are possible: either, apart from a boundary layer near the walls, a larger part of the box atmosphere is isothermal, or there is a steady decrease of temperature upwards. In accordance with Eqs. (58), (59), and (60), the cases correspond with stirred and stagnant atmospheres, respectively. In addition to this, when aerosol is introduced into the box, illumination by means of an electric torch of the droplets formed gives an additional, direct opportunity to observe the stability of the atmosphere. These observations have been always in accordance with the temperature profile measured.

Figure 27 shows the temperature profiles of five different liquid-air systems. The heaviest two liquids appear to develop a stagnant atmosphere whereas the three alcohols used (*b*, *c*, and *d*) yield a stirred atmosphere, apart from the boundary layers ( $\sim 1 \text{ cm}$ ) near the floor and the top of the tank. However, it is apparent that the heaviest alcohol (isopropyl alcohol, represented by the solid line) has a slight tendency to develop a stable layer in the lowest 10 cm. Another effect related to the degree of convection of the atmosphere is the decreased floor temperature in case of convection stirring. Convection, as an additional heat conductive process, will decrease the heat resistance between the heat source and the heat absorbing surroundings.

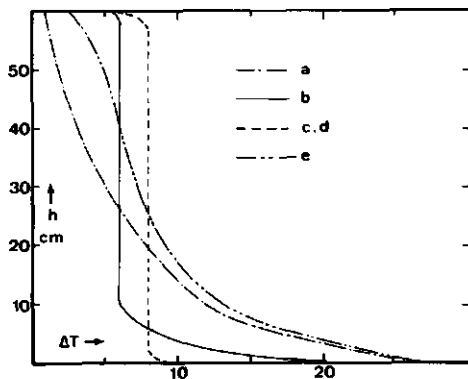


Fig. 27. Vertical temperature profiles of five different liquid-air systems at 60 W heating; *a* = di-isopropylether, *b* = isopropyl alcohol, *c* and *d* = ethyl and methyl alcohol, *e* = carbon tetrachloride.

Change of the gaseous component can also drastically alter the convection situation as is shown in fig. 28.

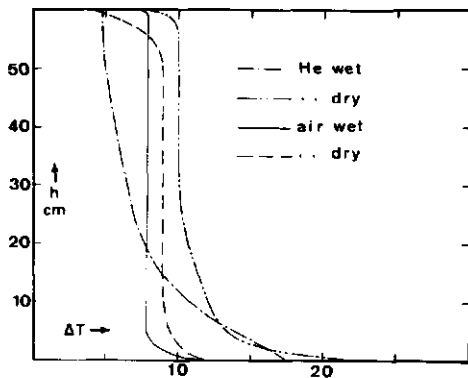


Fig. 28. Vertical temperature profiles of helium-air with and without a water layer on the floor. Power is 60 W.



Comparison of the curves for water-air and water-helium reveals that due to the relatively small molecular mass of helium the atmosphere is nonisothermal, corresponding with an inhomogeneous vapour-gas filling of the box. By comparison with the fairly isothermal situation in pure helium, it is seen that the watervapour-helium system is stagnant due to the presence of the heavier water vapour. This stabilizing effect of water vapour is absent in case of air in accordance with the larger molecular mass of air compared to water.

The influence of heating power on atmospheric stability has not been studied systematically but a few experiments exhibit the effects to be expected (see fig. 29). When the heating power is decreased from 60 to 30 W, the temperature profiles retain their general appearance but are shifted to lower temperatures. However, one detail is worth mentioning. Decrease of the heating power in case of a stagnant atmosphere (Freon 113 and *n*-hexane) increases the stagnation zone in the lower part of the box. This could probably be associated with a transition from case 3 ( $M_d > M_g$ , stagnant) to case 2 ( $M_d > M_g$ , stirred) under the influence of a temperature lowering far enough below the boiling point of the liquid. In fig. 29 it is seen that these vapour-gas systems fit also the general picture of either stagnant or stirred atmospheres.

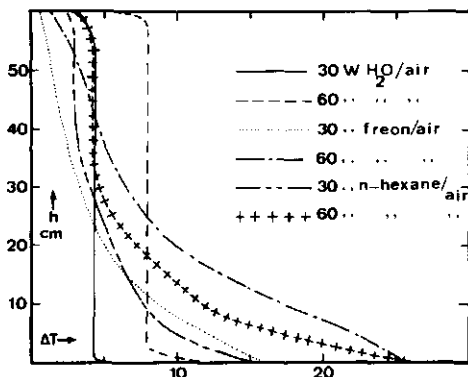


Fig. 29. Vertical temperature profiles of three vapour-gas systems at different heating powers; 30 and 60 W.

Table XII presents the results of the vapour-gas systems studied. In the last column, the observations concerning the atmospheric stability have been tabulated. The  $d\rho/dT$  values have been calculated using Eq. (65). The  $\Delta H_v$  and  $X_d$  data have been obtained from [119]. The validity of inequality Eq. (60) as a boundary condition for the stagnant case, is clearly shown. Apart from a transition region the observations are in nice agreement with the theoretical predictions. The extraordinary behaviour of the isopropyl alcohol-air system can be explained in the following manner. Compared to *n*-propyl alcohol, the isomer has a vapour pressure nearly two times larger. This leads to an enhanced diffusion of isopropyl-alcohol molecules to the cold walls, thereby decreasing  $X_d$  and violating the model used for deriving Eq. (65). An  $X_d$  value smaller than that used in calculation of  $d\rho/dt$ , would have led to a smaller  $d\rho/dt$  value, probably a negative one. Moreover, as remarked in the discussion of fig. 27, isopropyl alcohol is a transition case, since it has a stable layer in the lowest 10 cm of the box.

#### 4.3.7. Stirred electrophoresis

Very limited experimental data is available on the subject of stirred electrophoresis because the effect itself has been regarded undesirable and could be eliminated rather easily.

Table XIII summarizes some experimental data collected from literature and from one experiment carried out by the author in a polyethylene vessel of  $0.5 \text{ m}^3$  volume. Due to lack of exact knowledge on the electrical mobilities  $\mu_e$  of the aerosol particles studied in the experiments reported in Table XIII, a reasonable value of  $10^{-4} \text{ cm}^2 \cdot \text{V}^{-1} \cdot \text{s}^{-1}$  was chosen for the neutralized aerosol. Then a relatively reliable estimate of the  $\mu_e$ -values as given in Table XIII for the unneutralized aerosols produced by nebulization and dry dispersion can be obtained from Stein's charging characteristics [80] of his aerosols. It is assumed that the  $\mu_e$ -value for dry-dispersed aerosol applies also to Lieberman's aerosol [83]. The wall charge  $q_e$  can be calculated from

$$q_e = \beta_e \frac{2\epsilon V}{\nu_e} \quad (85)$$

which is equivalent to Eq. (45).

Both Lieberman's and Stein's data [83], [80] leads to consistent  $q_e$  values of roughly  $1.5 \times 10^{-7}$  C. Their spherical plastic vessels of 320 liters had an inner wall surface area  $S$  of about  $2.5 \text{ m}^2$  which yields nearly equal  $q_e$ -values with an average surface charge density of  $6 \times 10^{-8} \text{ C.m}^{-2}$ . Our polyethylene vessels having  $S = 3 \text{ m}^2$ , however, should have had an average surface charge density of  $7 \times 10^{-9} \text{ C.m}^{-2}$ . The difference between the charge density of our vessels and the other vessels is to be expected, because the vessels of Lieberman and Stein have been cleaned prior to their use for the experiments which certainly will result in significant surface charging (Stein reports charge islands with voltages of up to 10 kV [80]). Our vessel has not been cleaned prior to the experiment reported.

McMurry [40] using a  $65 \text{ m}^3$  teflon bag as aerosol container, quotes 70% removal per hour of  $1 \mu\text{m}$  polystyrene spheres from the bag atmosphere. This corresponds to a decay constant of about  $10^{-4} \text{ s}^{-1}$ . Assuming neutralized particles ( $\mu_e = 10^{-4} \text{ cm}^2 \cdot \text{V}^{-1} \cdot \text{s}^{-1}$ ) and an inner wall surface of  $200 \text{ m}^2$ , one calculates an effective charge  $q_e$  of  $6 \times 10^{-6}$  C and an effective charge density at the walls of  $3 \times 10^{-8} \text{ C.m}^{-2}$ . This compares fairly well with the above mentioned values for plastic vessels ( $\approx 6 \times 10^{-8} \text{ C.m}^{-2}$ , see Table XIII). Therefore, we believe that McMurry's observations on aerosol removal from his teflon bag must be attributed to stirred electrophoretic deposition.

Another study of aerosol behaviour in a vessel with non-conducting walls is the one by Zalabsky [41] (see pg. 25). He investigated the removal of Pt-oxide aerosol formed by heating a Pt-wire in air (see pg. 25) in a 24 liters glass vessel ( $S = 0.5 \text{ m}^2$ ). The aerosol was neutralized and will have had an electrical mobility of about  $2.5 \times 10^4 \text{ cm}^2 \cdot \text{V}^{-1} \cdot \text{s}^{-1}$ . Zalabsky has observed a half-life of 27 minutes ( $\beta = 4 \times 10^{-3} \text{ s}^{-1}$ ). From Eq. (85) one obtains a  $q_e$ -value of  $4 \times 10^{-9}$  C, and an effective wall charge density of  $10^{-8} \text{ C.m}^{-2}$  which again is not unreasonable in view of the afore mentioned values for plastic walls (Table XIII).

#### 4.3.8. Summary

Experiments have been performed with aerosols from Exploding Wires as well as with monodisperse particles in aerosol vessels. The aerosol behaviour can be treated quantitatively as a case of stirred atmospheres where the deposition rate limiting processes occur in the boundary layer at the walls. Conditions under which non-stirred settling or stratification could arise, are dealt with; experimental support is given to the theory developed in section 2.5.

Stirred deposition in dry, unheated vessels can be due to three mechanisms. Larger particles (diameter  $\geq$  several tenths of a  $\mu\text{m}$ ) are removed by gravitational deposition. Smaller particles deposit due to diffusive deposition; however, in the case of vessels with electrically non-conductive walls particles in the size range of 0.01 - 1  $\mu\text{m}$  can be removed by electrophoresis. For the diffusive deposition in vessels with conductive walls a relation is obtained between the diffusion boundary layer thickness and the particle diffusion coefficient. The effects of aerosol formation parameters, vessel height and initial mass concentration have been studied. Higher values of formation energy and vessel height, and lower initial mass concentration result in higher aerosol stability (lower deposition rate).

The use of unheated, dry vessels for the investigation of aerodynamic properties of aerosols (aerodynamic diameter and dynamic shape factor) has been investigated. Experimental results on the relation between dynamic shape factor of solid aggregates and their microstructure compare favourably with the Stöber-Kops model [89, 90]; indications are obtained of the better suitability of the vessel decay curve technique for large aggregates compared to the centrifuge.

Application of the model of stirred electrophoresis to experimental observations yields reasonable estimates of electrostatic surface charges on vessel walls of some plastics ( $10^{-7}$  -  $10^{-9}$  C.m<sup>-2</sup>) under certain assumptions.

Experimental results and discussions on stirred deposition due to electrophoresis, diffusion and coagulation will also be given in the chapter on smog chambers (4.6).

#### 4.4. Aerosol decay in heated dry vessels

##### 4.4.1. General observations and considerations

Heating an enclosed gas atmosphere increases the temperature of the gas compared to the enclosing walls. When natural convection is not suppressed (see section 4.3.6) the atmosphere will be stirred apart from a boundary layer at the walls across which a temperature gradient exists. This temperature gradient is the driving force for aerosol transport (thermophoresis) to the relatively cold walls in a manner treated quantitatively in section 2.2.4.

In the vessels used for study of the aerosol behaviour under heating conditions the generated convective flow velocities have been measured in a number of typical cases. These velocities were found to be about  $20 \text{ cm.s}^{-1}$  which agrees with rough calculations [5] yielding  $30 \text{ cm.s}^{-1}$ . Assuming a boundary layer thickness of about 0.5 cm this means that inertial deposition of the aerosols used (up to  $1 \mu\text{m}$  aerodynamic diameter) cannot have played a significant role in aerosol removal under these circumstances (relaxation time of a  $1 \mu\text{m}$  particle is several microseconds).

Visual inspection of the transparent walls of the vessels PERVEX (plexiglass) and GRACE (Pyrex glass) has revealed that the aerosol deposit is usually distributed over the walls. In case of floor heating of the PERVEX-vessel it could be established visually that negligible deposition takes place at the floor. Altogether, deposition is mainly on the cold walls, presumably by thermophoresis.

Since the heat source has been always located in the lower part of the vessels, the other walls should be considered to be a heat sink too. However, the thermophoretic force acting on the particles in the boundary layer at the top of the vessel is counteracted by the gravitational force. Roughly (see next sections) the thermophoretic deposition velocities in our experiments amount to about  $5 \times 10^{-4} \text{ cm.s}^{-1}$ . Since the gravitational settling velocity of the aerosols used ( $\sim 0.5 \mu\text{m}$ ) is much larger (about  $10^{-3} \text{ cm.s}^{-1}$ ), it is evident that the thermophoretic deposition on the ceiling has been strongly hampered in most cases. This is consistent with the observation of a much thinner deposit on the ceiling compared to the side walls.

Fig. 26 depicts the effect of heating the aerosol contained in the 100-vessel (pg. 101).

Firstly, the inhomogeneous filling of the vessel when it is not heated, during the initial seven hours is remarkable. The occurrence of this inhomogeneity at the relatively low (see the previous section) initial mass concentration of  $70 \text{ mg.m}^{-3}$  must be explained by the intensive thermal insulation of the vessel, viz. apart from the (upper) 10% of the vessel wall the vessel had been packed in 3 cm thick polystyrene foam. Very probably, most of the random temperature fields in the laboratory have been shielded in this way, thereby reducing strongly the unintentional thermal convection.

Heating of the vessel atmosphere with 50 W power of a quartz heater completely removes the heterogeneity and considerably increases the aerosol removal rate. Fourfold increase of the heating power to 200 W further increases aerosol instability such that after about 50 hours the mass concentration is about two orders of magnitude below that of the unheated case. At increasing heating power the decay curves become better exponential. This is due to the thermophoresis being more dominant over gravitational settling: the initial curving of the decay curves is caused by the initial preponderance of the latter deposition mechanism, which loses its importance after removal of the largest particles. This picture is supported by additional evidence (see fig. 30) for the effect of the initial mass concentration  $c_m(o)$  on the appearance of the decay curves. Only the largest  $c_m(o)$  results in significant curving, which gradually disappears after about 10 hours. Then the decay is also exponential and of a rate equal to that of the other aerosols.

The exponential character of the aerosol decay of the heated aerosol (apart from deviations owing to additional gravitational settling) means that thermophoresis has an insignificant particle size dependence. This agrees with those theories on thermophoresis (see section 2.2.4) predicting independence of size for larger particles ( $\frac{z}{r} < 1$ ).

As shown above, thermophoretic deposition is an efficient process compared to gravitational settling already under moderate heating conditions. Consequently, the duration of the initial coagulation stage of an instantaneously formed aerosol will be influenced by the

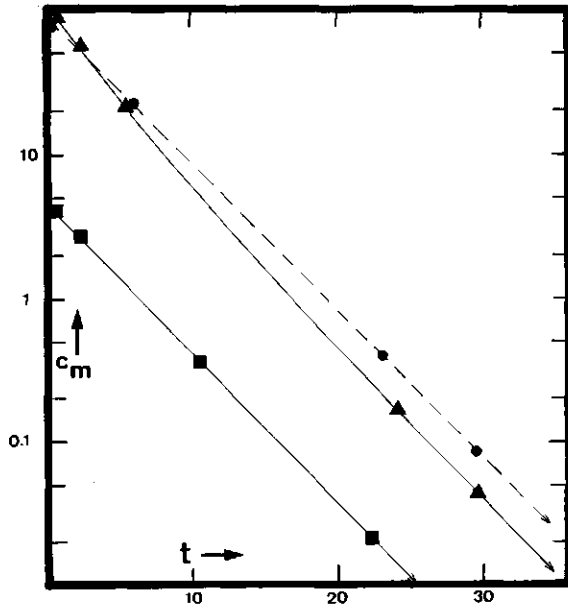


Fig. 30. Mass concentration decay of inhomogeneously heated gold aerosols in "100"-tank. The curves shown belong to the aerosols exploded with different  $c_m(o)$  and Espec.  $c_m$  in  $\text{mg}/\text{m}^3$ . Time  $t$  in hours. Espec ranges from  $20 \text{ kJ}\cdot\text{g}^{-1}$  to  $250 \text{ kJ}\cdot\text{g}^{-1}$ .

heating. The same is valid to the aggregate size, which is uniquely related to coagulation. Fig. 31 shows the effect of heating on the average mass  $\bar{m}$  per aggregate.  $\bar{m}$  reaches a final value (indicating vanishing coagulation) at an earlier point of time. This final value is lower for higher heating powers. This is caused primarily by the interference of thermophoresis in the coagulation process due to the high efficiency of thermophoretic deposition already when the particles are still too small to be removed at a considerable rate by gravitational settling. Curve D in the lower part of fig. 20 illustrates this once again.

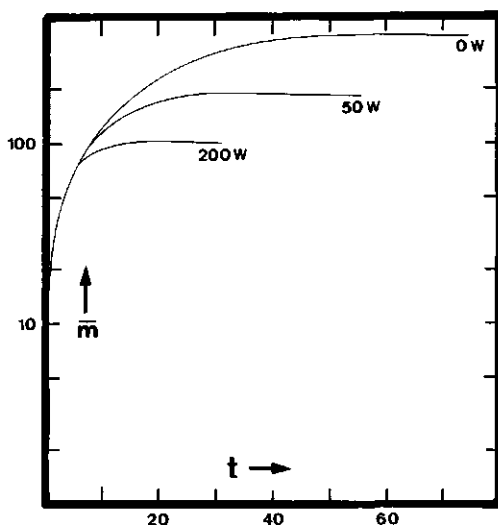


Fig. 31. Course of average particle mass  $\bar{m}$  (in pg) after formation of gold aerosol in 100-vessel for various heating power levels of heater on vessel floor. Time  $t$  in hours.

#### 4.4.2. Effect of heating power

A number of experiments with gold aerosols in various vessels with different heating powers is available for analysis. The results are given in Table XIV. The analysis of the PERVEK data is taken as an example, because two types of heating have been applied. Either a quartz heater placed on the floor has been used or the brass floor has been heated evenly. In the latter way gravitational deposition of aerosol on the heated floor ( $120 - 250 \text{ W}\cdot\text{m}^{-2}$ ) should be negligible according to fig. 4. As argued in the previous section, thermophoretic deposition on the top wall is hindered by gravitational settling. Hence, an additional correction for this has to be applied amounting to the ratio of top wall surface area to the vertical wall surface area ( $\sim 20\%$ ). Table XIV shows that without the corrections  $B_m = 0.16$  is obtained from both experiments with heated floor. A  $B_m^{\text{CORR}}$  value of 0.19 results when the correction ( $+ 20\%$ ) for the top wall effect is applied.  $B_m$  has been calculated from  $\frac{\alpha}{\lambda g}$  (see Eq. (26)) taking into account that



$$B_m = \frac{\alpha}{\lambda} \times \frac{\lambda}{g} \frac{\rho}{\eta} \frac{g}{g} T \quad (86)$$

where the second factor  $\frac{\lambda}{g} \frac{\rho}{\eta} \frac{g}{g} T$  is almost independent of temperature T (section 2.2.4). For helium and nitrogen this factor amounts to  $0.37 \text{ J.cm}^{-3}$  and  $0.50 \text{ J.cm}^{-3}$  respectively.

When Stetter's theory is used (section 2.2.4, Eq. (28a)) it follows that  $n_{th} = \frac{1}{B_m^{corr}} = 5.3$ . According to Stetter  $n_{th}$  ranges for air from 3 for small particles ( $r < 2$ ) to  $n_{th} = 8$  for large particles ( $r > 2$ ). Particles are larger than  $2$  ( $0.065 \mu\text{m}$ ) when the aerodynamics or the spatial dimensions are considered, but the primary particles constituting the aggregates have dimensions smaller than the mean free path of air molecules. The  $n_{th}$ -value of 5 indicates that the interaction between gas molecules and the primary particles is more or less direct.

The  $B_m$  values calculated from the results of the three experiments in PERVEX with the quartz heater (local heating, Table XIV) are higher than obtained from experiments in PERVEX with a heated floor. This can be explained by additional gravitational aerosol deposition on the floor which is not heated. This effect can be corrected for by subtracting the decay constant for settling  $\beta_s$  from the measured decay constant  $\beta_m$ . The decay constant of stirred settling  $\beta_s$  has been calculated from the average mass  $\bar{m}$  per coagulate using Eqs. (47), (71), (76) and the relation between  $\kappa$  and  $n$  as found (pg. 94). This correction for gravitational deposition on the floor and for the top wall effect gives  $B_m^{corr}$  values (0.19 - 0.22) which correspond fairly well with those found for the case of floor heating (Table XIV). Similar analysis of three experiments in the 100-vessel yields  $B_m^{corr}$  data which are also similar to those from the floor-heated PERVEX (since the  $\bar{m}$  value of the 100 W experiment in the 100-vessel is lacking a  $\beta_s$  value is used of  $0.6 \times 10^{-5} \text{ s}^{-1}$ , equal to the other 100-vessel experiments reported in Table XIV).

Unfortunately, the experimental results from the GRACE and ENAK vessel are not very useful, though for different reasons. The  $\bar{m}$  data for correction for  $\beta_s$  are lacking for the GRACE experiments. However, the uncorrected  $B_m$  values are compatible with those of the PERVEX and 100-vessel experiments. Therefore, this can be regarded as additional

experimental support for the correctness of these GRACE data since all cases concern the same kind of aerosols. The ENAK data fit the other results rather badly ( $B_m^{\text{corr}} \approx 0.1$ ). One may speculate whether this is due to incorrect Q measurement (voltage/current; but probably heat loss from the heater to the floor has played a relatively large role) or due to incorrect  $\beta_s$  correction (the basic  $\bar{m}$  values used for this correction are rather high).

The experimental  $B_m^{\text{corr}}$  value of approximately 0.2 can be compared with the B-values as calculated from theories of Epstein, Brock, and Derjaguin. These B-values ( $B_E$ ,  $B_B$  and  $B_D$  from Eqs. (27) and (28)) amount to  $1.2 \times 10^{-4}$ , 0.18 and 0.36, respectively (see Table XV, first line). Evidently,  $B_E$  and  $B_D$  do not correspond with our  $B_m^{\text{corr}}$  value of 0.20. Clearly, Epstein's formula ( $B_E$ ) is not valid for the conductive aerosols like those of gold. Our results do not support Derjaguin's model either; the  $B_D$  value is twice too large. The  $B_E$  value of 0.18 calculated from Brock's equation is in good agreement with our result. However, this is not surprising because Brock's equation (28c) is a semi-empirical one containing slip coefficients ( $c_m$  and  $c_t$ ) obtained from fitting with experimental data on thermophoresis in air.

In conclusion, aerosol behaviour in heated enclosures can be described by our model of stirred thermophoretic deposition. In some cases corrections for gravitational settling onto the floor or at the top of the vessel are required. The  $B_m$  values of 0.2 obtained from our experimental data on gold aerosols agree with the models of Stetter and Brock and do not support those of Epstein and Derjaguin.

#### 4.4.3. Effects of aerosol material, temperature and gas phase on thermophoresis

Table XIV also gives experimental results on removal of aerosols of materials other than gold. As argued earlier it is sensible to consider the floor heated PERVEX experiments firstly. Oil droplets and Exploding Wire platinum aerosols appear to be subject to thermophoretic deposition characterized by the same value for  $B_m^{\text{corr}}$ : 0.22. This value is quite similar to that found for gold aerosols (0.20, see previous section). Similar result have been obtained for aerosols of copper

oxide and NaCl in the 100-vessel. Although no exact stirred settling data are available for making the  $\beta_s$  correction, yet a  $B_m^{\text{CORR}}$  value can be deduced assuming a negligible  $\beta_s$  correction ( $d_a$  is low for these aerosols). The observed material independence of thermophoresis once again favours the theories of Stetter and Brock.

Table XIV also gives a  $B_m^{\text{CORR}}$  value obtained for 0.8  $\mu\text{m}$  polystyrene particles. This value of 0.11 deviates considerably. The corresponding  $n_{\text{th}}$  value is 9 which is almost equal to the maximum quoted by Stetter [72], viz. 8. This should be the maximum approached in the coarse particle region.

The experimental observations tabulated in Table XV on the influences of temperature and gas phase have limited validity because the data on  $Q$  (heating power) used for calculation of  $B_m^{\text{CORR}}$  (by means of (26) and (86)) are uncertain, viz. the  $Q$ -measurements are somewhat too low in case of the He experiments. Higher  $Q$ -values lead to lower  $B_m$ -values. However, a correction of more than a factor of two seems unlikely. Consequently, comparing the  $B_m^{\text{CORR}}$ -values of about 0.3 in case of He with the theoretical  $B$ -values as listed in Table XV, it should be concluded that there is reasonable agreement between theory and experiment as far as the theories of Stetter and Brock are concerned. The tendency for  $B$  to be larger for He than for air can be explained by the variation in  $n_{\text{th}}$  from 3 to 5, dependent on the nature of surface reflection of the gas molecules [72]. The value  $n_{\text{th}} = 3$  corresponds to molecules which are rigid spheres, i.e. molecules having only short-range interaction with the particle surface. In view of the simple and noble gas electronic structure of the helium atom, these atoms will tend to behave as hard spheres, which means a value of  $n_{\text{th}}$  near to 3. In other words, the observed higher  $B$  values (lower  $n_{\text{th}}$  values) for helium compared to air are in qualitative agreement with these theoretical considerations. The thermophoretic deposition is found to be larger for helium than for air, analogously to the better thermo-diffusion separation of noble gases than of other gases [72].

Any temperature effect on stirred thermophoresis is clearly absent in Table XV, as was predicted in section 2.2.4. In fact, as shown by Table XVI, even experiments performed at temperatures around 500  $^{\circ}\text{C}$  show no significant temperature effects.

#### 4.4.4. Hampered settling on heated vessel floors (low heating rates)

In the previous sections it became clear that thermophoresis predominates over gravitational settling of particles with diameters of about  $0.7 \mu\text{m}$  in heated vessels with heating power densities  $\frac{Q}{V}$  larger than about  $0.1 \text{ kW.m}^{-3}$ . Moreover, the results indicated that heating of the upward facing vessel walls could lead to important hampering or even hindering of gravitational settling of particles onto these walls. This has been studied in more detail using the PERVEX vessel by recording aerosol stability as a function of the heating power of its brass floor. Gold aerosols formed by explosion of  $0.1 \text{ mm } \phi$  gold wires at  $10 \text{ kV}$  capacitor voltage have been used. The aerosol decay has been followed by means of a condensation nucleus counter. Decay constants  $\beta_m$  could be obtained from the exponential part of the long term decay curves after coagulation has lost its dominance. The experimental results are displayed in fig. 32.

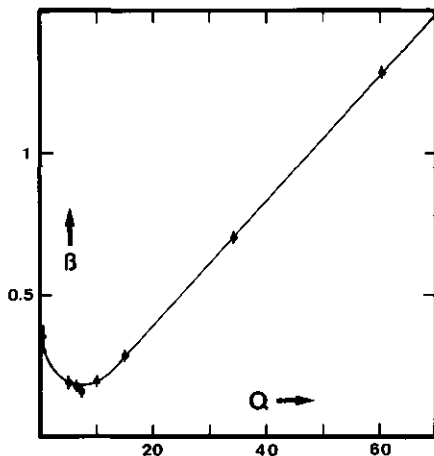


Fig. 32. Decay constants  $\beta$  (in  $10^{-4} \text{ s}^{-1}$ ) of gold aerosols in the PERVEX-vessel. The floor was heated with a variable power  $Q$  (in Watts).

With increasing power of the floor heating  $Q$  the decay constant  $\beta_m$  initially decreases (aerosol stability increases) due to the hampering of gravitational settling. At higher levels of heating power, the aerosol deposition is enhanced because the thermophoretic deposition on the cold walls (except the top wall) becomes overwhelming. The  $\beta_m$  values of the cases of highest heating levels (34 W and 60 W) have been used previously for calculation of  $B_m^{\text{corr}}$  (see Table XIV), which calculations have shown that thermophoresis is the governing aerosol removal process under these conditions. The measuring data are also tabulated in Table XVII. The results can be analysed as follows.

A contribution  $\beta_{th}$  to the measured decay constant  $\beta_m$  due to the thermophoresis to the cold walls (except the top side) can be calculated for each heating case because  $\beta_{th}$  is proportional to  $Q$  and  $\beta_{th} = \beta_m$  for both 60 W and 34 W. As a result  $\beta_{th} = 0.21 Q$ . Values of  $\beta_{eff} = \beta_m - \beta_{th}$  have been calculated for the various  $Q$  levels (Table XVII). This  $\beta_{eff}$  value shows how deposition on the floor is influenced by the floor heating. The low  $\beta_{eff}$  values for  $Q \geq 10$  W means that for these larger heating powers floor deposition is negligible. The decay constant  $\beta$  at  $Q = 0$  corresponds to an average aerodynamic diameter of  $0.74 \mu\text{m}$ . A negative correction  $\beta_{th}(f)$  can be made to  $\beta_{eff}$ , which correction involves the hampering thermophoretic effect. This "decay constant"  $\beta_{th}(f)$  can be assessed assuming the same heat transfer coefficient to apply for both the cold vertical walls and the warm floor. Hence,  $\beta_{th}(f) = \beta_{th} \frac{S_c}{S_f}$  where  $S_c$  = surface area of the cold walls, and  $S_f$  = floor surface area. For the PERVEX-vessel this should lead to  $\beta_{eff} = \beta_s - \beta_{th}(f) = \beta_s - 5.8 \beta_{th}$ . Consequently, for e.g.  $Q = 5$  W,  $\beta_{eff}$  should have been negligible, contrary to the observations (Table XVII). Probably, the assumption of similar heat transfer at the cold walls and at the floor is not very realistic. The floor could have been heated inhomogeneously. However, also eddy convective heat transfer through the boundary layer at the floor could have smoothed the temperature gradient at the floor and given rise to transport of aerosol to the floor through the boundary layer at the places of rising eddy instabilities. Clearly, the model given in section 2.2.5 (see also fig. 4) for calculation of the diameter of a particle which just floats above a heated plate does not apply completely in this case. Nevertheless, there is considerable

hampering of gravitational aerosol deposition although less than calculated. The half-life of the aerosol has been increased about two fold at  $Q = 7 W$  compared to the unheated case. Provided slight heating is not undesirable, this floor heating technique could be applied for stabilisation of aerosols. This technique is easier to perform than the drum rotation treated in section 2.5.4.

#### 4.4.5. Summary

Local heating of dry, aerosol containing vessels considerably enhances deposition due to thermophoresis. This could be described by a model developed for stirred thermophoretic deposition. Observations of the independence of the thermophoretic decay constant on aerosol material, temperature and (for  $d \geq 0.5 \mu\text{m}$ ) particle size are in agreement with this model. The theories of Stetter and Brock fit the observations very well. Observed effects of gas phase and particle size are of proper magnitude. The stability of aerosols in vessels can be considerably enhanced by moderate heating of the vessel floor.

#### 4.5. Aerosol decay in vessels with a heated pool of water on the floor

This section deals with aerosol behaviour in chambers heated from below and having some water on the floor. In this case heat transfer by the chamber atmosphere is not only by sensible heat but also by latent heat transport. This introduces some typical aerosol processes which can be used for aerosol studies or need to be reckoned with in evaluation of aerosol behaviour under similar conditions.

A chamber with a heated pool of liquid may show stratification (pg. 58) dependent on the liquid/gas system. The system  $\text{H}_2\text{O}/\text{air}$ , however, treated in this section is one of convective stirring enhanced due to latent heat transfer by water vapour.

##### 4.5.1. General observations and discussions

Compared to aerosol behaviour in heated dry vessels treated in the previous section 4.4, the instability of an aerosol in heated wet vessels is strongly enhanced (fig. 33). Typically, the aerosol decay rate of the wet case is not only larger than that of the dry case but

also the decay rate increases as time proceeds. Ultimately, this leads to a "catastrophic" disappearance of the aerosol at the end of its life.

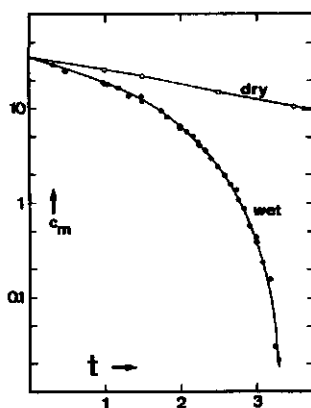


Fig. 33. Mass concentration decay  $c_m$  (in  $\text{mg m}^{-3}$ ) of gold aerosol in PERVEX with water layer on the floor (o) and under dry conditions ( $\bullet$ ). Time  $t$  in hours.

Visual observation in the glass and perspex vessels (GRACE and PERVEX resp.) has shown that a dense fog exists immediately after introduction of aerosol (usually Exploding Wire generated) into the chamber atmosphere. The reduced visibility persists until the dramatic aerosol removal occurs. At that time the chamber atmosphere becomes clear within a minute. Visual inspection of the fog by means of a laser beam (2 mW HeNe laser) has given the impression that the fog consists of droplets larger than the particles present in the dry case at the same point of time after aerosol formation. These droplets float around in the vessel indicating a well-stirred atmosphere. Compared to the wetting of the cold walls by the continuous vapour condensation, there is no significant additional water transport to these walls by depositing droplets. The laser beam has revealed also the existence of a layer of slightly less than 1 cm thickness, above the warm pool of water where larger droplets are seen to settle. It has appeared difficult to measure the water vapour content of the atmosphere prior to aerosol formation. A

rough measurement of the dew point of the PERVEK atmosphere (60 W) has yielded a supersaturation value of a few %. This is slightly less than to be expected on the basis of the temperature difference of several degrees between pool and atmosphere above it.

From these observations the following model for aerosol behaviour may be deduced. The atmosphere of an aerosol-free chamber with a warm pool of water is supersaturated with vapour from this pool. This supersaturation is the net result of the vapour supply from the pool and the vapour removal by condensation onto the cold walls of the chamber. Aerosol particles introduced into such atmospheres will act as condensation nuclei (exceptions see below) and grow rapidly to droplet sizes until supersaturation has almost disappeared. Allowing some initial fast coagulation until  $c_n = 5 \times 10^5 \text{ cm}^{-3}$ , this means that droplets of a few  $\mu\text{m}$  are formed by the removal of the supersaturation of several percent (Millikan chamber observations without electric field gave droplet diameters of 1 - 5  $\mu\text{m}$ ). These droplets continue their growth due to the supply of water vapour by the warm pool. Deposition of droplets of this size will be mainly by gravitational settling (owing to additional latent heat transfer the decay constant for thermophoretic deposition in PERVEK at 60 W floor heating will be less than  $10^{-5} \text{ s}^{-1}$  (see Table XIV) whereas a settling velocity for 2  $\mu\text{m}$  particles of  $1.3 \times 10^{-2} \text{ cm.s}^{-1}$  yields a decay constant  $\beta_s$  for settling of about  $2 \times 10^{-4} \text{ s}^{-1}$ ).

Consequently, the decay rate will increase because of the increasing particle size. The growth rate of each droplet will increase further due to the decreasing droplet concentration. This in turn gives rise to an enhanced decay rate. This is the typical "catastrophic" decay displayed in fig. 33. In the next section a relation will be derived using this model which will be found to agree with measurements giving additional support to the correctness of this model.

Usually, a dense fog formation is visible after introduction of aerosol into a space with a heated pool of liquid on the floor. However, a number of exceptions have been noted which are worthwhile to mention here.

Firstly, when liquid/gas systems other than water/air are used, the atmosphere heated from below may be stratified (4.3.6.3). Aerosol



introduction in these stratified atmosphere shows fog formation only in the lower part of that space, signifying that the supersaturation is limited to these regions. Additionally, between the cloud and the warm pool a clear layer of about 5 cm is present through which under special illumination individual droplets are seen raining from the cloud above. This has been observed for the three systems  $\text{CCl}_4/\text{air}$ , Freon 113/air and  $\text{H}_2\text{O}/\text{He}$ . Each droplet within the fog is in almost complete rest which is in accordance with the absence of stirring of these atmospheres as proved in 4.3.6.3. Presumably, this also causes the thickness (5 cm) of the layer of falling droplets to be larger than in case of stirred systems (less than 1 cm).

Secondly, when aerosols of notorious hydrophobic nature like silicone oil or liquid paraffin, are brought into the supersaturated atmosphere of the water/air system, there is no dense fog formation. The decay of hydrophobic aerosols is insignificantly altered by the presence of the warm pool of water. Only a minor fraction of the oil droplets has been observed to have a significantly larger size after some time. This suggests that only few oil droplets have grown by condensation of water vapour. Fig. 34 shows that there is no "catastrophic" decay of these hydrophobic aerosols, indicating also negligible condensation. The appearance of some larger drops can be explained in two ways. Either the oil drops have impurity sites at their surface where water molecules can reside and lead to further limited condensation, or the formation of the water layer by sorption irrespective of their contact angle  $|\theta|$  is very slow. Provided the latter explanation is correct, the study of the appearance of larger droplets in oil aerosols would be valuable for the insight in water condensation on small hydrophobic droplets.

As argued at the end of section 2.2.5, thermophoresis and diffusiophoresis contribute nearly equally to the aerosol deposition rate at R.T. in a vessel with a heated waterpool. It has been observed in PERVEX that addition of water reduces the temperature difference between the PERVEX atmosphere and the surroundings to just half its original value. As a result, the thermophoretic deposition rate will be halved. The rates of deposition by diffusiophoresis and thermophoresis should then be nearly equal in order to have almost identical aerosol decay rates under wet and dry conditions. This fits the above mentioned theoretical conclusion of section 2.2.5.

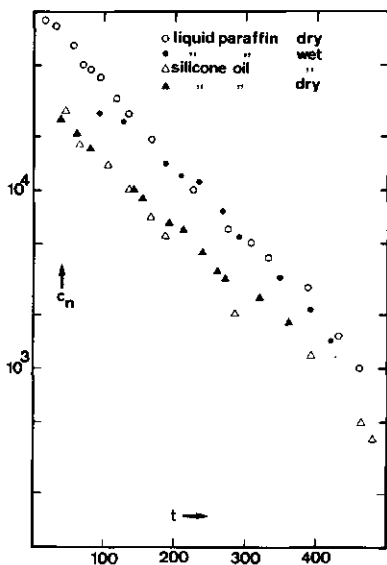


Fig. 34. Decay curves (particle number concentration ( $c_n$  in  $\text{cm}^{-3}$ ,  $t$  in minutes) of aerosols of liquid paraffin and silicone oil in PERVEX-box with heated floor (60 W). "Dry" and "wet": without and with waterlayer on the floor.

Thirdly, different aerosol behaviour is also found with platinum oxide aerosols in PERVEX from a glowing platinum wire of 0.1 mm diameter in air. The particles generated in this way are very difficult to observe by electron microscopy. The platinum oxide particles are either rather volatile or too small. Only a small fraction of the aerosol particles is visibly transformed into droplets immediately after aerosol generation. This fraction may be enlarged by increasing the glowing time which normally is a few minutes. The number concentration of the droplets gradually diminishes until, after about 1½ hours, no droplets are visible. Nevertheless, the condensation nuclei counter measures  $c_n$  still more than  $10^3 \text{ cm}^{-3}$ . The condensation nuclei concentration shows an initial fast decay (due to coagulation) followed by two periods of different exponential decay. The first period has a larger decay rate than the second one. Extending the glowing time (increasing aerosol production) shifts the transition between the two periods to

later points of time. The transition could be established to coincide with the onset of absence of droplets. This can be explained by assuming the existence of two aerosol fractions, of which one is active in condensation nucleation, the other remaining untouched. Presumably, this is on account of the different particle sizes of these fractions, of which the larger fraction is formed by coagulation. The rapid exponential decrease at the longest glowing time (20 minutes) has a half-life of about 20 minutes which corresponds to a reasonable droplet diameter of 4  $\mu\text{m}$ . The ability of the condensation nuclei counter to detect particles after the droplets have disappeared is due to the much larger supersaturations ( $\sim 25\%$ , corresponding with a critical diameter of 0.01  $\mu\text{m}$  |121|) in these counters compared to that in PERVEX (0.1 - few %, corresponding with critical droplet diameters of 2  $\mu\text{m}$  - 0.05  $\mu\text{m}$  |121|).

In conclusion, aerosol behaviour in a vessel with a heated pool of water on the floor depends on the ability of the particles to act as nuclei condensation. This aerosol property is known to be a function of supersaturation, particle size and material. When the particles act as nuclei for condensation a very fast growth takes place followed by (stirred) settling with an increasing decay rate due to further condensational growth. Non-stirred settling could occur under conditions leading to stratification (section 2.5.3). Aerosols on which negligible condensation takes place, disappear exponentially with a decay rate not very different from dry (thermophoretic) deposition. Very likely, the heated wet chambers can be used for study of aerosol formation in chemical reactions (smog chambers) by investigating droplet formation at a known given supersaturation of the chamber atmosphere. In this manner simulation can be achieved of the conditions prevailing in clouds, mists and plumes.

#### 4.5.2. Theory

We shall derive a calculational model of particle growth by condensation and subsequent deposition, the fit of which model with the observations (to be given in the next section) can be used for better understanding of the processes in a vessel with a heated pool of liquid.

A number of simplifications and approximations, however, is necessary

in order to arrive at a set of simultaneous differential equations which can be solved. The supersaturation of the vessel atmosphere being unknown, it is wise to omit the fog formation at the moment of aerosol introduction from the model. Coagulation cannot be treated because the resulting equations cannot be solved. The two remaining processes governing aerosol behaviour are condensational growth and stirred settling. Whether these simplifications and approximations are realistic will be considered later on.

The growth of the droplets due to condensation on the particles of the continuous supply of vapour from the warm pool is given by

$$c_m \frac{dr^3}{dt} = E \quad (87)$$

$$\text{with: } E = \frac{3Q_v M_m}{4\pi\rho \Delta H_v V} \quad (88)$$

$c_m$  = mass concentration of aerosol introduced

$r$  = droplet radius

$Q_v$  = heat released per second due to condensation on aerosol cloud

$M$  = molecular mass of condensing vapour

$m$  = average mass of original aerosol material in one droplet

$\rho$  = density of liquid

$\Delta H_v$  = latent heat of vaporisation

$V$  = vessel volume

Assuming all droplets to be in thermodynamic equilibrium with the atmosphere, they must have the same size. Hence, the mass concentration equivalent for Eqs. (4) and (17) describes the stirred settling of the fog

$$\frac{dc_m}{dt} = - A r^2 c_m \quad (89)$$

$$\text{where: } A = \frac{2\rho g}{9h\eta}$$

$\rho$  = density of liquid

$g$  = gravitational acceleration

$h$  = vessel height

$\eta$  = viscosity of the gas atmosphere

The set of simultaneous differential equations (87) and (89) can be solved if neither  $Q_v$  nor  $m$  is a function of time. This will in fact be assumed: thus the possible change of  $m$  due to coagulation is disregarded and  $Q_v$ , about which no information is available, is assumed to be constant. With these approximations the solution is found to be

$$c_m^{2/5} = \{c_m(o)\}^{2/5} - Gt \quad (91)$$

where:  $c_m(o)$  = aerosol mass concentration at  $t = 0$

$$G = \frac{2}{5} \left(\frac{5}{3} E\right)^{2/5} A^{3/5} \quad (92)$$

$E$  and  $A$  are given by Eqs. (88) and (90), respectively. In conclusion, when plots of the  $\frac{2}{5}$ -th power of the mass concentration versus time yield straight lines then aerosol decay is likely to be governed by the combination of condensational growth and stirred settling.

#### 4.5.3. Experimental results and discussions

Fig. 35 gives the results of the decay of the mass concentration of gold aerosol in the GRACE vessel at various heating powers of the water pool. These are typical curves all showing the "catastrophic" decay near the end of the aerosol life. The life-time of the aerosols is inversely related to the heating power level. Comparison with decay curves of the number concentration has revealed that the moment at which the aerosol has completely disappeared is the same in both cases. Provided the model is correct on which Eq. (91) is based, plots of  $c_m^{2/5}$  versus time should yield straight lines. Fig. 36 shows this to apply for the experiments performed in GRACE and PERVEX. Only the experiments at relatively low heating powers (30 W and 50 W) have an initial period which deviates. This initial period will be discussed later on in this section. The straight lines of the two-fifth power plots of the mass concentration versus aerosol life in the large ENAK vessel (cf. fig. 37) are an additional proof of the correctness of the model developed in the previous section. From the slopes  $G$  of a number of such decay lines the corresponding heat  $Q_v$  released per second due to condensation on the particles could be calculated. Eqs. (88), (90) and (92) have been used for this. An  $\bar{m}$  value of  $10^{-10}$  mg was calculated

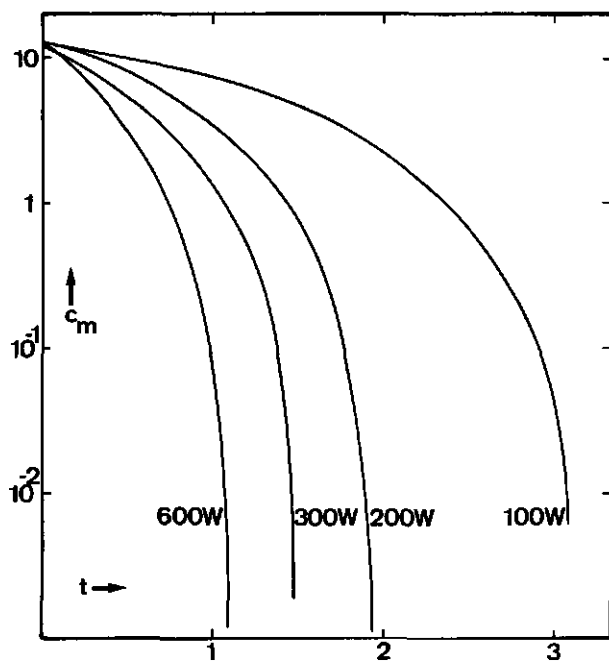


Fig. 35. Mass concentration decay ( $c_m$  in  $\text{mg}\cdot\text{m}^{-3}$ ,  $t$  in hours) of gold aerosols formed by means of the Exploding Wire technique in the GRACE vessel with a heated layer of water. The heating power was varied.

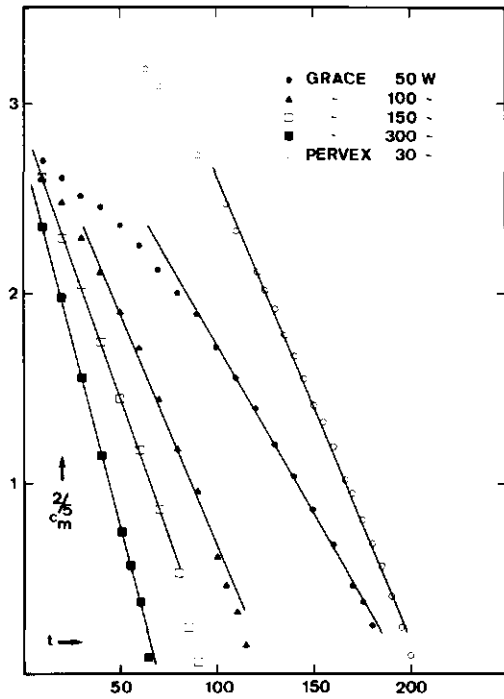


Fig. 36. Decay of aerosol mass concentration ( $c_m$  in  $\text{mg}\cdot\text{m}^{-3}$ ;  $t$  in minutes) in GRACE and PERVEX for various heating power levels of water layer.

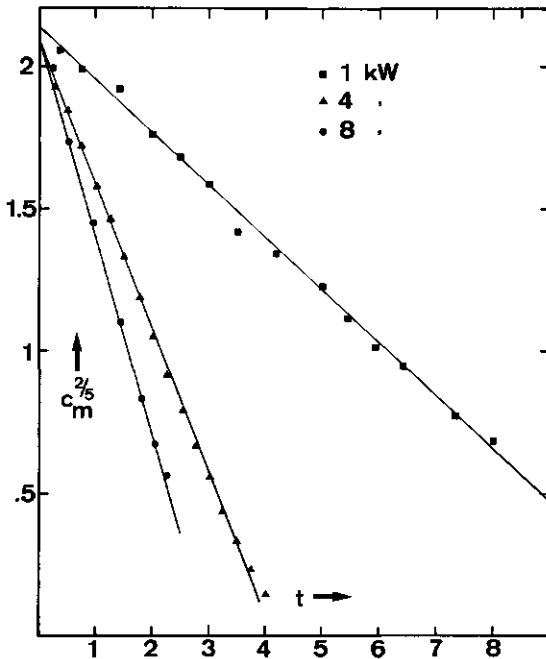


Fig. 37. Mass concentration decay of gold aerosols under wet conditions in ENAK at various heating power levels.  $c_m$  in  $\text{mg}\cdot\text{m}^{-3}$ ,  $t$  in hours.

from the  $c_m$  and  $c_n$  data and used for the  $Q_v$  calculation of which the results are given in Table XVIII. The percentage  $\frac{Q_v}{Q} \times 100\%$  of the pool heating power involved in the condensation on the cloud droplets ranges from 0.1 to 0.6%. Table XVIII shows the tendency of this percentage to increase with increasing heating power  $Q$  for a particular vessel.

In this section attention was given only to those decay curves or parts of decay curves which obey Eq. (92). The underlying model assumes negligible droplet formation at the point of time of aerosol introduction in the supersaturated atmosphere. The droplets formed by the removal of the supersaturation in the case of lower levels of heating power should contribute significantly to the aerosol behaviour. This explains the deviation from linearity in fig. 36 in the early stage



of the aerosol life. Only scattered observations are available for analysis of this part of the aerosol processes in a vessel with a heated pool of water: firstly, a number of experiments in PERVEX at low  $Q$  values and, secondly, an experimental series in GRACE where the water content of the atmosphere is varied at moderate  $Q$  by addition of NaCl to the pool of water.

Table XIX represents the measuring data in PERVEX at low heating powers. The half-lives in the second column originate from the part of the experimental decay curve after coagulation has ceased to dominate the aerosol behaviour. A correction  $\beta_{th}$  must be applied for the thermophoretic removal. It is assumed that thermophoresis has an activity only half that of the dry system at the same  $Q$  since the temperature difference between gas atmosphere and the vessel surroundings is also halved in the wet case. From the corrected  $\beta$  values ( $\beta_m - \beta_{th}$ ) droplet sizes are calculated using Eq. (71). The resulting droplet sizes look reasonable for  $Q \geq 10$  W, in view of the droplet sizes of a few  $\mu\text{m}$  observed in the Millikan chamber (pg. 119). The diameter obtained at  $Q = 0$  nicely agrees with that obtained with the Stöber centrifuge, viz.  $0.70 \mu\text{m}$ . However, the "droplet" size of  $0.64 \mu\text{m}$  at  $Q = 5$  W must be incorrect because the  $d$  value of  $0.64 \mu\text{m}$  at  $Q = 0$  should be the smallest. This anomaly could be explained by the hampering effect of the warm pool of water on the stirred settling of the particles. As shown earlier (pg. 116), this effect is most discernible in this  $Q$  range. It is possible to calculate the supersaturation of the atmosphere from these droplet sizes given in Table XIX using the water vapour pressure at the gas temperature and the droplet number concentration as well. Estimates of these two parameters are available. From a measured gas temperature of  $22^\circ\text{C}$  the water vapour content  $c_{\text{H}_2\text{O}}$  under equilibrium conditions is known to be  $22 \text{ g}\cdot\text{m}^{-3}$ . In this temperature range  $c_{\text{H}_2\text{O}}$  is nearly proportional to temperature. Consequently, an error of a few degrees results in a negligible error of about 10% in  $c_{\text{H}_2\text{O}}$ . From the aerosol decay curves one obtains a number concentration of about  $5 \times 10^4 \text{ cm}^{-3}$  at the moment stirred settling governs aerosol decay. From this the percentage of supersaturation %S can be calculated according to

$$\%S = \frac{c_n \pi \rho_{H_2O} d^3}{6 c_{H_2O}} \times 100 = 0.12 d^3 \quad (93)$$

with the droplet diameter  $d$  in  $\mu\text{m}$  and the density of water  $\rho_{H_2O}$  equal to  $1 \text{ g.cm}^{-3}$ . The obtained  $\%S$  values are given in Table XIX. They are of the same magnitude as those observed directly (a few %) giving support to the correctness of this approach. When care is taken to measure both temperature and  $c_n$ , and, moreover, the thermophoretic contribution is known, this approach allows assessment of the degree of supersaturation of atmospheres above warm pools. The  $\%S$  values in the system studied are comparable to those present in clouds [122] and, hence, droplet formation in clouds can be studied in vessels like PERVEX.

Beside the variation of the pool heating power the supersaturation can be controlled also by addition of salt to the warm pool. The effect of this on aerosol behaviour has been studied in GRACE with the heating power held constant at 100 W. The vessel contained 15 liters of water of which the salt content has been varied by addition of amounts of NaCl ranging from 0.1 kg up to 3 kg. In this case E.W. generated copper oxide aerosols have been used. Table XX summarizes the experimental conditions and results. In addition, the course of the calculation of droplet size  $d$ , percentage of supersaturation  $\%S$ , etc., is given. Qualitatively, increase of the salt concentration results in an increased aerosol stability ( $t_{\frac{1}{2}}$  increases and  $\beta$  shows the inverse effect). Assuming stirred settling of the formed droplets to be the major process, the Stokes settling velocities  $v_s$  were calculated. However, the  $v_s$  value of  $9.2 \times 10^{-3} \text{ cm.s}^{-1}$  found for  $200 \text{ kg NaCl.m}^{-3}$  (corresponding to a droplet diameter of  $1.7 \mu\text{m}$ ) is unlikely large in view of the visual absence of fog formation in these cases of highest salt concentrations. This again indicates the additional effect of thermophoresis which analogously to the above given analysis of PERVEX results is taken to have a decay constant  $\beta_{th}$  about half that of the dry system:  $\beta_{th} = 7.7 \times 10^{-5} \text{ s}^{-1}$ . The droplet sizes obtained after correction for thermophoresis are reasonable in view of the results in PERVEX (Table XIX) and the earlier mentioned droplet sizes deduced from Millikan chamber observations. As a result also the  $\%S$  values are comparable. A droplet

number concentration of  $10^5 \text{ cm}^{-3}$  has been used which is indicated by the condensation nuclei counter. Obviously, the supersaturation can be controlled very accurately by the salt addition in the wide range from 0.1% to nearly 2%. Assuming an error of  $\pm 10\%$  in the basic  $t_{1/2}$  data, the calculated values of  $d$  and  $\%S$  have an error of  $\pm 20\%$  for low NaCl concentrations increasing to nearly  $\pm 50\%$  for the highest NaCl concentrations.

From the measured degree of supersaturation the effect of adding NaCl on the water vapour concentration may be found and compared with the calculated value of  $\Delta c_{\text{H}_2\text{O}} = 29 \text{ g H}_2\text{O} \cdot \text{m}^{-3}$  per  $\text{g NaCl} \cdot \text{cm}^{-3}$  at  $39^\circ \text{C}$  which is the GRACE pool temperature. Fig. 38 shows that from 7 up to 20  $\text{kg NaCl} \cdot \text{m}^{-3}$  experimental and theoretical  $\Delta c_{\text{H}_2\text{O}}$  values are proportional, the theoretical values being about 75% larger.

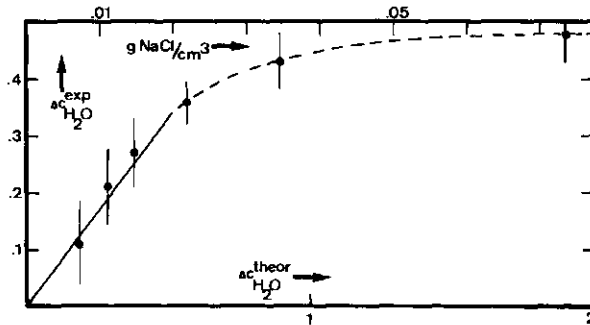


Fig. 38. Lowering of the water vapour concentration  $\Delta c_{\text{H}_2\text{O}}^{\text{exp}}$  (in  $\text{g H}_2\text{O} \cdot \text{m}^{-3}$ ) in the GRACE atmosphere as a function of the calculated water vapour concentration lowering  $\Delta c_{\text{H}_2\text{O}}^{\text{theor}}$  (lower scale) from the NaCl concentration (upper scale,  $\text{g NaCl} \cdot \text{cm}^{-3}$ ) in the pool.

This discrepancy can be easily accounted for by an increase of a few tenths °C of the pool temperature due to a change in the balance between latent and sensible heat transfers after the salt addition. Indeed, pool temperature increased about 0.5 °C after addition of 33 kg NaCl.m<sup>-3</sup>. The discrepancy between theory and experiment for higher salt concentration ( $\geq 20$  kg NaCl.m<sup>-3</sup>) is not surprising since the experimental technique used cannot yield information about the water content of atmospheres with supersaturation levels near zero and below.

In conclusion, it can be established that spaces containing a heated pool of liquid are a potential tool for investigation of condensation on aerosol particles. When low levels of heating power are used or when the evaporation of the pool is suppressed by salt addition to it, the droplet sizes and the degree of supersaturation are known. For the latter property knowledge of gas temperature and droplet number concentration is required. The aerosol decay at higher levels of heating power is accelerated, the two-fifth power of the mass concentration of the original aerosol decreasing linearly with time. Ultimately, a "catastrophic" disappearance is the result, leading to a well-defined point of time after which the atmosphere is essentially free of aerosol. In this stage the mechanisms governing aerosol behaviour are condensational droplet growth and stirred settling.

#### 4.5.4. Summary

The presence of a pool of heated liquid inside an aerosol containing vessel leads to condensation on the aerosol particles, followed by gravitational settling of the droplets formed. Hydrophobic aerosols (like various oils) are not subject to condensation in case of a heated water pool with low levels of supersaturation. Assuming 0.1% to 0.6% of the heating power from the pool to be involved in the condensation on the particles, good agreement is obtained between the experiments and a model of the aerosol mass concentration decay. The model allows also calculation of droplet sizes and reasonable estimates of the degree of supersaturation (a few %) of the atmosphere in absence of aerosols. This is also applied to cases of vapour pressure lowering by addition of salt to the pool.

#### 4.6. Photochemical reaction chambers (smog chambers)

##### 4.6.1. General

As mentioned in the introduction (section 1.2) of this thesis, one of the motives for the study of aerosol behaviour inside an enclosure is the influence which the enclosure walls can exert on processes taking place in an air parcel brought into an enclosure for the purpose of investigation. Such an air parcel can be an atmospheric sample or an artificial one. The majority of this kind of research involves the photochemistry of air contaminated with various gaseous pollutants (photochemical air pollution). In particular, the systems in air of unsaturated hydrocarbons/ $\text{NO}_x$  and  $\text{SO}_2$ / water vapour are subjects of intensive research in photochemical reaction chambers (smog chambers). Usually, the air is filtered prior to filling the smog chamber but recently the role of the particulate matter in the atmospheric photochemistry has also attracted attention. In some cases the aerosol formed or the condensation of less volatile reaction products on existing particles are studied which, obviously, requires insight in the interfering interaction between aerosol and the smog chamber walls. These effects have received only limited attention as may be clear from section 1.2 (though the examples given there are not exhaustive). Unfortunately, the possible effects of the illumination of smog chamber atmospheres on aerosol behaviour are not mentioned in literature.

##### 4.6.2. Thermophoretic effects

In the author's laboratory photochemical studies are performed in smog chambers. These investigations are focussed on the role which particles can play in photochemical reactions in the systems mentioned above. For this purpose a twin smog chamber called SUNKIST is used which consists of two identical  $1 \text{ m}^3$  Pyrex-glass boxes ( $b \times l \times h = 0.8 \times 1.25 \times 1 \text{ m}^3$ ). Between the two boxes a sunlamp battery is located which irradiates the box contents simulating a sun-lit atmosphere. By comparing the chemical reactions occurring in the box atmospheres, one of them being aerosol-free, information on the role of aerosol will be obtained. Apart from the window walls ( $0.8 \times 1 \text{ m}$ ), the walls of the boxes are covered externally with aluminium foil in order to have optimum use and distribution of the light shining into the boxes.

In order to assess the effect of thermophoresis the heat transfer by the box atmosphere must be determined. Using highly polished thermocouples the gas temperatures of the box atmospheres of SUNKIST have been measured. These temperatures were found to be about 2 °C above laboratory temperature. From this temperature difference  $\Delta T$  (in °C) a heat flux  $Q/S$  (in  $W.m^{-2}$ ) through the box walls equal to  $9 W.m^{-2}$  can be deduced by using

$$\frac{Q}{S} = 4.5 \Delta T \quad (94)$$

This rule of thumb (which can be derived from (25)) was obtained by the author for the  $Q/S$  range of 10 - 200  $W.m^{-2}$  from a great number of observations on a variety of internally heated vessels of e.g. glass, plexiglass and steel, all in a laboratory environment. From the heat flux of  $9 W.m^{-2}$  and assuming a heat sink surface area of the box equal to  $5.3 m^2$ , one obtains an effective power  $Q$  of heat transfer from the box atmosphere to the surroundings amounting to 41 W. This is about 5% of the total electric power consumed by the sun lamp battery (0.8 kW). Using Eq. (26) which relates the thermophoretic decay constant  $\beta_{th}$  to the heating power density  $\frac{Q}{V}$ , and a B-value of 0.2 (which is the experimental value; see pg.113) one obtains

$$\beta_{th} = 0.4 \frac{Q}{V} \quad (96)$$

for larger particles ( $r > \bar{l}$ ). Hence,  $\beta_{th}$  amounts to about  $1.6 \times 10^{-5} s^{-1}$  or the aerosol half-life equals nearly 12 hours. For the small particles ("transient nuclei" of median size about 0.02  $\mu m$ ) formed in smog chambers containing filtered air half-lives will be smaller, viz. about 7 hours ( $n_{th} \approx 3$  for  $r < \bar{l}$ ; see pg. 38).

#### 4.6.3. Photophoretic effects

Usually, in research on photochemistry of the troposphere interest is focussed on the reactions induced by near-UV light since this is the most energetic part of sun light. Consequently, there is often only limited information about the visible spectral light flux simultaneously radiated into smog chambers. In some cases black lamps are used which

have a relatively small light flux in the visual range. The light intensity spectrum inside SUNKIST has not been measured. However, certainly, its black lamps provide merely a good simulation of the near UV sunlight intensity but the visible light intensity is much less than that of sunlight. In order to have a basis for assessment of possible photophoretic effects in smog chambers, we assume here a light flux with a spectral distribution and integral flux equal to the sun light. Consequently, our considerations apply mainly to those experimental set-ups which either use sun lamps or outdoor facilities. This means that we assume that about  $0.1 \text{ W.cm}^{-2}$  radiates into the smog chamber, leading to a photophoretic velocity (pg. 46) (supposing absorbing particles with  $\text{Kn} < 1$ ) of about  $0.01 \text{ cm.s}^{-1}$  in the direction of the illuminated walls. In the case of boxes like SUNKIST (section 4.6.2) a photophoretic decay constant  $\beta_p$  results amounting to  $8 \times 10^{-5} \text{ s}^{-1}$  or an aerosol half-life of 24 hours. When small particles (nuclei of  $\text{Kn} > 1$ ) as formed in irradiated filtered air systems are subjected to this photophoresis one would obtain a half-life of about 15 hours (for  $\text{Kn} > 1$  then  $n_{th}$ -value in Eq. (39) should amount to about 3). These half-lives are not too short, but it should be kept in mind that actual deposition rates due to photophoresis will be even smaller since

- particles will not be completely absorbing,
- often the smog chamber radiation sources have total light fluxes lower than  $0.1 \text{ W.cm}^{-2}$  because of a lower visual light content than in actual sun light,
- due to application of light reflecting walls the light incidence is usually from various directions, resulting in random photophoretic forces which partially cancel.

Consequently, calculated photophoretic deposition rates will be maximum values.

#### 4.6.4. Diffusional and gravitational effects

Smog chamber experiments are usually performed without pre-existing aerosol. Then sizes of the particles formed are  $0.1 \mu\text{m}$  or less. Consequently, gravitational deposition will be of minor importance compared to e.g. diffusive deposition. The constant  $\beta_d$  for the latter removal process is given by Eq. (16) where  $\delta$ , the effective boundary layer thickness for diffusive wall deposition, is related to particle size or

diffusion coefficient by  $\delta = 4.6 D^{0.265}$  (as derived in section 2.2.2 (Eq. (15)). Consequently, Eq. (14) reduces to

$$\beta_d = 0.22 D^{0.735} \frac{S}{V} \quad (97)$$

A smog chamber like SUNKIST (1 m<sup>3</sup> volume, see pg.132) will have diffusive wall loss of nuclei of 0.02  $\mu\text{m}$  diameter with a decay constant  $\beta_d$  amounting to about  $2 \times 10^{-5} \text{ s}^{-1}$  or 10 hours half-life. This is a rather low deposition rate. Consequently, diffusive deposition will not play an important role in the interpretation of smog chamber data.

#### 4.6.5. Coagulation combined with deposition

During irradiation of the contents of a smog chamber three processes influence aerosol behaviour: the photochemical production of low-volatility material, coagulation and wall deposition. Some investigators have studied the combined action of the two first-mentioned processes, e.g. Friedlander's group [40]. The competition between the homogeneous nucleation of the photochemical reaction products and the condensation of these products on pre-existing particles or on freshly formed nuclei is a rather complicated matter and also goes beyond the scope of this study. It should be mentioned, however, that Friedlander has shown [123] that the largest part of the mass of the reaction product condenses on a pre-existing aerosol without excluding significant formation of new nuclei.

Since coagulation and deposition of the pre-existing aerosol have to be considered also, this combined effect is treated here. This mixed effect has been studied already in early periods of aerosol research (see pg. 19). Nolan [13] explained the observed decay of nuclei in an enclosure by assuming that coagulation and (diffusive) deposition occur at all concentrations, the former process dominating at higher concentrations and the latter dominating in the low concentration regime. The number concentration decay is then a combination of Eqs. (1) and (4)

$$-\frac{dc_n}{dt} = Kc_n^2 + \beta c_n \quad (98)$$



Provided  $K$  and  $\beta$  are constants (which is common experience, sections 1.2 and 2.1), integration leads to

$$c_n = \frac{\beta c_n(o) \exp(-\beta t)}{\beta + Kc_n(o) \{1 - \exp(-\beta t)\}} \quad (99)$$

#### 4.6.6. Experiments and discussion

As mentioned earlier, the simultaneous formation and dynamics of new particulate material in photochemical systems complicates considerably the analysis of aerosol behaviour under these conditions. Consequently, experiments discussed here are performed without such a continuous aerosol source. Instead, an aerosol has been chosen with a relatively small particle size. Aerosols have been produced by nebulizing a salt solution (pg. 63) yielding particles with a log-normal size distribution of  $d_g \approx 0.06 \mu\text{m}$  and  $\sigma_g = 1.7$  for 1 wt.% solutions, according to analysis of electron micrographs.

Fig. 39 exemplifies the decay of two NaCl aerosols decaying in the 100-vessel due to combined coagulation and stirred deposition. Both series of decay data have been used for fitting Eq. (99). This fitting leads to coagulation constants  $K$  of  $1.5 \times$  to  $2 \times 10^{-9} \text{ cm}^3 \cdot \text{s}^{-1}$  and decay constants  $\beta$  of  $3.2 \times$  to  $3.5 \times 10^{-6} \text{ s}^{-1}$ . Table XXI allows comparison between measured and calculated  $c_n$ -values. The standard deviation between measurement and calculation amounts to  $-2.8\% \pm 13\%$  and  $-7.7\% \pm 6\%$  for the two series, which should be regarded to be a good fit. From the decay constants obtained in this way one may deduce a particle diameter of  $0.061 - 0.065 \mu\text{m}$  assuming Eq. (16) for stirred diffusive deposition to be valid as well as the relation (15) between  $\delta$  and  $D$  obtained in section 4.3.1. Since this particle diameter of about  $0.06 \mu\text{m}$  is in good agreement with the above mentioned value for the particle size, this proves the correctness of the approach. In particular, the fit with the relation between  $\delta$  and  $D$  (Eq. (15)) is obvious. The obtained coagulation constant  $K$  of  $1.5 - 2.0 \times 10^{-9} \text{ cm}^3 \cdot \text{s}^{-1}$  is in agreement with Davies' theory [116]. Fig. 40 shows that our  $K$ -value ( $Kn = 2$ ) is close to Davies' theoretical relation. Strikingly, also the  $K$ -values obtained by Nolan and Kennan are in excellent agreement with theory. Since their results have been obtained also by analysis of decay curves of aerosols in enclosures, this indicates that this

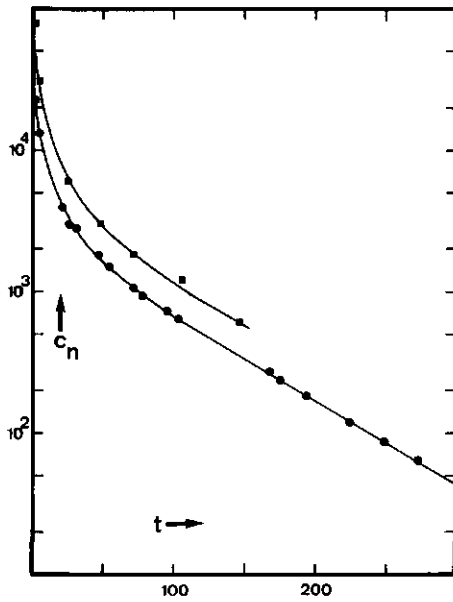


Fig. 39. Number concentration  $c_n$  (in  $\text{cm}^{-3}$ ) as a function of time  $t$  (in hours) of NaCl aerosols (from 1% NaCl solution nebulizing) in the 100-vessel.

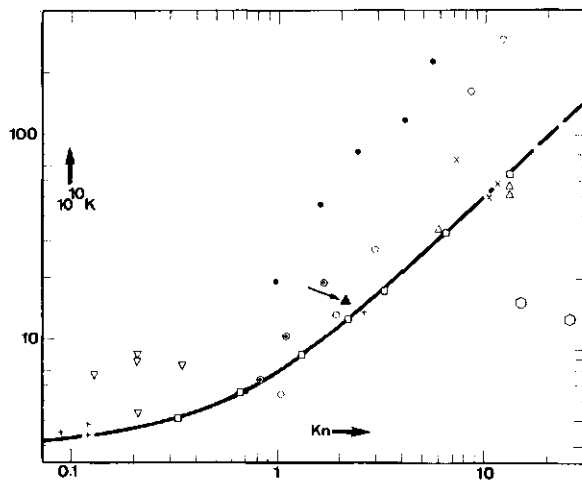


Fig. 40. Coagulation coefficient  $K$  of aerosols below  $Kn = 15$  (taken from [116]). The solid line represents the theoretical relation according to Davies [116].

- Experimental results:
- $\Delta$  Rooker and Davies [163]
  - $\times$  Mercer and Tillery [162]
  - $+$  Devir [130]
  - $\square$  Nolan and Kennan [131]
  - $\circ$  Wagner and Kerker [132]
  - $\odot$  Chatterjee [133]
  - $\bullet$  Quon [134]
  - $\nabla$  Gillespie and Langstroth [24]
  - $\circ$  Fuchs and Sutugin [135]
  - $\blacktriangle$  This work

technique is a powerful tool for coagulation reserach.

In an attempt to study the effect of irradiation on aerosol behaviour in SUNKIST (see section 4.6.2), this box has been filled with  $\text{Na}_2\text{SO}_4^-$  aerosol produced by nebulisation. Prior to entering the box the aerosol has been neutralized in a  $^{85}\text{Kr}$  TSI-neutralizer. The aerosol decay measurements have been carried out for the illuminated box as well as with the UV-lamps switched off. Two measurement techniques have

been applied simultaneously. The number concentration  $c_n$  has been measured by means of an Environment One Rich 100 condensation nuclei counter. For total airborne sulphur a Meloy SA 285 Total Sulphur Monitor (TSM) has been used. Zero readings were obtained by both instruments at the beginning of the experiments. The lamps have been on for two hours prior to aerosol injection. Since the TSM has been calibrated for  $SO_2$ , there could be uncertainty as to the absolute value of the measuring signal. However, according to literature [129] the chemical state of sulphur influences the TSM reading only in case of combined chemical reactivity and volatility at temperatures  $< 150^\circ C$  like e.g. for  $H_2SO_4$ . Evidently, decay constants can be correctly obtained by means of the TSM.

The results of the experiments are given in fig. 41. The total sulphur concentration has a half-life of 7.5 hours irrespective of illumination.

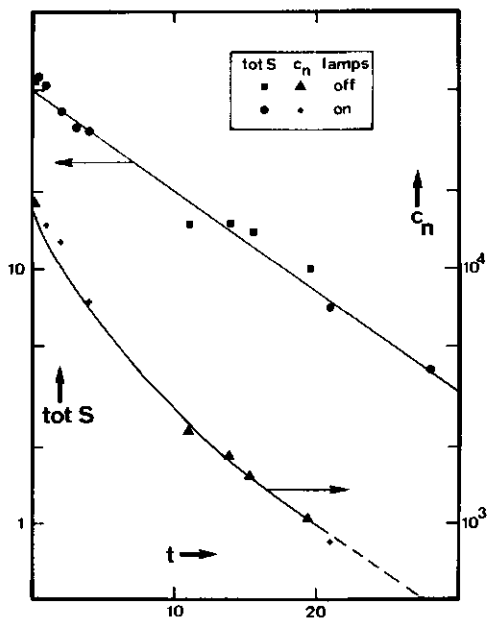


Fig. 41. Courses of number concentration  $c_n$  (in  $cm^{-3}$ ) and "total sulphur" concentration (tot S, in ppb S) of  $Na_2SO_4$  aerosol in SUNKIST: comparison between lamps on vs. off. t in hours.

A number of important conclusions can be drawn from these results. Firstly, there is no significant influence of the irradiation on aerosol behaviour inside SUNKIST. This means that the two processes treated in sections 4.6.2 and 4.6.3 (thermophoresis and photophoresis, resp.) do not play an important role in this case. Very probably, the reasons given in 4.6.3 for having low photophoretic deposition apply very well to SUNKIST. One of the major effects can be due to multiple reflections at the externally aluminized glass walls. Thermophoresis probably is less than calculated due to the difficulty of reliable temperature measurement of an illuminated box atmosphere like SUNKIST. Due to radiative heat transfer the observed  $\Delta T$  of 2 °C relative to the surroundings could have been too high.

Secondly, from the half-life of aerosol decay of 7.5 hours it can be concluded that diffusive deposition is not dominant. The particles of 0.06  $\mu\text{m}$  diameter should disappear by stirred diffusive deposition with a half-life of 48 hours. Consequently, diffusive deposition is negligible.

Thirdly, as shown in Table XXII the average particle diameter increases with time. Although this is due to a decreasing  $c_n$  decay rate, coagulation is not responsible for that as the mass concentration decreases too. Moreover, the related effective coagulation "constant" of  $5 \times 10^{-9} \text{ cm}^3 \cdot \text{s}^{-1}$  at  $c_n = 10^4 \text{ cm}^{-3}$  should be considered too large. Consequently, the deposition mechanism responsible for the aerosol decay removes the finer particles with a higher rate.

Now, no stirred deposition process is left from those treated in chapter 2 except stirred electrophoretic deposition (2.2) which process is also dealt with in section 4.3.7. Consequently, it is worthwhile to analyze the half-life of 7.5 hours ( $\beta = 2.6 \times 10^{-5} \text{ s}^{-1}$ ) in a similar way as in 4.3.7. Using  $\mu_e = 10^{-4} \text{ cm}^2 \cdot \text{V}^{-1} \cdot \text{s}^{-1}$ , this yields a total effective charge on the SUNKIST-walls of  $5 \times 10^{-8} \text{ C}$  or a surface charge density of  $8 \times 10^{-9} \text{ C} \cdot \text{m}^{-2}$ . This is a realistic value compared to those given in 4.3.7. In particular, the fact that the value for SUNKIST is comparable to that calculated for Zalabsky's glass vessel (Table XIII), viz.  $10^{-8} \text{ C} \cdot \text{m}^{-2}$ , is very satisfying. However, also the slightly different  $\frac{q_e}{S}$  values of  $7 \times 10^{-9} \text{ C} \cdot \text{m}^{-2}$  found for our polyethylene vessel and  $3 \times 10^{-8} \text{ C} \cdot \text{m}^{-2}$  for McMurry's large teflon bag all show the coherence of aerosol behaviour in vessels with

non-conducting walls. The walls of all these vessels have not been cleaned specially prior to the experiments and as a result will have had less surface charge than those of Stein and Lieberman (Table XIII).

From the increase (as shown in Table XXII) of the particle diameter during aerosol removal, it is obvious that the smallest particles deposit at a faster rate and, consequently, should have a higher electrical mobility  $\mu_e$ . This is in accordance with Eq. (43) provided particle size is below  $0.1 \mu\text{m}$  which is the case.

Finally, some conclusions can be drawn concerning the correctness of the "total sulphur" measurement by means of the TSM. The calculated diameters represented in Table XXII should be compared with the mass averaged diameter which can be calculated from the fact that  $d_g = 0.06 \mu\text{m}$  and  $\sigma_g = 1.7$ . These figures are characteristic of a count-size distribution which may be converted to a mass median diameter (mmd) [97] by

$$\ln(\text{mmd}) = \ln(d_g) + 3 \ln^2 \sigma_g \quad (100)$$

Hence, mmd amounts to  $0.14 \mu\text{m}$ . From this a mass-average particle diameter  $\bar{d}$  can be calculated [97] with the aid of

$$\ln \bar{d} = \ln(\text{mmd}) + 1.5 \ln^2 \sigma_g \quad (101)$$

This yields  $\bar{d} = 0.24 \mu\text{m}$ . Comparison with the measured  $d$ -value ( $0.28 \mu\text{m}$ ) at  $t = 0$  of Table XXII shows a reasonable agreement between these diameters. This means that the total sulphur monitor is a suitable apparatus for sulphate aerosol analysis (confirming [129]) and that the analysis of the decay curves of sulphate aerosols by means of the total sulfur monitor (flame photometric detector) is very useful.

#### 4.6.7. Summary

The effects of thermophoresis and photophoresis from the heat and light fluxes present in a photochemical reaction chamber have been calculated. Thermophoresis could cause aerosol deposition with a half-life of 5 - 10 hours. Photophoresis can give rise to a half-life of at least 2 hours. Observations on aerosol behaviour in a smog chamber revealed

the relatively great importance of electrophoretic deposition. In this chamber thermophoretic and photophoretic deposition are smaller than calculated for various reasons.

Analyses of aerosol decay data in a steel reaction chamber show the usefulness of the models for stirred deposition of small particles and nuclei. Also the utility of such aerosol measurements for assessing coagulation constants and diffusion deposition velocities has been demonstrated.

## 5. GENERAL SUMMARY

This thesis treats aerosol behaviour under various conditions in enclosed spaces. Knowledge of this behaviour is of importance for the use of aerosol-filled enclosures as a supply of aerosol, as a means for aerosol characterization and for so-called smog chambers for air pollution research (mainly for the investigation of photochemical processes by which usually particles are formed).

Chapter 1 gives a brief literature survey, indicating the limited attention given hitherto to aerosol behaviour in enclosed spaces. After decades of almost exclusive interest from meteorologists, since the beginning of the sixties, enclosed aerosols have become an important research subject in nuclear safety. Nuclear aerosol research, however, pertains mainly to high aerosol mass concentrations.

In chapter 2 a model is given, describing aerosol removal from enclosed spaces. Usually, aerosol deposition on the walls occurs from a cloud with homogeneous space distribution due to thermal convection. The rate-limiting step of deposition is the transport through the boundary layer at the walls. Relations are derived for a number of removal mechanisms: sedimentation, diffusion, thermophoresis, diffusio-phoresis, electrophoresis and photophoresis. From literature data and Fuchs' theory a relation is derived for the dependence of the boundary layer thickness  $\delta$  for diffusive deposition on the diffusion coefficient  $D$  of aerosol particles in usual containments. Boundary conditions for non-stirred deposition of aerosols by sedimentation and diffusion are given.

Chapter 3 summarizes the most important means used for experiments.

In chapter 4 the experimental results and conclusions are presented. It consists of four sections dealing with unheated dry enclosures, heated dry enclosures, enclosures with a heated pool of liquid, and smog chambers, respectively.

Observations on the behaviour of monodisperse and polydisperse aerosols in unheated dry enclosures support the model derived for sedimentation and diffusion. Additionally, the relation between  $\delta$  and  $D$  derived in chapter 2 is validated. Particles larger than a few tenths of a micron are removed by sedimentation; particles smaller than about  $0.1 \mu\text{m}$  are



subject to diffusive deposition, though often electrophoresis plays an important role (particularly, in case of particles of about  $0.1 \mu\text{m}$ ). It is shown that aerosol measurements in containments can be used for determination of dynamic shape factors and aerodynamic diameters.

Aerosols in heated dry containments are removed by thermophoresis. Observations on a large variety of aerosols and enclosures are in fair agreement with the model on thermophoretic removal derived in chapter 2. Interpretation of the experimental results yields the thermophoretic properties of aerosols. The results support the theories of Brock and Stetter, and are in disagreement with those of Derjaguin and Epstein. In accordance with theoretical predictions, thermophoretic decay constants are obtained independent of particle size ( $\geq 0.5 \mu\text{m}$ ), of particle material and of temperature. Gentle heating of the floor of a containment is shown to have a stabilizing effect on the enclosed aerosol.

Introduction of aerosol in a containment with a heated pool of liquid on the floor leads to particle growth by vapour condensation followed by an accelerating removal by sedimentation. Experimental observations support a model describing aerosol behaviour in such systems. The knowledge of this aerosol behaviour allows study of condensation on aerosol particles and particle growth under conditions of variable degrees of supersaturation. The degree of supersaturation can be varied by means of the heating power dissipated in the pool of liquid as well as by means of solving substances in the liquid.

Investigations of aerosol behaviour in photochemical smog chambers show insignificant deposition due to thermophoresis or photophoresis under these conditions. Observed aerosol stabilities could be explained by electrophoretic deposition, yielding a coherent picture with electrophoresis in other investigations. Coagulation constants of aerosol could be calculated from measurements on number concentrations of aerosols in enclosed spaces. The results obtained agree fairly well with Davies' theory on coagulation. Decay curves of number concentration of aerosols in metal vessels can be used for assessment of diffusion coefficients.

REFERENCES

- | 1| O.J. Lodge, *Nature* 31 (1885), 265.
- | 2| B.G. Ferris Jr, *J. Air Poll. Control Ass.* 28 (1978), 482.
- | 3| H.G. Boren, *Arch. Environ. Health* 8 (1964), 119  
(N.J. Furiiosi, et al., *Arch. Environ. Health* 27 (1973), 405  
could not establish any synergism between NaCl-aerosol and NO<sub>2</sub>  
on the response of exposed rats and monkeys).
- | 4| e.g. M.O. Amdur, in "Air Quality Criteria for particulate Matter"  
(U.S.A. Dept. Health, Education and Welfare, Washington, 1969),  
AP-49, 134.
- | 5| N.A. Fuchs, "The Mechanics of Aerosols" (Pergamon Press, Oxford,  
1964), p. 250.
- | 6| J.F. van de Vate, "The Safety of SNR-300 and the Aerosol Model;  
a Summary Report of the RCN Aerosol Research 1967 - 1971",  
RCN-174, 1972.
- | 7| J.F. van de Vate, et al., Fourth International Clean Air Congress  
May, 1977, Tokyo, Japan.
- | 8| Morton Corn, "Properties of non-viable particles in air", in  
A.C. Stern's "Air Pollution", Vol I (Third Ed., Acad. Press,  
New York, 1967), p. 294.  
(about extraterrestrial (meteoritic)dust cf. G.M. Hidy, The Dynamics  
of Aerosols in the Lower Troposphere, in "Assessment of Airborne  
Particles", ed. T.T. Mercer, et al., (C.C. Thomas, Springfield, U.S.A.,  
(1972)).
- | 9| K.T. Whitby and B. Cantrell, "Atmospheric Aerosols - Characteristics  
and Measurement" in Proc. Int. Conf. Envir. Sensing and Assessment,  
Las Vegas (USA), Sept. 14-19, 1975 (IEEE, New York, 1976), paper  
29-1.
- | 10| R.K.A.M. Mallant, et al. "Submicron Marine Aerosol: Size Distribution  
and Chemical Reactivity", Proc. Int. Conf. Gesellschaft für  
Aerosol forschung, Vienna, Sept. 26-28, 1978.
- | 11| H. Kennedy, *Proc. Roy. Irish Acad.* 33A (1916), 58.
- | 12| W.D. Flower, *Phil. Mag.* 5 (1928), 1084.
- | 13| P.J. Nolan, *Proc. Roy. Irish Acad.* 41A (1933), 61.
- | 14| J.J. Nolan and V.H. Guerrini, *Proc. Roy. Irish Acad.* 43A (1935), 5.

- [15] H. Rauscher, Wiener Anz. 70 (1933), 198.
- [16] L.W. Pollak and T.C. O'Connor, Geofis. Pura Appl. 31 (1955), 66.
- [17] R. Fürth, Geofis. Pura Appl. 31 (1955), 80.
- [18] P.J. Nolan and E. Kuffel, Geofis. Pura Appl. 31 (1955), 97.
- [19] L.W. Pollak, T.C. O'Connor and A.L. Metnieks, Geofis. Pura Appl. 32 (1956), 177.
- [20] T.C. O'Connor, Geofis. Pura Appl. 31 (1959), 107.
- [21] P.J. Nolan and J.A. Scott, Proc. Roy. Irish Acad. 63A (1955), 35.
- [22] G. McGreevy, Arch. Meteor. Geophys. u. Bioklim. 14A (1965), 149.
- [23] G.O. Langstroth and T. Gillespie, Can. J. Res. 25B (1949), 455.
- [24] T. Gillespie and G.O. Langstroth, Can. J. Chem. 29 (1951), 133 and 201.
- [25] J. Rosinski, D. Werke and C.T. Nagamoto, J. Coll. Sci. 17 (1962), 703.
- [26] Nuclear Aerosols in Reactor Safety, State-of-the-art report of the Expert Group of the committee on the Safety of Nuclear Installations, Nuclear Energy Agency of the Organisation for Economic Cooperation and Development OECD, Paris, France, CSNI-report no. 34 (1979).
- [27] "Airborne Radioactivity", selected papers from 1977 ANS Winter Meeting, San Francisco (Cal.), Nov. 29 - Dec. 2, 1977 (American Nuclear Society, 1978).
- [28] M.A. Greenfield, R.L. Koontz and D.F. Hausknecht, AI-AEC-12878 (1970).
- [29] M.A. Greenfield, R.L. Koontz and D.F. Hausknecht, J. Colloid Interf. Sci. 35 (1971), p. 102.
- [30] Quart. Techn. Progr. Report, LMFBR Safety Programs, Jan. - March 1971 AI-AEC-13014 (1971).
- [31] R.J. Davis, Am. Ind. Hyg. Ass. J. 32 (1971), 603.
- [32] See Ref. [26], Appendix D.
- [33] G.C. Lindauer and A.W. Castleman, Jr., J. Aerosol Sci. 2 (1971), 85.

- [34] F.L. Horn and A.W. Castleman, Jr., Proc. Int. Congress on the Diffusion of Fission Products, Saclay, France (Nov. 4 - 6, 1969), p. 93.
- [35] W. Schikarski and H. Wild, Staub 30 (1970), 251, and also: K. Keller, KFK 1490 (1971).
- [36] S. Jordan, Gesellschaft für Kernforschung, Karlsruhe, W. Germany (personal communication).
- [37] J.A. Gieseke, et al., HAAARM-3 Users Manual, BMI-NUREG-1991 (1978).
- [38] G. Nishio, et al., Nucl. Enging Design 34 (1975), 417.
- [39] D.F. Miller, Exploratory Study of Factors Affecting Aerosol Formation, EPA 650/3-75-002 (1974).
- [40] P.H. McMurry, On the Relationship between Aerosol Dynamics and the Rate of Gas-to-Particle Conversion, Thesis Calif. Instit. Technology, Pasadena (Cal.), 1977.
- [41] R.A. Zalabsky, A Study of Photochemical Aerosol Formation and the Coagulative Mass Transport in Natural and Laboratory Aerosol-Gas Mixtures, Thesis Univ. Arizona (1978).
- [42] a. M. von Smoluchowski, Z. Phys. Chem. 92 (1917), 140.  
b. H. Müller, Kolloidchem. Beih. 26 (1928), 257.
- [43] G. Zebel, Kolloid-Z. 156 (1958), 102.
- [44] P. Spiegler, J.G. Morgan, M.A. Greenfield, R.L. Koontz, NAA-SR-11997, vol. I (1967).
- [45] G. Zebel, "Coagulation of Aerosols" in "Aerosol Science", ed. C.N. Davies (Academic Press, London-New York, 1966), p. 37.
- [46] T. Gillespie, Proc. Roy. Soc. A216 (1953), 569.
- [47] J. Rosinski, et al., J. Coll. Sci. 17 (1962), 703.
- [48] L. Prandtl, "Führer durch Strömungslehre" (Brannschweig, 1949); reference given by Fuchs [3].
- [49] N.A. Fuchs, "The Mechanics of Aerosols" (Pergamon Press, Oxford, 1964), p. 250.
- [50] Watson, G.M., Perez, R.B., Fontana, M.H., "Effects of Containment Size on Fission Product Behaviour", ORNL-4033 (1967).

- [51] M. Knudsen and S. Weber, *Ann. Phys.* 36 (1911), 982.
- [52] R.A. Millikan, *Phys. Rev.* 22 (1923), 1.
- [53] C.N. Davies, *J. Aerosol Sci.* 10 (1979), 151.
- [54] A. Einstein, *Ann. Physik* 17 (1905), 549.
- [55] Ref. [5], p. 254.
- [56] K. Shifrin *et al.*, *Izv. Akad. Nauk. SSSR, ser. geogr. geofiz.*, 3 (1949), 238.
- [57] T. Gillespie and G.O. Langstroth, *Can. J. Chem.* 29 (1951), 133.
- [58] P.J. Nolan, *Proc. Roy. Irish Acad.* 47A (1941), 25.
- [59] J.F. van de Vate, *J. Colloid Interf. Sci.* 41 (1972), 194.
- [60] R.A. Cox and S.A. Penkett, *Atm. Environ.* 6 (1972), 365.
- [61] H.M. ten Brink (Netherlands Energy Research Foundation, Petten) personal communication.
- [62] T.T. Mercer and M.I. Tillery, *J. Coll. Interf. Sci.* 37 (1971), 785.
- [63] S.J. Rooker and C.N. Davies, *J. Aerosol Sci.* 10 (1979), 139.
- [64] A. Einstein, *Z.f. Physik* 27 (1924), 1.
- [65] P.S. Epstein, *Z.f. Physik* 54 (1929), 537.
- [66] C.F. Schadt and R.D. Cadle, *J. Phys. Chem.* 65 (1961), 1689.
- [67] S. Jacobsen and J.R. Brock, *J. Colloid Sci.* 20 (1965), 544.
- [68] K.H. Schmitt, *Z. Naturf.* 16a (1961), 144.
- [69] *Int. Rev. in Aerosol Physics and Chemistry*, vol. 2 "Topics in Current Aerosol Research", ed. G.M. Hidy and J.R. Brock, (Pergamon Press, Oxford, 1971), p. 48.
- [70] L. Waldmann, *Z.f. Naturf.* 14a (1959), 589.
- [71] G. Stetter, *Sitzungsber. Oesterr. Akad. Wissensch. (Mathem.-naturw. Klasse) Abt. II*, 169 (1960), 91.
- [72] G. Stetter, *Staub* 20 (1960), 244.
- [73] B.V. Derjaguin and Yu. Yalamov, *J. Colloid Sci.* 20 (1965), 555.

- [74] P.J. Whitmore and A. Meisen, *J. Aerosol Sci.* 4 (1973), 435.
- [75] W.J. Moore, "Physical Chemistry" (Longman, 1972).
- [76] P. Goldsmith and F.G. May, "Diffusion- and Thermophoresis in water vapour systems", a contribution to "Aerosol Science", ed. C.N. Davies (Academic Press, London-New York, 1966).
- [77] B.V. Derjaguin, Y.I. Yalamov and A.I. Storozhilova, *J. Coll. Interf. Sci.* 22 (1966), 117.
- [78] N.T. Tong, *J. Coll., Interf. Sci.* 51 (1975), 143.
- [79] B.Y.H. Liu and D.Y.H. Pui, *J. Aerosol Sci.* 6 (1975), 249.
- [80] R.L. Stein, *Am. Ind. Hyg. Ass. J.* 33 (1972), 775.
- [81] J. Bricard and J. Pradel, "Electric Charge and Radioactivity of Naturally occurring Aerosols", in "Aerosol Science" (Ed. C.N. Davies, Acad. Press, London, 1966).
- [82] K.T. Whitby, "Electrical Measurements of Aerosols", in "Fine Particles" (Ed. B.Y.H. Liu, Acad. Press, London, 1976).
- [83] A. Lieberman and J. Rosinski, *J. Coll. Sci.* 17 (1962), 814.
- [84] R.L. Stein, *et al.*, *J. Coll. Interf. Sci.* 42 (1973), 441.
- [85] R.L. Stein and W.H. Ryback, *J. Coll. Interf. Sci.* 38 (1972), 654.
- [86] C.P. Yu, *J. Aerosol Sci.* 8 (1977), 237.
- [87] L.B. Loeb, "Static Electrification", Springer Verlag, Berlin, 1958.
- [88] W. Stöber, *J. Aerosol Sci.* 2 (1971), 453.
- [89] J.A.M.M. Kops, The Aerodynamic Diameter and Specific Surface Area of Branched Chain-like Aggregates, Thesis, University of Eindhoven, 1976 (ECN-5, 1976).
- [90] W. Stöber, "*Dynamic shape factors of non-spherical aerosol particles*" in "Assessment of airborne particles" (Eds. T.T. Mercer, P.E. Morrow and W. Stöber; C.C. Thomas Publ., Springfield, USA, 1972), p. 249.
- [91] M.D. Allen, *et al.*, *J. Aerosol Sci.* 10 (1978), 43.
- [92] Ref. [49], p. 41.

- | 93| W. Stöber, A. Berner, and R. Blaschke, *J. Coll. Interf. Sci.* 29 (1969), 710.
- | 94| W. Stöber, *Staub* 30 (1970), 277.
- | 95| R.A. Vomela, and K.T. Whitby, *J. Coll. Interf. Sci.* 25 (1967), 568.
- | 96| W.J. Megaw and A.C. Wells, *Nature* 299 (1971), 624.
- | 97| G. Herdan, "Small Particle Statistics" (Elsevier, Amsterdam, 1950).
- | 98| S.K. Friedlander, *J. Meteorology* 18 (1961), 753.
- | 99| G.C. Lindauer and A.W. Castleman, *Transact. Am. Nucl. Soc.* 12 (1969), 897.
- | 100| L.J. Goldberg, *Am. J. Hyg.* 68 (1958), 85.
- | 101| I.S. Goldberg, *et al.*, *J. Aerosol Sci.* 9 (1978), 209.
- | 102| J. Pich, *J. Aerosol Sci.* 10 (1976), 131.
- | 103| J. Pich, *J. Aerosol Sci.* 11 (1977), 989.
- | 104| N.A. Fuchs, *Kolloidnyi Zhurnal* 36 (1974), 1183.
- | 105| H. Frostling, *J. Aerosol Sci.* 4 (1973), 411.
- | 106| P.E. Morrow and T.T. Mercer, *Amer. Ind. Hyg. Ass. J.* 25 (1964), 8.
- | 107| A. Plomp, J.F. van de Vate, *et al.*, *Atm. Envir.* 13 (1979), 189.
- | 108| P.J. Nolan and L.W. Pollak, *Proc. Roy. Irish Acad.* 41A (1946), 9.
- | 109| W. Walkenhorst, *Staub* 19 (1959), 15.
- | 110| W. Stöber and H. Flachsbart, *Env. Sci. Techn.* 3 (1969), 1280.
- | 111| J. Porstendörfer and J. Heyder, *J. Aerosol Sci.* 3 (1972), 141.
- | 112| R.F. Phalen, *J. Aerosol Sci.* 3 (1972), 395.
- | 113| M. Tomaidēs and K.T. Whitby, *Proc. 7th Int. Conf. Condensation and Ice Nuclei, Prague-Vienna 1969*, p. 122.
- | 114| A.G. Barkow, F.G. Karioris and J.J. Stoffels, *Adv. X-ray Analysis* 6 (1963), 210.
- | 115| H. Ulich and W. Jost, "Kurzes Lehrbuch der Physikalischen Chemie" (Darmstadt, 1960), p. 81.
- | 116| C.N. Davies, *J. Aerosol Sci.* 10 (1979), 151.

- [117] W. Walkenhorst and W. Coenen, Staub 3 (1977), 106,
- [118] R. Whytlaw-Gray and H.S. Patterson, Smoke (Arnold, London, 1932), p. 16.
- [119] Landolt-Börnstein, Zahlenwerte und Funktionen, Vol. 2, Parts 2 and 4, Springer (1960).
- [120] J.H. van der Hage, Condensation of Water on Insoluble Substrates, Thesis, University of Utrecht, 1974.
- [121] A.G. Amelin, "Theory of Fog Condensation" (Israel Program for Scientific Translation, Jerusalem, 1967).
- [122] N.H. Fletcher, "The Physics of Rain Clouds" (Cambridge, 1969).
- [123] S.K. Friedlander, "Theory of New Particle Formation in the Presence of an Aerosol" in Proc. Int. Conf. Gesellschaft für Aerosol forschung, Vienna, 26-28 September, 1978.
- [124] J.A. Davidson, et al., J. Coll. Interf. Sci. 25 (1967), 381.
- [125] J. Porstendörfer, J. Aerosol Sci. 3 (1972), 141.
- [126] D. Rimberg and J.W. Thomas, J. Coll. Interf. Sci. 32 (1970), 101.
- [127] G. Deželić and J.P. Krahtovil, J. Coll. Interf. Sci. 16 (1961), 561.
- [128] M.J. Heard, et al., Atm. Envir. 4 (1970), 149.
- [129] R.L. Tanner, et al., Atm. Envir. 14 (1980), 121.
- [130] S.E. Devir, J. Colloid Sci. 18 (1963), 744.
- [131] P.J. Nolan and E.L. Kennan, Proc. Roy. Irish Acad. A52 (1949), 171.
- [132] P.E. Wagner and M. Kerker, J. Chem. Phys. 66 (1977), 638.
- [133] A. Chatterjee, et al., J. Colloid Interf. Sci. 53 (1975), 71.
- [134] J.E. Quon, Int. J. Air Water Poll. 8 (1964), 335.
- [135] N.A. Fuchs and A.G. Sutugin, J. Colloid Sci. 20 (1965), 492.



Table I. Thickness  $\delta$  of laminar boundary layer across which diffusive deposition of particles and gases on vessel walls occurs.

"particles" in air	"particle" diameter ( $\mu\text{m}$ )	$\delta$ (cm)	diffusion coefficient ( $\text{cm}^2 \cdot \text{s}^{-1}$ )	literature reference
H <sub>2</sub> O	$(5 \times 10^{-4})^a$	3.5	0.24	61
SO <sub>2</sub>	$(7 \times 10^{-4})^a$	2.5	0.10	60
CaCO <sub>3</sub>	0.01	0.4	$5.2 \times 10^{-4}$	63
"room particles"	0.02	0.6	$1.3 \times 10^{-4}$	62
NaCl	0.06	0.26	$1.7 \times 10^{-5}$	this work
"room particles"	$0.07^a$	0.23	$1.2 \times 10^{-5}$	58

<sup>a</sup> Calculated from D using Eq. (13).

Table II. Conversion of the diameter  $d$  of spheres with density  $\rho$  into the aerodynamic diameter  $d_a$  according to Eq. (50).  
 Diameters in  $\mu\text{m}$ ;  $\rho$  in  $\text{g cm}^{-3}$ .

$d$	$\rho = 0.5$		$\rho = 2$		$\rho = 5$		$\rho = 10$		$\rho = 15$		$\rho = 20$	
	$d_a$	$\frac{d_a}{d}$	$d_a$	$\frac{d_a}{d}$	$d_a$	$\frac{d_a}{d}$	$d_a$	$\frac{d_a}{d}$	$d_a$	$\frac{d_a}{d}$	$d_a$	$\frac{d_a}{d}$
0.01	0.0056	0.564	0.021	2.06	0.047	4.66	0.083	8.28	0.113	11.3	0.140	14.0
0.02	0.0111	0.555	0.039	1.97	0.085	4.23	0.143	7.20	0.189	9.5	0.229	11.5
0.05	0.0279	0.558	0.090	1.81	0.177	3.54	0.279	5.58	0.358	7.16	0.424	8.48
0.1	0.0577	0.577	0.167	1.67	0.305	3.05	0.461	4.61	0.580	5.80	0.682	6.82
0.2	0.123	0.615	0.312	1.56	0.536	2.68	0.788	3.94	0.982	4.91	1.15	5.08
0.5	0.332	0.664	0.738	1.47	1.21	2.42	1.74	3.48	2.15	4.30	2.50	5.00
1.0	0.685	0.685	1.45	1.45	2.33	2.33	3.33	3.33	4.10	4.10	4.75	4.75
2.0	1.39	0.695	2.86	1.43	4.57	2.29	6.50	3.25	7.98	3.99	9.23	4.62
5.0	3.51	0.702	7.10	1.42	11.3	2.26	16.0	3.20	19.6	3.92	22.6	4.52
10.0	7.05	0.705	14.2	1.42	22.5	2.25	31.8	3.18	39.0	3.90	45.0	4.50

Table III. Survey of aerosol vessels used.

Name	Shape	Volume (m <sup>3</sup> )	Height (m)	Wall material
PERVEX	box	0.15	0.6	Lucite brass floor
100	vertical cylinder	1.2	1.7	steel
200	box	1.0	1.0	steel
300	box	0.075	0.5	stainless steel
ENAK	vertical cylinder	20	4.2	aluminium
GRACE	vertical cylinder	0.3	1.2	glass
SAUNA	vertical cylinder	0.15	0.6	Incoloy steel
SUNKIST	box	1.0	1.0	glass

Table IV. Diameters of quasi-monodisperse polystyrene aerosols and their decay constants  $\beta$  in 200 vessel (2 m height).

diameter of sphere (d in $\mu\text{m}$ )			n	$f_n$ (b)	$\beta$ measured ( $10^{-6}\text{s}^{-1}$ )	$\beta_s$ ( $10^{-6}\text{s}^{-1}$ )	$\beta$ calculated ( $10^{-6}\text{s}^{-1}$ )
DOW (a)	ECN	literature					
1.305	1.26	1.09  124 , 1.21  125	1		27	28	28
0.796	0.78	0.81  126 , 0.77  124	1		11	12	12
"			2	1.19	15	16	16
"			3	1.28	18	18	18
"			4	1.38	21	21	21
0.557	0.52	0.50  125 , 0.51  124  0.53  127	1		6	6	6
"			2	1.19	7	8	8
"			3	1.28	9	9	9
"			4	1.38	11	10	10
0.234	0.22	0.207  125 , 0.22  128	1		2.9	1.4	2.3
"			2	1.19	2.8	1.8	2.6
0.126	0.107	0.100  125	1		4	0.5	2.7
"			2	1.19	3.6	0.6	2.4
"			3	1.28	3.3	0.7	2.3
0.091	0.071		1		5	0.3	4
"			2	1.19	3.5	0.4	3.0

(a) As quoted by manufacturer.

(b) According to Stöber [94].

Table V. Relationship between specific energies of formation  $E_{\text{spec}}$  and microstructure of gold aerosols.

Espec (kJ/g)	$d_{lg}$ ( $\mu\text{m}$ )	$\sigma_{lg}$	Specific surface energy		$n_1$ ( $10^{-12}$ g)
			(J/g)	ratio to Espec	
270	0.014	1.5	47	$0.17 \times 10^{-3}$	$5.7 \times 10^{-5}$
130	0.018	1.5	36	$0.28 \times 10^{-3}$	$1.2 \times 10^{-4}$
70	0.026	1.5	26	$0.37 \times 10^{-3}$	$3.7 \times 10^{-4}$
20	0.030	1.5	23	$1.2 \times 10^{-3}$	$5.6 \times 10^{-4}$
6	0.032	1.5	20	$3.3 \times 10^{-3}$	$6.8 \times 10^{-4}$

Table VI. Experimental results for gold aerosols formed by Exploding Wires at different specific formation energies (Espec).

Espec (kJ.g <sup>-1</sup> )	primary particles		aerodyn. diam. <sup>a</sup>		effective aerodyn. diam. <sup>b</sup>	
	$\frac{d}{10^{-4}}$ $\mu\text{m}$	$\sigma$ Ig	$(d_a)$ $\mu\text{m}$	$(\sigma_a)$ g	$d_a(c_m)^c$ $\mu\text{m}$	$d_a(c_n)^d$ $\mu\text{m}$
270	140 $\pm$ 15	1.5 $\pm$ 0.1	0.61	1.22	0.64	0.62
130	180 $\pm$ 20	1.5 $\pm$ 0.1	0.61	1.19	0.64	0.68
20	300 $\pm$ 40	1.5 $\pm$ 0.1	0.79	1.18	0.81	0.78

<sup>a</sup> as obtained by aerosol centrifuge.

<sup>b</sup> calculated from measured decay constants using Eqs. (17) and (18).

<sup>c</sup> from decay curve of mass concentration.

<sup>d</sup> from decay curve of number concentration.

Table VII. Aerosol decay in 200-vessel as a function of vessel height.

height (m)	observed half-life (h)	decay constant (h <sup>-1</sup> )	effective <sup>a</sup> aerodynamic diameter ( $\mu$ m)
2	10.5	$6.6 \times 10^{-2}$	1.0
1	8	$8.7 \times 10^{-2}$	0.81
0.5	5	$13.9 \times 10^{-2}$	0.72

<sup>a</sup> calculated from the decay constants using Eqs. (17) and (18).

Table VIII. Properties of iron oxide cluster aggregates (basic data from Kops [89]).

$d_a$ ( $\mu\text{m}$ )	$d_{sp}$ ( $\mu\text{m}$ )	$d_e$ ( $\mu\text{m}$ )	$\kappa =$ $\frac{d_{sp}}{d_e} F(d_a)F(d_e)$
0.62	10.4	0.97	16.0
0.68	12.3	1.08	16.5
0.76	12.3	1.19	14.3
0.80	16.6	1.28	17.7
0.93	17.0	1.47	15.1
1.01	19.1	1.58	15.6
1.10	18.1	1.74	13.2



Table IX. Measurements on  $U_3O_8$  and Cu oxide aerosols in the  $1.2 \text{ m}^3$  100-vessel.

$d_a$ ( $\mu\text{m}$ )	$m$ (pg)	$d_e^a$ ( $\mu\text{m}$ )	$n^b$	$\kappa$	$\frac{\kappa}{F(d_e)}$	miscellaneous
0.39	0.077	0.26	$4.9 \times 10^2$	4.30	2.59	<u><math>U_3O_8</math> aerosols.</u> After 24 hours: $d_a$ -distribution is log-normal with $(d_a)_g = 0.78 \mu\text{m}$ and $\sigma_g = 1.26$ . From decay curves: $d_a = 0.78 \mu\text{m}$ and $\bar{m} = 2.1 \text{ pg}$ . As a result: $n = 1.4 \times 10^4$ , $\kappa = 8.42$ and $\frac{\kappa}{F(d_e)} = 6.95$ .
0.44	0.11	0.29	$7.0 \times 10^2$	4.23	2.68	
0.49	0.21	0.36	$1.3 \times 10^3$	5.00	3.60	
0.57	0.50	0.49	$3.2 \times 10^3$	6.28	4.67	
0.68	1.26	0.66	$8.1 \times 10^3$	7.91	6.32	
0.80	2.60	0.84	$1.7 \times 10^4$	9.13	7.62	
0.92	3.62	0.94	$2.3 \times 10^4$	8.65	7.35	
1.10	5.33	1.07	$3.4 \times 10^4$	6.83	5.91	
0.32	0.10	0.32	$2.0 \times 10^3$	6.03	3.94	<u>Cu oxide aerosol.</u> After 24 hours: $d_a$ -distribution is log-normal with $(d_a)_g = 0.41 \mu\text{m}$ and $\sigma_g = 1.22$ . From decay curve: $d_a = 0.45 \mu\text{m}$ and $\bar{m} = 0.71 \text{ pg}$ . As a result: $n = 1.3 \times 10^4$ , $\kappa = 10.2$ and $\frac{\kappa}{F(d_e)} = 8.03$ .
0.35	0.16	0.37	$2.9 \times 10^3$	6.51	4.46	
0.39	0.25	0.43	$4.6 \times 10^3$	7.02	5.05	
0.44	0.39	0.50	$7.4 \times 10^3$	7.50	5.64	
0.49	0.66	0.59	$1.2 \times 10^4$	8.39	6.55	
0.57	1.04	0.70	$2.0 \times 10^4$	8.48	6.84	

$a \rho = 8.3 \text{ g cm}^{-3}$  and  $6 \text{ g cm}^{-3}$  for  $U_3O_8$  and Cu oxide, resp.

$b d_{1g} = 0.026 \mu\text{m}$  and  $0.020 \mu\text{m}$ ,  $\sigma_{1g} = 1.49$  and  $1.48$  for  $U_3O_8$  and Cu oxide, resp.

Table X. Increase  $f$  of the aerodynamic diameter of  $U_3O_8$  aggregates due to change to spheres.

$d_a$ ( $\mu\text{m}$ )	$\kappa$	$d'_a$ ( $\mu\text{m}$ )	$f$
0.39	4.3	0.89	2.3
0.44	4.2	0.98	2.2
0.49	5.0	1.19	2.4
0.57	6.3	1.54	2.7
0.68	7.9	2.05	3.0
0.80	9.1	2.57	3.2
0.92	8.7	2.87	3.1
1.10	6.8	3.00	2.7

Table XI. Calculated (using Eq. (84)) and measured half-lives of two gold aerosols A and B of different initial mass concentration (5 and 80 mg.m<sup>-3</sup> resp.) in the 200-vessel.  $K = 1.5 \times 10^{-9} \text{ cm}^3 \cdot \text{s}^{-1}$ .

time after formation (h)	half-life (h)			
	calculated <sup>a</sup>		measured <sup>b</sup>	
	A	B	A	B
0.25	21	7.8	16	6
2.5	11	6.3	16	6
5	10	6.3	16	6

<sup>a</sup> Using Eq. (84).

<sup>b</sup> From fig. 25.

Table XII. Review of vapor/gas systems studied and comparison of calculated  $d\rho/dT$  values with observations.

Vapor/Gas System	$M_d$	$M_g$	$\Delta H_v$ (kJ/mol)	$X_d$	T(K)	$d\rho/dT$ [g/(cm <sup>3</sup> ·K)]	Observation
Water/air	18	29	41	$3.6 \times 10^{-2}$	300	$-4.7 \times 10^{-6}$	stirred
Methyl alcohol/air	32	29	35	0.22	300	$-2.7 \times 10^{-6}$	stirred
Ethyl alcohol/air	46	29	39	$8.5 \times 10^{-2}$	300	$-1.0 \times 10^{-6}$	stirred
n-propyl alcohol/air	60	29	42	$3.9 \times 10^{-2}$	300	$-1.3 \times 10^{-6}$	stirred
Isopropyl alcohol/air	60	29	42	$6.8 \times 10^{-2}$	300	$+6.4 \times 10^{-6}$	stirred
Isoamyl alcohol/air	88	29	45	$5.7 \times 10^{-3}$	300	$-3.1 \times 10^{-6}$	stirred
n-hexane/air	86	29	29	0.29	300	$+2.0 \times 10^{-5}$	stagnant
Di-isopropyl ether/air	102	29	29	0.28	300	$+2.5 \times 10^{-5}$	stagnant
1,1,1-trichloroethane/air	133	29	33	0.22	300	$+3.4 \times 10^{-5}$	stagnant
Carbon tetrachloride/air	154	29	30	0.22	300	$+3.7 \times 10^{-5}$	stagnant
Freon-133/air	187	29	28	0.53	300	$+1.1 \times 10^{-4}$	stagnant
Water/helium	18	4	41	$3.6 \times 10^{-2}$	300	$+5.2 \times 10^{-7}$	stagnant

Table XIII. Analysis of aerosol decay constants  $\beta_e$  observed in chambers with non-conductive walls assuming dominating electrophoresis (Eq. (85)).

aerosol formation and treatment	aerosol volume ( $m^3$ )	chambers wall material	observed $\beta_e$ ( $s^{-1}$ )	assumed $\mu_e$ ( $cm^2 \cdot V^{-1} \cdot s^{-1}$ )	wall charge $q_e$ (C)	effective wall charge density $\frac{q_e}{S}$ ( $C \cdot m^{-2}$ )	literature
nebulization and neutralization	0.32	poly-styrene	$2 \times 10^{-4}$	$10^{-4}$	$1.2 \times 10^{-7}$	$5 \times 10^{-8}$	Stein [80]
nebulization	0.32	"	$8 \times 10^{-4}$	$2.5 \times 10^{-4}$	$1.8 \times 10^{-7}$	$7 \times 10^{-8}$	"
dry dispersal	0.32	"	$2.5 \times 10^{-3}$	$10^{-3}$	$1.4 \times 10^{-7}$	$6 \times 10^{-8}$	"
dry dispersal nebulization	0.32	Lucite	$2 \times 10^{-3}$	$10^{-3}$	$1.2 \times 10^{-7}$	$5 \times 10^{-8}$	Lieberman [83]
nebulization and neutralization	0.5	poly-ethylene	$7 \times 10^{-5}$	$2.5 \times 10^{-4}$	$2 \times 10^{-8}$	$7 \times 10^{-9}$	this work
nebulization and neutralization	65	teflon	$10^{-4}$	$10^{-4}$	$6 \times 10^{-6}$	$3 \times 10^{-8}$	McMurry [40]
chemical reaction/heating	0.024	glass	$4 \times 10^{-3}$	$2.5 \times 10^{-4}$	$4 \times 10^{-9}$	$10^{-8}$	Zalabsky [41]

Table XIV. Analysis of aerosol decay in heated vessels.

aerosol vessel	vessel volume (m <sup>3</sup> )	aerosol material	heating power (W)	half-life (h)	decay constant (10 <sup>-5</sup> s <sup>-1</sup> )	$\bar{m}$ (10 <sup>-13</sup> g)	settling decay constant (10 <sup>-5</sup> s <sup>-1</sup> )	see Eqs. (28) B <sub>m</sub> B <sub>corr</sub>	miscellaneous
100	1.2	Au*, air	50	8.2	2.3	1.8	0.6	0.28	90% insulation
"	"	"	100	5.1	3.8	-	(0.6)	0.32	"
"	"	"	200	2.9	6.6	1.0	0.6	0.20	"
PERVEX	0.15	"	18.5	2.7	7.1	8.8	3.3	0.19	local heating
"	"	"	33	1.8	10.7	5.4	3.0	0.20	"
"	"	"	64	1.0	19	2.8	2.5	0.22	"
"	"	"	34	2.8	7.0	-	-	0.16	floor heating
"	"	"	60	1.5	12.8	-	-	0.19	"
ENAK	20	"	200	18	1.1	10	0.85	0.28	local heating
"	"	"	500	14	1.4	8.0	0.88	0.54	"
GRACE	0.3	"	120	0.85	22	-	-	0.28	"
"	"	"	200	0.60	32	-	-	0.24	"
"	"	"	320	0.38	50	-	-	0.23	"
"	"	"	410	0.27	72	-	-	0.27	"
"	"	"	550	0.16	12(2)	-	-	0.33	"
"	"	"	680	0.13	15(4)	-	-	0.34	"
"	"	"	810	0.12	16(5)	-	-	0.30	"
"	"	"	900	0.10	190	-	-	0.32	"
"	"	oil, "	300	0.25	7.7	-	-	0.38	"
PERVEX	0.15	"	60	1.3	15	-	-	0.19	"
"	"	Pt*, "	60	1.3	15	-	-	0.22	"
"	"	"	60	1.3	15	-	-	0.22	"
100	1.2	Cu-ox, air	125	4.0	4.8	-	-	0.23	"
"	"	NaCl, air	125	4.4	4.4	-	-	0.21	"
"	"	polystyrene, air	200	3.6	5.4	2.8	1.4	0.11	"

\* Exploding Wire generated.

Table XV. B values as calculated from Eqs. (27) - (28) ( $B_S$ ,  $B_E$ ,  $B_B$  and  $B_D$ ) and from measuring data (29) ( $B_m^{corr}$ ).

aerosol/gas temperature	$B_m^{corr}$	$B_S$	$B_E$	$B_B$	$B_D$
Au/air R.T.	0.20 <sup>a</sup>	0.2 <sup>b</sup>	$1.2 \times 10^{-4}$	0.18	0.36
Au/N <sub>2</sub> 100°C	0.21	0.2 <sup>b</sup>	$1.5 \times 10^{-4}$	0.18	0.36
Au/He R.T.	0.41	0.2 - 0.3 <sup>c</sup>	$7.1 \times 10^{-4}$	0.18 <sup>d</sup>	0.36 <sup>d</sup>
Au/He 100°C	0.41	0.2 - 0.3 <sup>c</sup>	$8.3 \times 10^{-4}$	0.18 <sup>d</sup>	0.36 <sup>d</sup>
NaCl/He	0.48	0.2 - 0.3 <sup>c</sup>	0.72	0.58 <sup>d</sup>	1.2 <sup>d</sup>

<sup>a</sup> average  $B_m^{corr}$  value taken from Table XIV.

<sup>b</sup>  $n_{th}$  assumed to be 5 for air in view of results from Table XIV.

<sup>c</sup>  $n_{th}$  lies between 5 and 3 dependent on the nature of the interaction between He and particles.

<sup>d</sup> Eqs. (28c) and (28d) have been used with values of  $c_m$  and  $c_t$  only to be used for air in default of accommodation coefficient for He.

Table XVI. Effect of temperature ( $\bar{T}$ ) on thermophoretic deposition of copper oxide aerosol.

$Q^*$ (W)	$\bar{T}$ (°C)	$\beta$ ( $10^{-4} s^{-1}$ )	$B_m$
65	90	1.9	0.23
212	500	5.8	0.20
220	600	4.6	0.16

\* Calculated from temperature differences as measured between gas and walls (Eq. (94)).



Table XVII. Results on hampered aerosol deposition in PERVEX-vessel with floor heating at low power levels.

Q (W)	$t_{\frac{1}{2}}$ (h)	$\beta_m$ ( $10^{-5} s^{-1}$ )	$\beta_{th}^*$ ( $10^{-5} s^{-1}$ )	$\beta_{eff}^{**}$ ( $10^{-5} s^{-1}$ )
0	5.5	3.5	0	(+ 3.5)
5	10	1.9	1.1	+ 0.8
6.6	11	1.8	1.4	+ 0.4
7	12	1.6	1.4	+ 0.2
10	9.5	2.0	2.1	- 0.1
15	7	2.8	3.1	- 0.3
34	2.6	7.0	7.0	0.0
60	1.4	12.8	12.4	+ 0.4

\*  $\beta_{th} = 0.21 \times Q.$

\*\*  $\beta_{eff} = \beta_m - \beta_{th}.$

Table XVIII.  $Q_v$  values calculated from the aerosol experiments performed in condensing water vapour in various aerosol vessels, using Eq. (92).

Aerosol vessel	Q (W)	$G^*$ ( $\text{kg}\cdot\text{m}^{-3}$ ) <sup>2/5</sup> s <sup>-1</sup>	$Q_v$ (W)	$\frac{Q_v}{Q} \times 100\%$
ENAK	$8 \times 10^3$	$7.8 \times 10^{-7}$	45	0.56
ENAK	$4 \times 10^3$	$5.5 \times 10^{-7}$	18	0.45
ENAK	$2 \times 10^3$	$4.0 \times 10^{-7}$	8.5	0.42
ENAK	$10^3$	$2.7 \times 10^{-7}$	3.2	0.32
GRACE	600	$3.0 \times 10^{-6}$	2.8	0.46
GRACE	300	$1.9 \times 10^{-6}$	0.87	0.29
GRACE	200	$1.6 \times 10^{-6}$	0.57	0.28
GRACE	100	$1.2 \times 10^{-6}$	0.28	0.28
200	900	$1.2 \times 10^{-6}$	2.1	0.23
200	600	$1.0 \times 10^{-6}$	1.3	0.22
200	400	$8.3 \times 10^{-7}$	0.82	0.20
200	200	$5.5 \times 10^{-7}$	0.29	0.15
PERVEX	60	$1.5 \times 10^{-7}$	0.067	0.11

\* See Eqs. (91) and (92) on pg. 124

Table XIX. Droplet size  $d$  and percentage supersaturation  $\%S$  as calculated from decay curves of gold aerosols in PERVEX with a pool of water on the floor heated with various heating powers  $Q$ .

$Q$ (W)	$t_{\frac{1}{2}}$	$\beta_m$ ( $10^{-4} \text{ s}^{-1}$ )	$\beta_{th}^a$ ( $10^{-5} \text{ s}^{-1}$ )	$v_s^b$ ( $10^{-3} \text{ cm.s}^{-1}$ )	$d$ ( $\mu\text{m}$ )	$\%S^d$
0	6.8 h	2.8	0	1.68	0.68 <sup>e</sup>	0
5	5.8 h	3.3	0.8	1.50	(0.64)	-
10	130 min	8.9	1.5	4.4	1.14	0.18
15	75 min	15	2.2	7.8	1.54	0.44
30	53 min	22	4.4	10.8	1.83	0.73
60	28 min <sup>e</sup>	41	8.8	20	2.55	2.0

<sup>a</sup> From  $\beta_{th} = 0.5 \times 0.44 \times \frac{Q}{1.5 \times 10^5}$  according to experience that the temperature difference between gas atmosphere and cold walls is halved by changing from dry to wet atmospheres.

<sup>b</sup>  $v_s = (\beta_m - \beta_{th}) h = (\beta_m - \beta_{th}) 60$ .

<sup>c</sup> This value of 0.68  $\mu\text{m}$  corresponds very well with the  $d$  value obtained by centrifuge viz. 0.70  $\mu\text{m}$ .

<sup>d</sup> Calculated using Eq. (93).

<sup>e</sup> Similar  $t_{\frac{1}{2}}$  values have been obtained with copper aerosols of very low mass concentration indicating that the initial aerosol mass plays no role in the total droplet mass.

Table XX. Droplet size d and percentage supersaturation %S as calculated from decay curves of copper aerosols in the GRACE vessel with a 100 W heated pool of water containing various amounts of NaCl.

kg NaCl.m <sup>-3</sup>	t <sub>1/2</sub> (min)	$\beta$ (10 <sup>-5</sup> s <sup>-1</sup> )	v <sub>s</sub> (10 <sup>-3</sup> cm.s <sup>-1</sup> )	$\beta - \beta_{th}^a$ (10 <sup>-5</sup> s <sup>-1</sup> )	v <sub>s</sub> <sup>b</sup> (10 <sup>-3</sup> cm.s <sup>-1</sup> )	d μm	%S
200	150	7.7	9.2	0	0	-	-
130	140	8.3	9.9	0.6	0.7	-	-
70	120	9.6	11.6	1.9	2.3	0.8	0.09
33	110	10.5	12.6	2.8	3.4	1.0	0.18
20	92	12.6	15.1	4.9	5.9	1.3	0.40
13	80	14.4	17.3	6.7	8.0	1.6	0.74
10	73	15.8	19.0	8.1	9.7	1.73	0.93
7	65	17.8	21.3	10.1	12.1	1.93	1.30
0	60	19.3	23.1	11.6	13.9	2.09	1.65

<sup>a</sup>  $\beta_{th}$  was taken equal to  $7.7 \times 10^{-5} \text{ s}^{-1}$ , see also footnote <sup>a</sup> of Table XIX.

<sup>b</sup> Calculated from  $\beta - \beta_{th}$ .

Table XXI. Measured and calculated number concentrations  $c_n$  of NaCl aerosols produced by nebulizing an aqueous NaCl solution in the 100-vessel.

time (h)	$c_n$ measured ( $\text{cm}^{-3}$ )	$c_n^*$ calculated ( $\text{cm}^{-3}$ )	time (h)	$c_n$ measured ( $\text{cm}^{-3}$ )	$c_n^{**}$ calculated ( $\text{cm}^{-3}$ )
1	$2.8 \times 10^4$	$2.4 \times 10^4$	1	$9 \times 10^4$	$9.5 \times 10^4$
3.5	$2.2 \times 10^4$	$1.7 \times 10^4$	5.5	$3 \times 10^4$	$2.8 \times 10^4$
6	$1.3 \times 10^4$	$1.2 \times 10^4$	25	$6 \times 10^3$	$6.1 \times 10^3$
24	$3.8 \times 10^3$	$4.1 \times 10^3$	48	$3 \times 10^3$	$2.8 \times 10^3$
26	$2.9 \times 10^3$	$3.7 \times 10^3$	72	$1.8 \times 10^3$	$1.6 \times 10^3$
31	$2.8 \times 10^3$	$3.1 \times 10^3$	106	$1.2 \times 10^3$	$9 \times 10^2$
48	$1.8 \times 10^3$	$1.9 \times 10^3$	144	$6 \times 10^2$	$6 \times 10^2$
55	$1.5 \times 10^3$	$1.6 \times 10^3$			
72	$1.1 \times 10^3$	$1.1 \times 10^3$			
79	$9 \times 10^2$	$9.4 \times 10^2$			
96	$7.2 \times 10^2$	$6.9 \times 10^2$			
103	$6.4 \times 10^2$	$6.1 \times 10^2$			
168	$2.7 \times 10^2$	$2.2 \times 10^2$			
175	$2.4 \times 10^2$	$2.0 \times 10^2$			
192	$1.8 \times 10^2$	$1.6 \times 10^2$			
222	$1.2 \times 10^2$	$1.1 \times 10^2$			

\* assuming:  $c_n(0) = 3 \times 10^4 \text{ cm}^{-3}$ ,  $K = 2 \times 10^{-9} \text{ cm}^3 \cdot \text{s}^{-1}$ ,  $\beta = 3.5 \times 10^{-6} \text{ s}^{-1}$ .

\*\* assuming:  $c_n(0) = 2 \times 10^5 \text{ cm}^{-3}$ ,  $K = 1.5 \times 10^{-9} \text{ cm}^3 \cdot \text{s}^{-1}$ ,  $\beta = 3.2 \times 10^{-6} \text{ s}^{-1}$ .

Table XXII. Courses of "total sulphur" (tot S), number concentration  $c_n$  and particle diameter  $d$  as a function of time  $t$  of a  $\text{Na}_2\text{SO}_4$ -aerosol in SUNKIST.

t (h)	tot S (ppb)	$c_n$ ( $\text{cm}^{-3}$ )	$d^*$ ( $\mu\text{m}$ )
0	55	$1.8 \times 10^4$	0.28
1	52	$1.5 \times 10^4$	0.29
2	41	$10^4$	0.30
4	35	$8 \times 10^3$	0.31
11	15	$2.3 \times 10^3$	0.35
14	15	$1.8 \times 10^3$	0.38
15.5	14	$1.6 \times 10^3$	0.39
19.5	10	$10^3$	0.41
21	6	$8 \times 10^2$	0.37

\* Calculated from "total sulphur", assuming  $\text{Na}_2\text{SO}_4$  present with  $\rho = 1.5 \text{ g cm}^{-3}$ .

## SAMENVATTING

Dit proefschrift behandelt het gedrag van aerosol<sup>\*)</sup> onder verschillende omstandigheden in afgesloten ruimten. Kennis van dit gedrag is van belang voor het gebruik van met aerosol gevulde ruimten als voorraadvat en als middel om aerosol te karakteriseren, en van zgn. smogkamers voor onderzoek van luchtverontreiniging (voornamelijk betreffende fotochemische processen waarbij vaak aerosol gevormd wordt).

Een beknopt literatuur-overzicht (hoofdstuk 1) laat zien dat weinig aandacht werd gegeven aan het aerosolgedrag in afgesloten ruimten. Na een exclusieve belangstelling van de meteorologen voor het onderwerp, werd het sinds het begin van de zestiger jaren een belangrijk onderwerp bij onderzoek in verband met nucleaire veiligheid. Het nucleaire aerosolonderzoek richt zich, echter, in hoofdzaak op voor luchtverontreinigings-onderzoek irrelevant hoge massaconcentraties.

In het tweede hoofdstuk wordt een model gegeven voor het aerosolgedrag in afgesloten ruimten. Als regel vindt afzetting van aerosoldeeltjes plaats op de wanden vanuit de door warmte-convecties geroerde en gehomogeniseerde ruimte. Het transport door een relatief dunne grenslaag op de wand is de snelheidsbepalende stap voor de afzetting. Verbanden worden vervolgens gegeven voor een aantal afzettingsmechanismen: sedimentatie, diffusie, thermoforese, diffusioforese, electroforese en fotoforese. Uit literatuurgegevens en een theorie van Fuchs wordt een praktisch verband afgeleid tussen de grenslaag-dikte  $\delta$  voor diffusie-afzetten en de diffusiecoëfficiënt  $D$  van aerosoldeeltjes. Voorwaarden voor het optreden van niet-geroerde depositie door uitzakken en diffusie worden afgeleid.

Na een korte beschrijving (hoofdstuk 3) van de belangrijkste experimenteer-middelen wordt in het vierde hoofdstuk verslag gedaan van de waarnemingen en een interpretatie hiervan gegeven. Dit hoofdstuk behandelt

---

\*) Onder aerosol wordt verstaan (zie Van Dale's Groot Woordenboek der Nederlandse Taal, Nijhof, Den Haag, 1976) "het totaal van in de atmosfeer zwevende vaste en vloeibare deeltjes". De deeltjes zijn groter dan moleculen maar klein genoeg om meetbaar zwevend te zijn. Enkele voorbeelden van een aerosol zijn: nevel, heiligheid, rook, mist, wolken en zandstormen.

een viertal ruimten: onverwarmde droge ruimten, verwarmde droge ruimten, ruimten met verwarmde vloeistof op de bodem en smogkamers.

Met waarnemingen van het gedrag van monodisperse en polydisperse aerosolen in onverwarmde, droge ruimten wordt het afgeleide model voor sedimentatie en diffusie ondersteund. De waarnemingen bevestigen grotendeels de juistheid van het in hoofdstuk 2 afgeleide verband tussen  $\delta$  en D. Deeltjes groter dan enkele  $0,1 \mu\text{m}$  worden verwijderd door sedimentatie; deeltjes kleiner dan ongeveer  $0,1 \mu\text{m}$  zijn onderhevig aan diffusie-afzettingen maar ook vaak speelt electroforese een belangrijke rol (vooral bij deeltjes van ca.  $0,1 \mu\text{m}$ ). Het blijkt mogelijk om met behulp van waarnemingen betreffende het aerosolgedrag in onverwarmde droge ruimten, dynamische vormfactoren en aerodynamische diameters van aerosoldeeltjes te bepalen.

Thermoforetisch afzettingen is het dominerende proces in lokaal-verwarmde droge ruimten. De waarnemingen gedaan met een groot aantal verschillende aerosolen ondersteunen het in hoofdstuk 2 afgeleide model voor thermoforetisch afzettingen. Interpretatie van de waarnemingen levert de thermoforetische eigenschappen van aerosolen. De resultaten ondersteunen de theorieën van Brock en Stetter betreffende thermoforese maar wijken belangrijk af van die van Derjaguin en Epstein. In overeenstemming met de theorie wordt een thermoforetische vervalconstante gevonden onafhankelijk zowel van de deeltjesgrootte ( $\geq 0,5 \mu\text{m}$ ), als van het deeltjesmateriaal en van de temperatuur. Experimenten tonen aan dat lichte verwarming van de bodem van een aerosol-bevattende ruimte een belangrijke verbetering van de aerosolstabiliteit kan opleveren.

Plaatsing van een hoeveelheid verwarmde vloeistof in een ruimte met aerosol, leidt tot deeltjesgroei door condensatie van damp gevolgd door versnellende sedimentatie. Een model voor het aerosolgedrag onder deze omstandigheden wordt door de waarnemingen ondersteund. Condensatie op aerosoldeeltjes bij verschillende graden van oververzadiging kan onderzocht worden met dit systeem. De oververzadiging kan berekenbaar gevarieerd worden met het in de vloeistof gedissipeerde vermogen en door het oplossen van verschillende stoffen.

Een onderzoek van het aerosolgedrag in een fotochemische smogkamer toonde aan dat er geen significante thermoforetische en fotoforetische depositie van  $0,06 \mu\text{m}$  deeltjes plaatsvindt. De waargenomen aerosolstabiliteit blijkt



verklaard te kunnen worden door electroforetische depositie en geeft een samenhangend beeld met electroforetisch afzetten bij andere experimenten. Coagulatie-constanten van aerosolen kunnen berekend worden uit aantal-concentratie metingen in afgesloten ruimten. De resultaten passen goed bij de theorie van Davies voor coagulatie. Diffusieconstanten van aerosolen kunnen bepaald worden uit de lange-termijn afneming van de aantal-concentratie in metalen vaten.

CURRICULUM VITAE

De schrijver van deze studie werd op 4 mei 1937 te Vlaardingen geboren. Na van 1949 tot 1954 de Rijks Hogere Burgerschool B te s'-Hertogenbosch te hebben doorlopen, werd hij ingeschreven als student chemie aan de Rijks-Universiteit te Utrecht. In 1958 werd het kandidaatsexamen Chemie E (Natuur- en Scheikunde hoofdvak, Wiskunde bijvak) afgelegd. In 1961 volgde het doctoraalexamen Chemie met als uitgebreide specialisaties Kernfysica en Radiochemie. Na voor eerste militaire oefening een speciale opdracht te hebben vervuld, werd in 1963 als wetenschappelijk medewerker in dienst getreden van het toenmalige Reactor Centrum Nederland (RCN). Na enige jaren de thermoelektrische eigenschappen van nucleaire brandstof te hebben bestudeerd (in verband met mogelijke directe energie-omzetting), werd in 1967 begonnen met een onderzoek van aerosolen vanwege de veiligheid van snelle kweekreactoren. De kennis van aerosolgedrag en de beschikbaarheid van een aantal onderzoekfaciliteiten leidden in 1972 tot uitbreiding van het aerosolonderzoek met onderwerpen op het gebied van luchtverontreiniging in het algemeen. Het in dit proefschrift weergegeven experimentele onderzoek is verricht bij het voormalige RCN (thans Energieonderzoek Centrum Nederland).